ELECTRON PARAMAGNETIC RESONANCE STUDIES OF Mn^{2+} IN SOME DIA-AND PARAMAGNETIC SINGLE CRYSTALS

By

RAM SHARMA SARASWAT

DEPARTMENT OF PHYSICS

INDIAN INSTITUTE OF TECHNOLOGY KANPUR

DECEMBER, 1976

ELECTRON PARAMAGNETIC RESONANCE STUDIES OF Mn^{2+} IN SOME DIA-AND PARAMAGNETIC SINGLE CRYSTALS

A Thesis Submitted
In Partial Fulfilment of the Requirements
for the Degree of

DOCTOR OF PHILOSOPHY

By

RAM SHARMA SARASWAT

to the

DEPARTMENT OF PHYSICS

INDIAN INSTITUTE OF TECHNOLOGY KANPUR

DECEMBER, 1976

i dedicate this thesis

to

my dear 'amma' and 'chachaji'

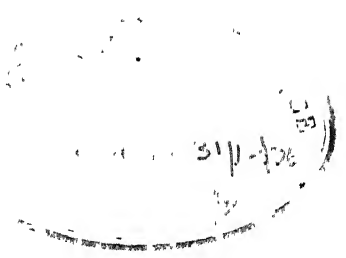

CERTIFICATE

This is to certify that the work presented in this thesis entitled 'Electron Paramagnetic Resonance Studies of Mn^{2+} in Some Dia- and Paramagnetic Single Crystals' is the original work of Mr. Ram Sharma Saraswat done under my supervision and it is not submitted elsewhere for a degree.

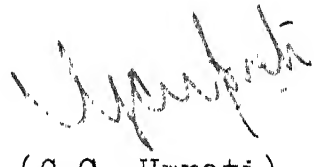

(G.C. Upreti)
Assistant Professor
Department of Physics
Indian Institute of Technology,
Kanpur-208016, INDIA

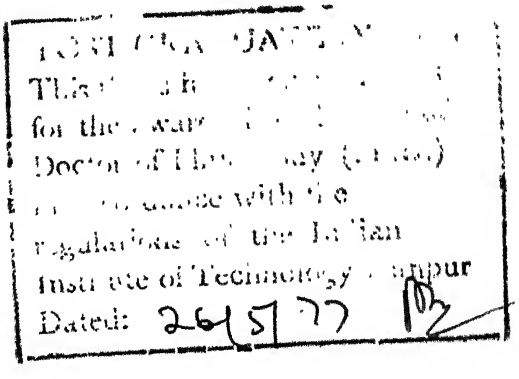

ACKNOWLEDGEMENTS

I express my deep sense of gratitude and indebtedness to Dr. G.C. Upreti for introducing me to the field of EPR and for his stimulating guidance and valuable discussions during the period of the present investigation. Sincere thanks are due to Professor Rollie J. Myers of Univ. of California at Berkeley for sending a copy of the thesis of Dr. Michael Robert St.John and its use in understanding and interpreting some of our experimental observations is gratefully acknowledged.

I am thankful to Professors P. Venkateswarlu, T.M. Srinivasan, D.R. Rao, R.K. Ray and H.D. Bist for their interest shown in the progress of this work.

It gives me great pleasure to convey my sincere thanks to my friends and colleagues, particularly M/S Vimal Jain, Akhilesh Jain, Vivek Malhotra and Mishraji (P.K.), for their warm friendship and cooperation throughout. I am thankful to Dr. U.V. Kumar for many timely helps and discussions and to Dr. (Mrs.) Kunda Muley for her help in initial stages of this work. For the help in work and pleasant company during my IIT stay, I thank my friends, particularly Guruji (PCU), Rastogi, Nigam, Roberts, Kaushik, Dayal, Ansari and Jagannath.

I am thankful for the technical assistance provided by M/S R.L. Arora, C.M. Sharma, S.D. Sharma, Kuldip Singh in particular and by the staff of various sections. My thanks are due to Mr. G.S. Hegde for microanalysis, to M/S S.L. Kanaujia and D.S. Rawat for assistance in lab. work, to Mr. J.K. Misra for carefully typing the thesis, Mr.R.K. Bajpai for tracing the figures and Mr. Lallu Singh for Cyclostyling.

Financial assistance from C.S.I.R. India during 1972-75 is gratefully acknowledged.

Finally, I feel it quite necessary, but not sufficient to convey my regards and thanks to my uncles, aunties and brothers for the affection and encouragement they have extended to me throughout and in addition to my brothers and their family members at Kanpur particularly for making my Kanpur stay very pleasant during the period of this work.

RSsaraswat

(R.S. Saraswat)

TABLE OF CONTENTS

		Page
List of Tables		vi
List of Figures		viii
Preface		xi
Chapter I	Introduction	1
II	Theory	11
	A. Theory of EPR of Iron Group Ions	12
	B. Spin-Hamiltonian Analysis of Mn^{2+} Spectra	33
	C. Theory of EPR of Mn^{2+} in Paramagnetic Single Crystals	41
III	Experimental	72
IV	Electron Paramagnetic Resonance Study of Mn^{2+} doped in Magnesium, Cobalt and Nickel Acetate Tetrahydrate Single Crystals	79
V	Electron Paramagnetic Resonance of Mn^{2+} in Some Tutton Salts	99
VI	Electron Paramagnetic Resonance Study of Mn^{2+} in $ZnSO_4.7H_2O$ and $CoSO_4.7H_2O$ Single Crystals	125
VII	Electron Paramagnetic Resonance Study of Mn^{2+} doped in Hexaquonitrates of Magnesium and Nickel	142
Appendix A	Literature Survey of EPR Studies of Various Paramagnetic Impurity Ions in Paramagnetic Hosts	162
B	Perturbation Theoretic Expressions for Hf Forbidden Doublet Separations in the EPR of Mn^{2+} in a Crystal Field of Orthorhombic Symmetry	167

LIST OF TABLES

Table		Page
II-1	Matrix elements of spin-Hamiltonian matrix for Mn^{2+} (S=5/2).	40
II-2	Spin-Hamiltonian parameters of Ni^{2+} in various nickel salt single crystals.	63
IV-1	Crystal structure parameters of tetrahydrate acetates of magnesium, cobalt and nickel.	82
IV-2	Spin-Hamiltonian parameters (non-Zeeman parameters are in units of 10^{-4} cm^{-1}) of Mn^{2+} in single crystals of tetrahydrate acetates of magnesium, cobalt and nickel at X-band.	89
IV-3	Widths of EPR lines and corresponding estimated values of $T_1(Co^{2+})$ at various temperatures for Mn^{2+} doped in single crystals of $Co(CH_3COO)_2.4H_2O$.	94
V-1	Spin-Hamiltonian parameters (non-Zeeman parameters are in units of 10^{-4} cm^{-1}) of Mn^{2+} in single crystals of some potassium and ammonium Tutton salts.	108-10
V-2	Linewidths of various fine structure groups of Mn^{2+} complex, for which H||Z, in $CoK_2(SO_4)_2.6H_2O$ and $FeK_2(SO_4)_2.6H_2O$ Tutton salt single crystals at 300 K.	113
V-3	The Zeeman-field intensity (H) and the corresponding linewidth (ΔH) of Mn^{2+} resonance lines for H||Z in $FeK_2(SO_4)_2.6H_2O$ at 77 K.	116
V-4	The Zeeman-field intensity (H) and the corresponding linewidth (ΔH) of Mn^{2+} resonance lines for H||Z in $Ni(NH_4)_2.(SeO_4)_2.6H_2O$ at 300 K.	121
VI-1	Spin-Hamiltonian parameters (non-Zeeman parameters are in units of 10^{-4} cm^{-1}) of Mn^{2+} in single crystals of heptahydrate sulphates of zinc, magnesium and nickel at 300 K and at X-band.	131

Table		Page
VI-2	Linewidths (in gauss) of various fine structure groups of Mn^{2+} complex, for which H||Z, in two forms of $CoSO_4.7H_2O$ at 300 K.	137
VII-1	The Zeeman-field intensity (H) and the corresponding linewidth (ΔH) of Mn^{2+} resonance lines for H||Z in $Ni(OH_2)_6.(NO_3)_2$ single crystals at 300 K.	159

LIST OF FIGURES

Figure		Page
II-1	Energy level splittings of the ground state of Mn^{2+}, for the case of negative D, and the $\Delta M = \pm 1$, $\Delta m = 0$ transitions, ZFS is the splitting due to the crystalline field, and hfs due to the hyperfine interaction.	31
II-2	Schematic diagram showing the relation among the systems involved in the Mn^{2+} line narrowing mechanism due to rapid relaxing Co^{2+} ions.	55
III-1	Block diagram of the EPR spectrometer.	74
III-2	Device to rotate the single crystal inside the cavity about a horizontal axis.	76
IV-1	Projection of the atoms in the bc* plane for crystals of tetrahydrate acetates of Mg, Co and Ni. Here c*-axis is perpendicular to both a- and b-axes. W_1, W_2, $\bar{W}_1$ and $\bar{W}_2$ are the water molecules and O_1 and O_2 are the oxygens of the two acetate groups.	84
IV-2	The EPR spectra of Mn^{2+} in $Mg(CH_3COO)_2.4H_2O$ at 300 K and at 77 K for H along the Z-axis of one set of equivalent Mn^{2+} complexes.	85
IV-3	The EPR spectra of Mn^{2+} in $Ni(CH_3COO)_2.4H_2O$ at 300 K and at 77 K for H along the Z-axis of one set of equivalent Mn^{2+} complexes.	86
IV-4	The EPR spectra of Mn^{2+} in $Co(CH_3COO)_2.4H_2O$ at 300 K and at 77 K for H along the Z-axis of one set of equivalent Mn^{2+} complexes.	87
V-1	The monoclinic crystal structure of $Mg(NH_4)_2(SO_4)_2.6H_2O$ projected along its c_o axis. The numbers inside the circles represent the positions of the atoms or molecules along the c_o axis in units of the unit cell dimension along the c_o axis (100 = 6.211 Å). For the other molecule of the unit cell, the positions of Mg and $H_2O(3)$ are given.	102

Figure		Page
V-2	The EPR spectra of Mn^{2+} in MPSH, CPSH and FPSH at 300 K for H along the Z-axis of one set of equivalent Mn^{2+} complexes.	104
V-3	The EPR spectra of Mn^{2+} in MPSH, CPSH and FPSH at 77 K for H along the Z-axis of one set of equivalent Mn^{2+} complexes.	105
V-4	The EPR spectra of Mn^{2+} in ZPSH at 300 K and at 77 K for H along the Z-axis of one set of equivalent Mn^{2+} complexes.	106
V-5	The EPR spectra of Mn^{2+} in $Ni(NH_4)_2(SeO_4)_2.6H_2O$ at 300 K for H along and at different angles from the Z-axis of one set of equivalent Mn^{2+} complexes.	107
VI-1	The EPR spectrum of Mn^{2+} in $ZnSO_4.7H_2O$ at 300 K for H along the Z-axis of one set of equivalent Mn^{2+} complexes.	130
VI-2	The EPR spectra of Mn^{2+} in $CoSO_4.7H_2O$(I) at 300 K and at 77 K for H along the Z-axis of one set of equivalent Mn^{2+} complexes.	134
VI-3	The EPR spectra of Mn^{2+} in $CoSO_4.7H_2O$ (II) at 300 K and at 77 K for H along the Z-axis.	135
VI-4	The EPR spectra of Mn^{2+} in $CoSO_4.7H_2O$(II) at 300 K for H along the X and Y axes.	136
VII-1	The crystal structures of (a) $Mg(OH_2)_6.(NO_3)_2$ and (b) $Ni(OH_2)_6.(NO_3)_2$.	147
VII-2	The EPR spectrum of Mn^{2+} in $Mg(OH_2)_6.(NO_3)_2$ at 300 K for H along the Z-axis of one set of equivalent Mn^{2+} complexes.	149
VII-3	The EPR spectrum of Mn^{2+} in $Mg(OH_2)_6.(NO_3)_2$ at 300 K for H along the X-axis of one set of equivalent Mn^{2+} complexes.	150
VII-4	The EPR spectrum of Mn^{2+} in $Mg(OH_2)_6.(NO_3)_2$ at 300 K for H along the K_1-axis.	152

Figure		Page
VII-5	The EPR spectrum of Mn^{2+} in $Mg(OH_2)_6.(NO_3)_2$ at 300 K for H along the K_2-axis.	153
VII-6	The EPR spectrum of Mn^{2+} in $Mg(OH_2)_6.(NO_3)_2$ for H along the K_2-axis showing the allowed and forbidden hyperfine transitions in the central group $+1/2 \leftrightarrow -1/2$ at 300 K. The transitions are labeled by a number n so that $\Delta m = \pm n$.	154
VII-7	The EPR spectrum of Mn^{2+} in $Ni(OH_2)_6.(NO_3)_2$ at 300 K for H along the Z-axis. The two high field groups recorded with ten times increased gain (X 10) are shown in the inset.	156
VII-8	The EPR spectra of Mn^{2+} in $Ni(OH_2)_6.(NO_3)_2$ at 300 K for H along the X and Y axes.	157
B-1	Schematic diagram showing the allowed ($\Delta M=\pm 1$, $\Delta m=0$) and forbidden ($\Delta M = \pm 1$, $\Delta m = \pm 1$; $\Delta M = \pm 1$, $\Delta m = \pm 2$) hyperfine transitions in the EPR of Mn^{2+} in an orthorhombic crystalline field for the Zeeman field at an angle slightly away from the Z-axis. The transitions numbered from 1 through 50 correspond to $\Delta M = \pm 1$, $\Delta m = \pm 1$ and those numbered from 1' through 8' correspond to $\Delta M = \pm 1$, $\Delta m = \pm 2$. The identification of the forbidden transitions is given in the text.	180

PREFACE

Electron Paramagnetic Resonance (EPR) studies of transition metal ions have usually been carried out by doping them as impurity in non-magnetic (i.e. diamagnetic) hosts. Similar studies can, in principle, be carried out by incorporating the paramagnetic ions in paramagnetic hosts, but these studies have been hindered by the broadening of impurity resonance lines due to the host-impurity interaction. However, if sharp spectra are observable, these studies should provide same information as obtained by doping impurity ions in diamagnetic hosts and in addition should also contain information on magnetic interactions themselves and on the host ion properties. Therefore a comparison of the EPR results of a paramagnetic ion doped in isomorphous dia- and paramagnetic single crystals would single out the features arising due to these interactions. With this in mind EPR studies of Mn^{2+} doped in the paramagnetic single crystals (crystals of Nickel, Cobalt and Ferrous salts) have been undertaken. This thesis describes the EPR studies of Mn^{2+} in single crystals of Tetrahydrate acetates of Co, Ni and Mg, $(M(CH_3COO)_2.4H_2O)$; Potassium Tutton salts of Co, Fe, Zn and Mg, $(MK_2(SO_4)_2.6H_2O)$, Ammonium Nickel Selenate Hexahydrate, $((NH_4)_2Ni(SeO_4)_2.6H_2O)$; Heptahydrate

sulphates of Co and Zn, ($MSO_4.7H_2O$) and Hexaquonitrates of Ni and Mg, ($M(OH_2)_6.(NO_3)_2$).

Chapter I describes, in brief, a general introduction to the subject of EPR in solids, particularly in single crystals. This is followed by a brief introduction to the magnetic interactions between impurity and host paramagnetic ions, viz. dipolar and exchange interactions.

Chapter II, dealing with theory, has been divided into three sections. Section A deals with the brief theory of EPR, the crystal field effects and the spin-Hamiltonian formalism. The discussion is restricted to the iron group transition metal ions in general, and to Mn^{2+} ion in particular. Also described, in brief, are the various physical processes (mechanisms) responsible for the zero-field splitting of Mn^{2+}, a S-state ion. Section B presents the spin-Hamiltonian analysis of Mn^{2+} EPR spectra. Section C deals with the theory of the EPR of paramagnetic impurity ions in paramagnetic hosts to elucidate when the sharp spectra are attainable and how to extract the additional information, relayed by the magnetic interactions, from the observed spectra.

Chapter III, on experimental, deals with a brief description of the experimental set up used in the studies - Varian V-4502 X-band EPR spectrometer fitted with V-4540

variable temperature accessory, a crystal rotating device and a quartz dewar used for the studies at liquid nitrogen temperature. The growing of single crystals from aqueous solution is also discussed.

Chapter IV presents a comparative EPR study of Mn^{2+} in a family of isomorphous dia- and paramagnetic single crystals, viz. Tetrahydrate acetates of Co, Ni and Mg (abbreviated as CoAc , NiAc and MgAc, respectively). This study gives information regarding the magnetic interactions between the impurity and host ions through their effect on EPR spectra of Mn^{2+} ions. Mn^{2+} is found to substitute for the divalent metal ions and exhibits two magnetically inequivalent complexes corresponding to the bimolecular unit cell of the three crystals. The observed additional features in the EPR of Mn^{2+} in CoAc and NiAc from those in MgAc are attributed to the magnetic interactions between Mn^{2+} and the respective host paramagnetic ions. In both CoAc and NiAc we observe a shift in the g_z-value caused probably by the local static magnetic field at Mn^{2+} sites created by the host paramagnetic ions. The observation of sharp EPR spectra of Mn^{2+} in NiAc and CoAc has been discussed in terms of spin-quenching and host spin-lattice relaxation narrowing, respectively. The linewidths of Mn^{2+} in NiAc show anisotropy and field dependence which are explained in terms of spin-quenching ideas. In CoAc,

however, the Mn^{2+} linewidths increase as one goes from outer fine structure groups to the central group which may be due to unequal influence of exchange interaction between Co^{2+} and Mn^{2+} upon various $\Delta M = \pm 1$ transitions of Mn^{2+}. Further the linewidths of Mn^{2+} in CoAc increase very rapidly with decreasing temperature, which is actually an indication that host spin-lattice relaxation narrowing is operative. In the end the use of impurity probe to measure extremely fast T_1 at high temperature ($\sim$ 300K) is illustrated by estimating T_1 of Co^{2+} in CoAc from the observed Mn^{2+} linewidths in CoAc.

Chapter V describes EPR investigations of Mn^{2+} doped in isomorphous para- and diamagnetic crystals of $MK_2(SO_4)_2.6H_2O$ Tutton salts, where M = Co, Fe, Mg and Zn. Here again Mn^{2+} is found to substitute for M^{2+} exhibiting two magnetically inequivalent complexes. The EPR spectra are analysed using a spin-Hamiltonian of orthorhombic symmetry. The additional features in the EPR of Mn^{2+} in Co Tutton salt, compared to that in diamagnetic Zn or Mg salts, are similar to those observed in the case of CoAc:Mn^{2+} and are explained in the same way. Further the additional features in the EPR of Mn^{2+} in Ferrous Tutton salt, viz. large Mn^{2+} linewidths, their unusual variation with fine structure groups, their decrease with the lowering of temperature and their field dependence at liquid nitrogen temperature, are discussed in terms of

various mechanisms describing the widths of Mn^{2+} lines in Ferrous salts. Besides, an interesting observation is large 'D' value of Mn^{2+} for Potassium Tutton salts than for corresponding Ammonium Tutton salts. This chapter also describes the EPR study of Mn^{2+} in $(NH_4)_2Ni(SeO_4)_2.6H_2O$ Tutton salt. Besides the common features of Mn^{2+} spectra in other Tutton salts, some additional features, such as g_z-shift, anisotropic and field dependent linewidths, are observed in the EPR of Mn^{2+} in $(NH_4)_2Ni(SeO_4)_2.6H_2O$. These features are explained in terms of the magnetic interactions between Mn^{2+} and Ni^{2+} and spin-quenching ideas.

In Chapter VI, the results of EPR study of Mn^{2+} in heptahydrate sulphates of Co and Zn crystals, $CoSO_4.7H_2O$ and $ZnSO_4.7H_2O$, are presented. The crystals of $CoSO_4.7H_2O$ are monoclinic, while those of $ZnSO_4.7H_2O$ are orthorhombic and isomorphous to $NiSO_4.7H_2O$ and $MgSO_4.7H_2O$. The detailed crystal structure data of $CoSO_4.7H_2O$ is not available. Our studies reveal the presence of two types of crystals obtained for $CoSO_4.7H_2O$ which are morphologically different and grow in two different temperature ranges about the room temperature. The two types of crystals give different EPR spectra of Mn^{2+}. The additional features of EPR spectra of Mn^{2+}, due to the magnetic interactions between Co^{2+} and Mn^{2+}, are similar to those in other Co salts, discussed in Chapters IV and V. EPR

spectra of Mn^{2+} in $ZnSO_4.7H_2O$ exhibited four magnetically inequivalent complexes and are analysed for the best fit parameters.

EPR studies of Mn^{2+} in highly hygroscopic crystals of hexaquonitrates of Ni and Mg are described in Chapter VII. Crystal structure studies show that various iron group hexaquometal nitrates of formula $M(OH_2)_6.(NO_3)_2$ are not isomorphous. Our EPR studies of Mn^{2+} in $Mg(OH_2)_6.(NO_3)_2$ and $Ni(OH_2)_6.(NO_3)_2$ also reveal that these are not isomorphous. Mn^{2+} spectra in $Ni(OH_2)_6.(NO_3)_2$ show a g-value shift and anisotropic and field dependent linewidths. These features are explained in terms of the magnetic interactions between Mn^{2+} and Ni^{2+} ions and spin-quenching ideas. Analysis of the hf forbidden transitions of Mn^{2+} in $Mg(OH_2)_6.(NO_3)_2$ is also included in this chapter.

Two appendices are included at the end. Appendix A contains the literature survey on the EPR studies of various paramagnetic impurities in paramagnetic hosts. In Appendix B expressions are derived for the doublet separations of the forbidden hf transitions in the EPR of Mn^{2+} in orthorhombic crystalline field, using perturbation theory.

Each chapter is written as to be self-contained and as such repetitions of some statements became unavoidable. At the end of each chapter a list of references is given.

A great deal of the contents of Chapters I and II has been gathered from certain review articles and text books. These are given as 'General References' and are not directly referred to, by a reference number, in the text. The names of the journals are abbreviated in accordance with the 'World List of Scientific Periodicals', IV edn. Butterworths, London (1963).

CHAPTER I

INTRODUCTION

ABSTRACT

A brief introduction is given to the subject of electron paramagnetic resonance (EPR) in solids, particularly in single crystals. Various applications of EPR technique are enumerated. A brief description of the magnetic interactions, viz. dipolar and exchange interactions, is followed by a description of the nature of problems studied in the present thesis.

Many and varied have been the applications of magnetic resonance techniques since Zavoisky[1] discovered electron paramagnetic resonance (EPR) in condensed matter as the first of a group which comprises NMR, NQR, ferro and antiferromagnetic resonances, cyclotron resonance and other techniques such as various kinds of double resonances. EPR is the resonance absorption of microwave radiation, usually between the ground state energy levels of a system, possessing permanent magnetic dipoles, under the application of an applied static magnetic (Zeeman) field. In principle, EPR technique may be applied to investigate any atomic or molecular system with unpaired electrons and in practice, it has been applied to a large variety of problems. Most widely investigated are paramagnetic ions in crystals[2], unpaired electrons in semiconductors[3] and organic free radicals[4], colour centres and radiation damage centres[5]. Essentially all of the information, obtained on radicals stabilized in irradiated biomolecules such as nucleic acids[6] and proteins[7], have been obtained from EPR spectroscopy. EPR may be used to identify radicals, describe their molecular structure and determine their concentration.[4] Also this technique is useful in detecting the occurrence of free radicals in chemical reactions, where they play an important role in reaction-mechanism.[8] EPR has also been

successfully tried as a cancer **diagnostic** tool by detection of free radicals in the living tissue.[9]

EPR is a very powerful tool and is widely used in solid state research. The paramagnetic ions in crystals have been studied extensively using EPR technique and probably lead the field in terms of volume of results. EPR has contributed much to the information concerning the energy levels lying within few cm^{-1} from the ground state of a paramagnetic system and to the understanding of various interactions in solids. The following magnetic and structural information can be obtained from the EPR data on the compounds containing transition ions, where the paramagnetism arises from the electrons in an unfilled d or f shell.

(1) One can determine the energy levels within few cm^{-1} from the ground level of a paramagnetic system. This information is useful while interpreting bulk properties e.g. susceptibility and specific heat, specially at very low temperatures, when such properties depend only on the energy levels within a few cm^{-1} of the ground level.

(2) Though the resonance spectrum arises from electronic transitions, the information on the nucleus of the paramagnetic ion can be obtained if there is a hyperfine structure arising from interaction between electrons and nucleus.

For example, the nuclear spin and approximate values of the nuclear magnetic dipole and electric quadrupole moments can be found.

(3) The presence of the orbital angular momentum makes the net magnetic moment of the paramagnetic ions extremely sensitive to their electronic environment. This is because the orbital motion is affected directly, unlike the spins which may only feel the environment through spin-orbit coupling. Thus EPR is able to distinguish the local symmetry of an ion's environment precisely and single crystal work allows the identification of complexes with different orientations. The nature and strength of the binding between a paramagnetic ion and its ligands are also extractable from EPR data as well as simple properties like the ion's oxidation state.

(4) The widths of resonance lines in a well resolved spectrum depend on a number of factors including the rate at which the microwave energy absorbed by the electron spins is transferred into thermal (lattice vibrations) energy, i.e. on the spin-lattice relaxation time and the magnetic dipolar and exchange interactions between the paramagnetic ions. Thus information about these factors can be obtained from the observed linewidths in EPR spectra.

Abragam and Pryce[10] formulated the interpretation of EPR spectra in terms of a spin-Hamiltonian where an effective spin is used, which correctly describes the low lying states. Inspite of the fact that spin-Hamiltonian provides a convenient device for the interpretation of EPR spectra, it disguises the fact that orbital contributions are involved by incorporating them into experimentally determined parameters. This has often proved very confusing to those not well acquainted with the field. Lot of work has been done along these lines and the comprehensive treatise of Abragam and Bleaney[11] gives an excellent review of the subject.

All the above mentioned information can be obtained only from a well resolved EPR spectrum. The observation of EPR in concentrated materials is hindered by broadening of resonance lines due to magnetic interactions between paramagnetic ions and thus makes them unpopular for EPR studies.

The main interaction in concentrated magnetic materials is the dipolar interaction, usually written as:

$$\mathcal{H}_{dip} = \frac{\vec{\mu}_i \cdot \vec{\mu}_j}{r^3} - 3\,\frac{(\vec{\mu}_i \cdot \vec{r})(\vec{\mu}_j \cdot \vec{r})}{r^5} = \vec{\mu}_i \cdot \vec{H}_{dip} \qquad (I.1)$$

where $\vec{r}$ is the vector joining the magnetic moments $\vec{\mu}_i$ and $\vec{\mu}_j$. Eq. (I.1) points out clearly that the dipolar interaction can be viewed as the energy of the dipole $\vec{\mu}_i$ in the field

created by the other magnetic moment $\vec{\mu}_j$. As the distances, usually found in the crystals, are of the order of few Angstroms (Å), the dipolar field from the nearest neighbours comes to be of the order of few hundred gauss. But in the case of concentrated materials, the dipolar interaction must be summed over the entire lattice due to the poor convergence of the sum. This poor convergence is due to the reason that volume of crystalline solid increases at the same rate at which the dipolar interaction falls off. The net result of this summation of dipolar fields will yield a distribution of the magnetic field strengths throughout the crystal. The different dipoles will then experience different magnetic fields and consequently will give different resonance conditions. Owing to this spread in Larmor frequencies (i.e. resonance condition) a broadening will occur. This is termed as inhomogeneous broadening and may give linewidths as large as $\sim$ 1000 G.

Another important interaction is the exchange interaction, which arises from the use of antisymmetrized wave-functions as opposed to single product of one electron wave functions. When the wave functions of unpaired spins, which are not pure but are formed by taking into account the covalent bonding of the ion with ligands, are allowed to overlap, the combined effects of the coulomb repulsion

between the electrons and the antisymmetry of the wave functions required by the Pauli exclusion principle result in a coupling of spins, known as exchange interaction. This was proposed by Dirac[12] and Heisenberg[13] in 1926. The simplest form of this is a scalar isotropic type, termed as Heisenberg exchange, and is written as:

$$\mathcal{H}_{ex} = -2J \vec{S}_1 . \vec{S}_2 \qquad (I.2)$$

As a result of this spin coupling the problem no longer remains localized to a single ion plus ligands, but becomes a many body problem involving cooperative interactions of the lattice as a whole. This coupling may either be such that the net magnetic moment is zero (termed as antiferromagnetic), or be such that all the spins are aligned in the same direction (termed as ferromagnetic).

As a consequence of these interactions in paramagnetic materials, the observation of EPR is not possible because of either the lack of resolution of spectra, or the change of character of the problem to that of elemental excitations in solid as a whole. Because of these problems, EPR in concentrated materials has not proved to be that fruitful as expected. The effects of these interactions can be overcome by isolating the paramagnetic ions from each other. This is usually done by doping small amount of these ions

into appropriate diamagnetic hosts. Sometimes this isolation occurs naturally as in some biological systems. Most of the EPR work to date has been done in magnetically dilute systems and the comprehensive treatise by Abragam and Bleaney[11] provides an excellent review of the subject.

Nonetheless the EPR of paramagnetic ions incorporated into paramagnetic host lattices, if resolved, should contain the same information as available in a diamagnetic host lattice and in addition should also contain information relayed to it via the magnetic interactions about the interactions themselves and about the paramagnetic host ion properties. A literature survey of such studies has been carried out and has been given in Appendix A. It has been found that a number of iron-group and lanthanide ions have exhibited sharp EPR spectra when doped in various paramagnetic iron-group or lanthanide ion host lattices and unusual features have often been observed in their EPR spectra. Our aim in this thesis will be to elucidate exactly when the sharp line EPR spectra of paramagnetic impurity in paramagnetic hosts are attainable and how to extract the additional information from the observed EPR spectra. The work presented in this thesis will be on iron group paramagnetic hosts doped with Mn^{2+}, a S-state ion. The hosts chosen are the single crystals of nickel, cobalt and ferrous salts.

REFERENCES

1. E. Zavoisky, J.Phys.(USSR) 9, 211 (1945) and 10, 197 (1946).

2. B.Bleaney and K.W.H.Stevens, Rept. Progr. Phys. 16, 108 (1953); K.D.Bowers and J.Owen,ibid.18,304 (1955); J.W.Orton,ibid.22, 204 (1959).

3. G.Lancaster, 'Electron Spin Resonance in Semiconductors', Hilger and Watts, London (1966).

4. D.J.E. Ingram, 'Free Radicals as Studied by Electron Spin Resonance', Butterworths, London (1958).

5. D.M.S. Bagguley and J.Owen, Rept. Progr. Phys. 20, 304 (1957).

6. A. Müller, Prog. Biophys. Mol. Biol.17, 491 (1967).

7. W.Gordy, W.B. Ard and H.Shields, Proc. Natl.Acad.Sci. 41, 983 (1955).

8. K.U.Ingold, 'Magnetic Resonance in Chemistry and Biology', Chap.9, Marcel Dekker, Inc. New York (1975).

9. A.J. Vithayathil, J.L. Ternberg and B.Commoner, Nature 207, 1246 (1965).

10. A.Abragam and M.H.L. Pryce, Proc. Roy.Soc. (London) A 205, 135 (1951).

11. A.Abragam and B.Bleaney, 'Electron Paramagnetic Resonance of Transition Ions', Clarendon Press, Oxford (1970).

12. P.A.M.Dirac, Proc. Roy.Soc. (London) A 112, 661 (1926).

13. W.Heisenberg, Z.Phys. 38, 411 (1926).

GENERAL REFERENCES

1. W.Low, 'Paramagnetic Resonance in Solids', Solid State Phys. Supplement 2, Academic Press, New York (1960).

2. H.M. Swartz, J.R. Bolton and D.C. Borg, 'Biological Applications of Electron Spin Resonance', Wiley-Interscience, New York (1972).

3. D.J.E. Ingram, 'Biological and Biochemical Applications of Electron Spin Resonance', Adam Hilger Ltd., London (1969).

4. S.A. Al'tshuler and B.M. Kozyrev, 'Electron Paramagnetic Resonance', Academic Press, New York (1964).

5. G.E. Pake, 'Paramagnetic Resonance', Benjamin, New York (1962).

6. D.H.Martin, 'Magnetism in Solids', Iliffe, London (1967).

CHAPTER II

THEORY

ABSTRACT

This chapter has been divided into three sections. Section A gives a brief theory of EPR, the crystal-field effects and the spin-Hamiltonian formalism, with reference to iron group ions in general, and Mn^{2+} ion in particular. Also described, in brief, are the various physical processes (mechanisms) responsible for the zero-field splitting of Mn^{2+}, a S-state ion. A general spin-Hamiltonian analysis of Mn^{2+} EPR spectra in orthorhombic crystalline field has been presented in Section B. Section C deals with the general problem of EPR of paramagnetic impurity ions in paramagnetic hosts. It is shown that well resolved spectra of an impurity ion with long spin-lattice relaxation time can be observed if either the host ions have very short spin lattice relaxation time, or have their magnetic moments reduced significantly by spin quenching. Also discussed is what additional information, in principle, can be obtained from the observed spectra of paramagnetic impurity ions in paramagnetic hosts.

SECTION A

THEORY OF EPR OF IRON GROUP IONS

INTRODUCTION

Paramagnetism, a consequence of the existence of magnetic moments, is a property common to all atoms or ions with an odd number of electrons. However, the presence of incomplete 3d, 4f and 5f electronic shells in the ground state of the atoms and ions of iron, lanthanide and actinide group elements, respectively, is responsible for their paramagnetism. The application of paramagnetic resonance technique and the development of the associated crystal field theory have led to a good understanding of the magnetic properties of the ions of various transition groups in crystals.

When a free ion, with a resultant angular momentum $\vec{J}$, is placed in a magnetic field, H, the energies of the various states are given as:

$$E_{M_J} = g\beta H M_J \qquad \text{(II.1)}$$

where, $M_J = J, J-1, \ldots, -J+1, -J.$

If an alternating field of frequency ν is applied at right angles to H, the magnetic dipole transitions are induced between these energy states according to the selection rule $\Delta M_J = \pm 1$, giving rise to the resonance condition:

$$h\nu = g\beta H \qquad \text{(II.2)}$$

where g is the spectroscopic splitting factor and effectively measures the rate at which the energy states diverge with the applied magnetic field, h is the Planck's constant and β is the Bohr magneton. Further the intensities of these transitions are given by the square of the magnetic dipole transition probability $P_{M_J, M_J \pm 1}$, where

$$P_{M_J, M_J \pm 1} = \text{const.} \times [J(J+1) - M_J(M_J \pm 1)]^{\frac{1}{2}} \qquad \text{(II.3)}$$

Hence the different $M_J \leftrightarrow M_J \pm 1$ transitions will have different intensities.

CRYSTAL-FIELD EFFECTS:

While studying paramagnetic ions in diamagnetic crystal lattices, there are two types of interactions; (a) interactions between the paramagnetic ions, and (b) interactions between the paramagnetic ion and the diamagnetic neighbours (or ligands). Former interaction can be reduced effectively to a negligibly small value by doping small amounts of paramagnetic ions in the diamagnetic host. Thus each paramagnetic ion is

taken to be independent and isolated from other paramagnetic ions. The latter interactions of paramagnetic ion with diamagnetic ligands modify the magnetic properties of the paramagnetic ions. This can be understood from the crystal-field theory which assumes that the paramagnetic ion experiences a crystalline electric potential whose sources are point charges (ions) or point dipoles (e.g. H_2O molecules) lying wholly outside the paramagnetic ion. In other words the ligands influence the magnetic ion through the electric field which they produce at its site. This electric field modifies the usual orbital motion of unpaired electrons and gives rise to a new energy term which must be added to the Hamiltonian of the free ion to give new energy states.

The crystal field interaction is affected by the electrostatic screening of unpaired electrons when outer electron shells are occupied. Therefore it becomes necessary to distinguish the strength of crystal-field involved, as follows:

(1) Weak Crystal Field:

Here the crystal field interaction is weaker than the spin-orbit coupling and this is the case with the rare-earth and certain actinide compounds. It is due to the fact that the electron's paramagnetic shell, 4f or 5f, lies fairly

deep within the ion and is well shielded from the crystal field by closed shells of 5s and 5p electrons or 6s and 6p electrons, respectively. To a first order approximation the free ion calculations are valid here.

(2) Intermediate Crystal Field:

In this case the crystal field interaction is stronger than spin-orbit coupling and is considered first. This situation can be described by regarding the orbital motion as clamped by crystal field and making it unable to respond to an applied magnetic field. This is known as 'quenching of orbital angular momentum'. Here magnetic properties are all due to spin which is coupled only weakly to crystal field through spin-orbit coupling. Here g-factor (spectroscopic splitting factor) is close to the free spin value, 2.0023, and is quite different from free ion Lande's g-factor. This situation typifies the hydrated ions of iron group.

(3) Strong Crystal Field:

For the ions of 4d and 5d transition groups there is a tendency of covalent bonding due to which the orbitals of paramagnetic ion and neighbouring ligands overlap appreciably. Here crystal field assumption no longer holds because the sources for the crystal field are not wholly external to the paramagnetic ion. In addition to 4d and 5d groups, this situation is also found in cynides of 3d group such as Fe^{3+} in $K_3Fe(CN)_6$.[1]

SPIN-HAMILTONIAN:

The EPR study involves measuring of the microwave transitions within a group of energy states which lies typically some hundreds or thousands of cm^{-1} below all other states. It is usual, though somewhat inappropriate when orbital momentum is incompletely quenched, to refer the members of this group as 'spin' states derived from a particular 'orbital' state. This type of formalism is known as the spin-Hamiltonian formalism. The effective spin 'S' of the ground state can be known by equating the number of these low lying states to (2S + 1). In other words, the spin-Hamiltonian approximation is to replace the Hamiltonian of the ion (with all its states) by another Hamiltonian which accurately describes only the low lying states.

Usually in practice one guesses a form for the spin-Hamiltonian incorporating any known symmetry properties and see whether the coefficients can be chosen to reproduce results in agreement with experimental observations. If the fit is a poor one, one guesses another form.

HYPERFINE STRUCTURE:

The hyperfine structure in EPR spectrum results due to the interaction of nuclear magnetic moment of paramagnetic ion with its electronic moment. The origin of this can be

understood simply by assuming that the nuclear moment produces a magnetic field H_N at the magnetic electrons and the modified resonance condition is:

$$h\nu = g\beta |\vec{H} + \vec{H}_N| \qquad (II.4)$$

The nuclear moment, being space quantized in the direction of internal magnetic field (due largely to electrons), can take up $(2I + 1)$ positions corresponding to $(2I + 1)$ values of m_I, the nuclear magnetic quantum number (I being the nuclear spin quantum number). As the interaction energy is more fundamental than H_N, the nucleus and surrounding electrons are considered as a composite magnetic system having $(2I + 1)(2J + 1)$ possible states for a free ion i.e. each M_J state being split into a closely spaced group of $(2I + 1)$ states. Here the transitions are allowed with the selection rules $\Delta M_J = \pm 1$ and $\Delta m_I = 0$. Since in this thesis we will be concerned only with Mn^{2+}, for which $J = S$ and hence $M_J = M_S$. Hereafter we will use M for M_S and m for m_I.

FORM OF SPIN-HAMILTONIAN:

In general the total Hamiltonian, including all the interactions can be written as:

$$\mathcal{H}_{Total} = \mathcal{H}_F + \mathcal{H}_C + \mathcal{H}_{LS} + \mathcal{H}_Z + \mathcal{H}_{SS} + \mathcal{H}_N \qquad (II.5)$$

where, $\mathcal{H}_F$ is free ion Hamiltonian ($\sim 10^5$ cm^{-1})

$\mathcal{H}_C$ is contribution due to crystal field ($\sim 10^4$ cm^{-1})

$\mathcal{H}_{LS}$ is magnetic interaction between electronic spin and orbital angular momentum ($\sim 10^2$ cm^{-1} for iron group ions)

$\mathcal{H}_Z$ is interaction with Zeeman field (~ 1 cm^{-1})

$\mathcal{H}_{SS}$ is spin-spin interaction term (~ 1 cm^{-1})

$\mathcal{H}_N$ is hyperfine interaction term ($\sim 10^{-2}$ cm^{-1})

In the case of iron group ions ($\mathcal{H}_F + \mathcal{H}_C$) is solved first and other terms are considered as perturbations over it. The order of perturbation to be carried out is limited by its contribution to the energy level evaluation. For the case where the ground state is orbitally non-degenerate, the second order contribution from $\mathcal{H}_{LS}$ is comparable to the first order contribution of $\mathcal{H}_Z$, and hence the perturbation is carried out to the second order. Higher order terms are much small. Thus the new Hamiltonian, called the spin-Hamiltonian, where only terms upto the second order have been included, is,

$$\mathcal{H}_S = \beta \vec{H}.\tilde{g}.\vec{S} + \vec{S}.\tilde{D}.\vec{S} + \vec{S}.\tilde{A}.\vec{I} - \beta_N \vec{H}.\tilde{g}_N.\vec{I} + \vec{I}.\tilde{Q}.\vec{I} \qquad (II.6)$$

Here $\tilde{g}$, $\tilde{D}$, $\tilde{A}$, $\tilde{g}_N$ and $\tilde{Q}$ are all second rank tensors. The first term represents Zeeman interaction with the applied field $\vec{H}$; the presence of orbital momentum is taken into account by allowing the splitting factor 'g' to differ from the spin-only value (2.0023) and, if need be, to be similar in form to a tensor. The second term in $\tilde{D}$ represents the quadrupolar coupling to the crystal field. The third and fifth terms in $\tilde{A}$ and $\tilde{Q}$ express the hyperfine interaction between $\vec{S}$ and spin $\vec{I}$ of nucleus and the quadrupolar coupling between $\vec{I}$ and the electric field gradient in the ion, respectively. The fourth term represents nuclear Zeeman interaction with applied field $\vec{H}$. These tensors are diagonalized in a system of orthogonal axes, known as principal axes. These differ for the ions with different crystalline environments and even for ions with the same environment but different relative orientations of ligands. In principal axes system $\mathcal{H}_S$ can be written as:

$$\begin{aligned}\mathcal{H}_S = {} & \beta (g_x H_x S_x + g_y H_y S_y + g_z H_z S_z) + D[S_z^2 - S(S+1)/3] \\ & + E(S_x^2 - S_y^2) + A_x S_x I_x + A_y S_y I_y + A_z S_z I_z \\ & + Q' [I_z^2 - I(I+1)/3] + Q'' (I_x^2 - I_y^2) \qquad \text{(II.7)}\end{aligned}$$

Here g_{xx}... etc. are written as g_x... etc, $D = \frac{3}{2} D_z$, $E = \frac{1}{2} (D_x - D_y)$, $Q' = \frac{3}{2} Q_z$ and $Q'' = \frac{1}{2} (Q_x - Q_y)$. The fourth term in Eq. (II.6) being very small is neglected.

The spin-Hamiltonian for Mn^{2+} with $^6S_{5/2}$ ground state must contain terms in S_i^4 $(i = x,y,z)$ since the lowest term in the cubic potential is x^4. Hence the spin-Hamiltonian of Mn^{2+} in a cubic field is of the form:

$$\mathcal{H}_S = g\beta\vec{H}.\vec{S} + \frac{1}{6}a\left[S_x^4 + S_y^4 + S_z^4 - \frac{1}{5}S(S+1)(3S^2+3S-1)\right] + A(\vec{S}.\vec{I}) \qquad \text{(II.8)}$$

For the case of crystal field of orthorhombic symmetry the spin-Hamiltonian for Mn^{2+} can be written as.

$$\begin{aligned}\mathcal{H}_S = {} & \beta\vec{H}.\tilde{g}.\vec{S} + D\left[S_z^2 - \tfrac{1}{3}S(S+1)\right] + E\left(S_x^2 - S_y^2\right) \\ & + \frac{1}{6}a\left[S_x^4 + S_y^4 + S_z^4 - \frac{1}{5}S(S+1)(3S^2+3S-1)\right] \\ & + \vec{S}.\tilde{A}.\vec{I} + Q'\left[I_z^2 - \tfrac{1}{3}I(I+1)\right] + Q''\left(I_x^2 - I_y^2\right)\end{aligned} \qquad \text{(II.9)}$$

Here the cubic field term, a, is assumed to have the same axis system as the other two fine structure terms, D and E. The advantage of using a spin-Hamiltonian is that the rather complicated behaviour of the lowest energy states of paramagnetic ion in a magnetic field can be described in a relatively simple way by specifying the effective spin together with a small number of parameters which measure the magnitude of the various terms in the Hamiltonian. Hereafter the word spin means effective spin and axes, the principal axes. We will now consider the spin-Hamiltonian parameters individually.

(1) The Spectroscopic Splitting Factor 'g':

This spectroscopic splitting factor is analogous to the Lande's g-factor, g_L for a free ion, but in general has different values for an ion in a crystal; the reason being the part of magnetic moment arising from the orbital motion of electrons is modified by the crystal field. Thus for the paramagnetic ions in solids, this g-factor, called spectroscopic splitting factor, is purely an experimentally determined parameter. From Eq. (II.6) it is a second rank tensor, its symmetry being the symmetry of the crystal field. The contributions to g-factor may be made by other terms in the Hamiltonian or by effects not completely described by crystal field theory. An example is the configuration interaction occurring in covalent crystals.[2] Watanabe[2] not only explained large positive g shifts for Mn^{2+} ion in some covalent systems, but also suggested the reason for the large cubic fine structure constant, a, which accompanies the large g shift. The explanation for Mn^{2+} ion involves admixture of a configuration with six d electrons on the ion and a hole on the ligands into the d^5 ground configuration.

(2) Fine Structure Parameters:

'D' and 'E' parameters are generally known as second order fine structure constants and are the measure of the

internal splitting in the group of energy states, described by spin-Hamiltonian in the absence of Zeeman field. 'D' represents the axial part and 'E' the rhombic part of the crystal field. For Mn^{2+}, fourth order cubic field parameter, 'a', also contributes to the zero field splitting and is important for interpretation of EPR spectra. We have restricted ourselves in this thesis upto these parameters, though there are other fourth order parameters for Mn^{2+}.

(3) Hyperfine Structure Parameters:

For a paramagnetic ion in solid, the Zeeman interaction corresponds to the interaction of an anisotropic electronic magnetic moment with an external field and is represented by the term $\beta \vec{H}.\tilde{g}.\vec{S}$ in the spin-Hamiltonian. Similarly the magnetic hyperfine structure is the result of the interaction between this anisotropic electronic magnetic moment and the magnetic field due to the nuclear magnetic moment and can be represented by the term $\vec{S}.\tilde{A}.\vec{I}$. It diagonalizes to the form, shown in Eq. (II.7), in the principal axes system. Mn^{2+}, with symmetric ^6S ground state, should not show any hyperfine structure according to the first principles. But experimentally the hyperfine structure is observed. This is accounted for by the so called 'anomalous hyperfine splitting', which arises because of the existence of a finite electron spin-density at the nucleus. This can be regarded

as a consequence of either configuration interaction with configurations having unpaired electrons such as $3s\ 3d^5\ 4s$,[3] and/or as due to a difference in the spatial wave functions of electrons which differ only in their spin-orientation.[4] The latter phenomenon is known as core polarization and results naturally from an unrestricted Hartree-Fock calculation. Core polarization is the magnetic polarization of an atomic or ionic core of closed shells by an unfilled external shell with a total spin S. In the case of Mn^{2+}, core polarization provides a satisfactory physical model and the calculated values are in reasonable agreement with the experimental values.[5] Hyperfine coupling constants are sensitive to the nature of bonding and their variation can be utilized to find the same.

Although the hyperfine interaction $\vec{S}.\tilde{A}.\vec{I}$ produces most of the effects associated with hyperfine structure, one more term due to the interaction of the nuclear magnetic moment with the magnetic field is always present. It can be written as fourth term in Eq. (II.6):

$$\mathcal{H} = -\beta_N \vec{H}.\tilde{g}_N.\vec{I} \qquad \text{(II.10)}$$

Another term which often contributes to the hyperfine structure is the quadrupole interaction,

$$\mathcal{H} = \vec{I}.\tilde{Q}.\vec{I} \qquad \text{(II.11)}$$

the last term in Eq. (II.6). In the principal axes system it can be written in terms of Q' and Q'' (see Eq.(II.7)). The forbidden hyperfine doublet separations can be used to compute these parameters.

FINE STRUCTURE OF Mn^{2+} - ZERO FIELD SPLITTINGS OF Mn^{2+}:

Mn^{2+} ion has a half filled 3d shell and comes under the case of intermediate crystal field. The ground state has all the five spins coupled parallel and from Hund's rule is given by $^6S_{5/2}$. As there is no orbital momentum in this state, to first order, it will have no interaction with a crystal field. However, in practice, the 6-fold degeneracy is partially lifted into one doublet and one quartet (separation $\sim 0.1\ cm^{-1}$) even by a cubic crystal field. The fields of lower symmetry further split the quartet into two doublets and change the magnitude of the splitting. To have a theoretical explanation of this interaction, higher order processes are to be considered. In the absence of any satisfactory theoretical explanation for the zero field splittings (abbreviated as ZFS) of S-state ions, the study of ZFS of Mn^{2+} has become a challenging problem. Van Vleck and Penny[6] for the first time discussed qualitatively the origin of the axial field splittings of S-state ions considering the admixture of excited orbitally asymmetric states into the ground state via spin-orbit

coupling. These excited admixtures, being perturbed by the axial field, gave a second order energy term, $D[3S_z^2 - S(S+1)]$. However, the estimates of the splittings from such calculations were very high and were inadequate to explain quantitatively the observed splittings. Pryce[7] showed that the use of spin-spin interaction alongwith the admixture of states gave a finite and relatively lower order contribution to the splitting. Bersohn and Das[8] proposed a method of ZFS calculation via perturbation of the one electron orbitals either by the variation method or by solving first order perturbation equations numerically. Watanabe[9] carried out the first quantitative calculations of both spin-orbit and spin-spin contributions. In addition to the Pryce term, Watanabe also considered admixture of excited $|^4P>$ into $|^6S>$ state by spin-orbit coupling and found the van Vleck-Penny term to be always negative ($D < 0$) whereas Pryce term having either sign depending upon the sign of the crystalline electric field gradient. Watanabe's values were considerably smaller than the experimental values. Kondo[10] suggested that the discrepancy might be removed by considering anisotropic covalent admixtures. He considered both spin-spin and spin-orbit contributions to 'D' and 'E' and computed contributions to ZFS of Mn^{2+} ion in MnF_2 and strained MgO. Even using small value for electron transfer, he obtained reasonable agreement between calculated and observed ZFS. This indicates that the overlap contribution

to ZFS was dominant. Blume and Orbach[11] considered ZFS in S-state ion in a deformed cubic host and obtained first order non-zero matrix elements of axial and rhombic fields by spin-orbit admixture of excited $|^4P>$ state into ground $|^6S>$ state. The values obtained for the spin-Hamiltonian coefficients were equal in magnitude but opposite in sign to the experimental values of Watkins et al.[12], Shiren[13] and Feher.[14] Sharma et al.[15] performed these calculations again by taking correct choice of phase for the $|^4G>$ state. Orbach et al.[16] also made attempts to fit the axial field splitting of S-state ions by using a method due to Sternheimer[17] and obtained s-, d- and g- like admixtures to unperturbed functions by adding axial field potential to Hartree-Fock potential, derived from Watson's 3d functions[18] and integrating one electron Schrodinger equation numerically. These were used to calculate the matrix elements of axial field perturbation. These results dominate the Watanabe's computed results but fall somewhat short of the experimental values. Sharma et al.[19] gave a comprehensive treatment of the ZFS of Mn^{2+} ion in point multipole approximation. Various contributions to 'D' and 'E' were considered and quantitative results computed for the most important mechanisms for the specific cases for MnF_2 and $ZnF_2:Mn^{2+}$. The values of 'D' and 'E', obtained by summing over various contributions, were

compared to the experimental values.[20,21] In a subsequent paper Sharma et al.[22] included both overlap and charge transfer covalency effects and the calculations were done for the case of ZnF_2: Mn^{2+}. The sums of the overlap contribution and of point multipole model contribution to 'D' and 'E' were compared with the experimental results of Tinkham[20] and the agreement both in order of magnitude and sign was found to be good. Next Lowther,[23] using the effective spin-orbit Hamiltonians,[24] evaluated the magnitude of its contribution to 'D' and 'E' for ZnF_2:Mn^{2+} from a point-charge multipole model. This contribution was non-negligible and was comparable in magnitude to most of Sharma et al.'s mechanisms. Folen[25] recently used the results of EPR measurements of transferred hyperfine interactions in K_2ZnF_4: Mn^{2+} in conjunction with LCAO theory (involving intra spin-spin and spin-orbit interactions) to determine the electronic overlap contribution to 'D' parameter of Mn^{2+}. This yields the value of 'D' = 35.9×10^{-4} cm^{-1}, while the experimental value is 36.0×10^{-4} cm^{-1}. A calculation similar to that of Folen has been carried out by Narayana[26] for the system K_2MgF_4:Mn^{2+}. Watanabe[27] concluded that the cubic field splitting parameter 'a' should be proportional to inverse tenth power of R (interionic distance) and should be positive regardless

of the sign of Dq (parameter for strength of cubic field). He also proposed an EPR experiment on S-state ions under high hydrostatic pressure, which reduces R and induces increase in 'a', to test the theory.[27] Sharma[28] studied the effect of the strength of the cubic field on ZFS of Mn^{2+} in axial field and found that the usual belief- that ZFS diminishes as the strength of cubic field decreases is not always true. In some cases the ZFS decreases as the strength increases. Moreover ZFS was found to be sensitive to the strength of the cubic field and might even change sign on varying the strength. Sharma[28] also plotted 'D' against 10Dq for $MgCl_2:Mn^{2+}$, $CdCl_2:Mn^{2+}$, MnF_2, $ZnF_2:Mn^{2+}$ and $CdBr_2:Mn^{2+}$. In addition, 'L' from various mechanisms was plotted against 10Dq in $MgCl_2:Mn^{2+}$.

Lots of calculations have also been carried out taking into account the relativistic effects in explaining the ZFS of S-state ions. Van Huevelen[29], applying Wybourne's electrostatic model[30] of relativistic crystal field, calculated the ZFS of Mn^{2+} in cubic and tetragonal crystal-fields and found the calculated values about half of the experimentally observed values. Similar calculations were made by Hagston and Lowther,[31] by Serway,[32] by Schlottmann et al.[33] and by Chatterjee et al.[34] All these authors found the relativistic contribution dominating even the Blume-Orbach contribution in

the systems studied. Thus the relativistic contribution can not be neglected in the calculations of ZFS of Mn^{2+}.

A recent article by Newman and Urban[35] reviews the various mechanisms responsible for ZFS of S-state ions (Gd^{3+} mainly). In this article they also mention to have carried out a superposition model analysis for Mn^{2+} and Fe^{3+} in MgO which shows that a model, which is linear in the single ligand contributions, is quite consistent with all the n = 2 strain parameters given by Feher[14], and thus throws doubt on the relative importance of the Blume-Orbach process. Recently Chatterjee et al.[36] have calculated the contributions to 'D' for Mn^{2+} (site I) in $La_2Mg_3(NO_3)_{12}.24H_2O$ using already known and some new perturbation mechanisms upto and including fourth order using the relativistic wave functions and have shown that the largest contribution to the observed value of 'D' comes from the second order perturbation mechanism, in agreement with the prediction of van Heuvelen.[29]

It is thus clear that none of the many attempts made to calculate the ZFS of Mn^{2+} can be regarded as entirely satisfactory. The main problem is the present lack of sufficient ancillary data to check crucial aspects of these calculations, e.g. in the case of Mn^{2+} there is apparently no

phenomenological data on the axial components of the crystal field. Newman et al.[35] in their review emphasize the need for making planned experiments such as using variable frequency EPR technique explicitly aimed at testing the theoretical models. After a complete understanding of this problem, it should be possible to extend the role of S-state ions as 'test bodies', for their spectra will provide information on the electronic structure as well as on the atomic structure of their crystalline environment.

ALLOWED AND FORBIDDEN TRANSITIONS:

When the oscillating microwave field is perpendicular to the static Zeeman field, the allowed electronic transitions are magnetic dipole transitions with the selection rule $\Delta M = \pm 1$. Further the microwave field exerts a negligible effect on the nuclear moments, the selection rule involving nuclear transitions is $\Delta m = 0$ giving rise to hyperfine structure. Thus the transitions with the selection rules $\Delta M = \pm 1$ and $\Delta m = 0$ are termed as allowed transitions. Fig. II-1 shows the various interactions and the allowed transitions in the EPR of Mn^{2+}. In addition, transitions other than the allowed ones are sometimes observed. Transitions with $\Delta M \neq \pm 1$ are termed as electronic (fine) forbidden transitions and occur due to the mixing of states with different M due to the non-diagonal terms.[37] The $\Delta M = \pm 2$

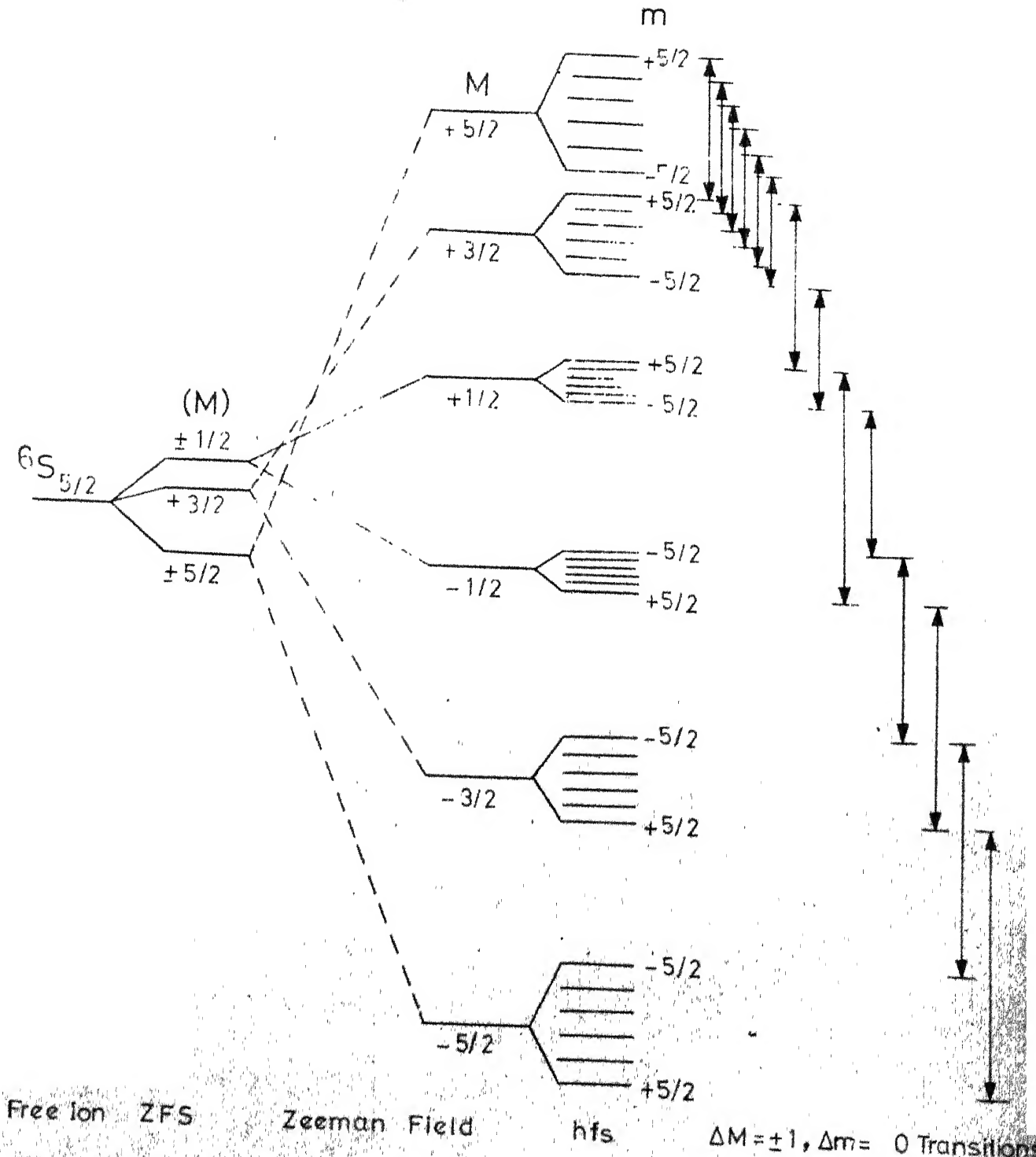

Fig. II-1: Energy level splittings of the ground state of Mn^{2+}, for the case of negative D, and the $\Delta M = \pm 1$, $\Delta m = 0$ transitions. ZFS is the splitting due to the crystalline field, and hfs due to the hyperfine interaction

transitions occur at Zeeman fields about half the magnitude for $\Delta M = \pm 1$ transitions.

The transitions with $\Delta m \neq 0$ are called forbidden hyperfine transitions which occur because of the mixing of various hyperfine states. The second order cross-terms between the hyperfine and the fine structure operators in the spin Hamiltonian can lead to this mixing.[38] For an orthorhombic crystalline field the cross-terms will be of the type $(DS_zS_\pm)(AS_\mp I_\pm)$ and $(ES_zS_\pm)(AS_\mp I_\pm)$. These second order cross-terms lead to the admixture of the hyperfine states. The nuclear part of a wave function $|m>$ is then a linear combination of the components $|m>$, $|m \pm 1>$, $|m \pm 2>$ ... etc so that the apparent forbidden transitions become weakly allowed with the selection rules $\Delta M = \pm 1$, $\Delta m = \pm 1$; $\Delta M = \pm 1$, $\Delta m = \pm 2$; ... etc. The expressions for the doublet separations arising out of $\Delta m = \pm 1$ and $\Delta m = \pm 2$ forbidden hyperfine transitions are derived in Appendix B from perturbation theory.

SECTION B

SPIN-HAMILTONIAN ANALYSIS OF Mn^{2+} SPECTRA

In the preceding section we have discussed how to describe the group of lowest lying energy states in terms of a small number of parameters of spin-Hamiltonian, which can give these energy states as its eigen values in terms of these parameters. This section describes how the values of these parameters may be determined from the observed EPR spectra.

The first step will be to decide the symmetry of the spectrum and the effective spin 'S', which in turn will determine the type of spin-Hamiltonian to be used. Considering the selection rules $\Delta M = \pm 1$, $\Delta m = 0$ for allowed transitions, the spectra of Mn^{2+} in crystals should normally contain five sextets (i.e. 30 lines) for each Mn^{2+} complex in the unit cell, assuming that the microwave quantum used is greater than the ZFS. The point symmetry of the site, to which Mn^{2+} is substituted, determines which of the parameters are non-zero. The value of the non-zero parameters is determined by the local environment around the paramagnetic ion. Here the knowledge of the crystal structure and the impurity ion involved, combined with the experience of the kind of spectru

usually observed under similar circumstances, will certainly be an invaluable aid to the analysis.

After determining these general features of the EPR spectra, one proceeds to find the magnetic axes (principal axes) X, Y and Z of each of the magnetic complexes. These axes are a set of mutually perpendicular directions which may be different for each magnetic complex in the unit cell of a crystal. These directions are found from the angular variation study of the spectrum by obtaining extrema in the fine structure spreads of the EPR spectra. The Z-axis is defined as the direction along which the spectrum shows maximum fine structure spread. Similarly the X-axis is perpendicular to the Z-axis and has a smaller spread than the Z-axis. Finally the Y-axis is perpendicular to both Z and X-axes and has the smallest spread. If the unit cell of the crystal contains more than one magnetic complexes with different orientations, the orientation of (X, Y, Z) axes must be determined for each complex. Besides, one usually comes across the paramagnetic susceptibility principal axes K_1, K_2 and K_3. These coincide with (X, Y, Z) axes, if there is only one magnetic complex per unit cell, or if all the complexes in the unit cell are equivalent. The axes (K_1,K_2,K_3) are an average of the (X,Y,Z) axes of the different magnetic complexes. Also it is not necessary that (K_1,K_2,K_3) axes

coincide with the crystallographic (a,b,c) axes.

As the symmetry of the Mn^{2+} complexes (discussed in this thesis) is not higher than orthorhombic, an appropriate spin-Hamiltonian used in the analysis is:

$$\mathcal{H} = \beta \vec{H}.\tilde{g}.\vec{H} + D\left[S_z^2 - (1/3)\,S\,(S+1)\right] + E\,(S_x^2 - S_y^2) + (1/6)a\left[S_x^4 + S_y^4 + S_z^4 - (1/5)\,S\,(S+1) \times (3S^2 + 3S - 1)\right] + \vec{S}.\tilde{A}.\vec{I} \qquad \text{(II.12)}$$

where the various terms have their usual significance and $S = I = 5/2$ for Mn^{2+}. In literature, sometimes other notations for spin-Hamiltonian parameters are used, which are related to our notations as follows:

$$D = b_2^0 = 3B_2^0 \qquad E = b_2^2/3 = B_2^2$$

$$a = 2b_4^0 = 120\,B_4^0 \quad \text{(cubic case)} \qquad F = 3b_4^0 = 180\,B_4^0 \quad \text{(axial case)}$$

Assuming $g\beta H \gg |D|$, $|E|$, $|a|$ and $|A|$ and carrying out perturbation calculations upto third order, the field expressions for the allowed fine structure transitions for the Zeeman field, H, parallel to the Z-axis are:[39]

$$H_1(M = 5/2 \leftrightarrow 3/2) = H_{oz} - 4D + \frac{9E^2}{(H_1+D)} - \frac{5E^2}{(H_1+3D)} + \frac{15LE^2}{(H_1+3D)^2} - \frac{9DE^2}{(H_1+D)^2} - 2a$$

$$H_2(M = 3/2 \leftrightarrow 1/2) = H_{oz} - 2D - \frac{9E^2}{(H_2+D)} + \frac{9E^2}{(H_2-D)} - \frac{5E^2}{(H_2+3D)} + \frac{9DE^2}{(H_2+L)^2} + \frac{9DE^2}{(H_2-D)^2} + \frac{15DE^2}{(H_2+3L)^2} + 5a/2$$

$$H_3(M = 1/2 \leftrightarrow -1/2) = H_{oz} - \frac{9E^2}{(H_3-D)} + \frac{5E^2}{(H_3+3D)} + \frac{5E^2}{(H_3-3D)} - \frac{9E^2}{(H_3+D)} - \frac{9DE^2}{(H_3-D)^2} - \frac{15DE^2}{(H_3+3D)^2} + \frac{15DE^2}{(H_3-3D)^2} + \frac{9DE^2}{(H_3+D)^2}$$

$$H_4(M = -1/2 \leftrightarrow -3/2) = H_{oz} + 2D + \frac{9E^2}{(H_4+L)} - \frac{9E^2}{(H_4-D)} - \frac{5E^2}{(H_4-3D)} - \frac{15DE^2}{(H_4-3D)^2} - \frac{9DE^2}{(H_4+D)^2} - \frac{9LE^2}{(H_4-D)^2} - 5a/2$$

$$H_5(M = -3/2 \leftrightarrow -5/2) = H_{oz} + 4L + \frac{9E^2}{(H_5-D)} - \frac{5E^2}{(H_5-3D)} + \frac{9DE^2}{(H_5-D)^2} - \frac{15DE^2}{(H_5-3D)^2} + 2a$$

(II.13)

In the above expressions the contribution of terms involving 'D' and 'E' is taken upto the third order of perturbation theory, while the terms in 'a', because of their very small contribution, have been considered only in the zeroth order.

The field expressions for hyperfine structure transitions for H parallel to the Z-axis are:

$$H(m \leftrightarrow m) = - Am - \frac{B^2}{H_{oz}} [I(I + 1) - m^2 + (2M-1)\, m] \qquad (II.14)$$

where 'A' is used for 'A_z' and 'B' is the average of 'A_x' and 'A_y' ($B = (A_x + A_y)/2$). The field expressions for H parallel to the X and Y axes can be obtained by using the following transformations:

H||Z	H||X	H||Y
D	$-(D-3E)/2$	$-(D+3E)/2$
E	$-(D+E)/2$	$(D-E)/2$
$b_4^{\,o}$	$(3b_4^{\,o}-b_4^{\,2}+b_4^{\,4})/8$	$(3b_4^{\,o}+b_4^{\,2}+b_4^{\,4})/8$
H_{oz}	H_{ox}	H_{oy}
A_z	A_y	A_y

Here $b_4^{\,o}$, $b_4^{\,2}$ and $b_4^{\,4}$ are fourth order parameters out of which we have considered only $b_4^{\,o}$ and neglected $b_4^{\,2}$ and $b_4^{\,4}$ because of their very small contribution.

The EPR spectra along the principal axes are first analysed using the above expressions for the fine structure transitions and then the expressions for hyperfine transitions are also included in the analysis. The position of a fine structure transition is taken as the centre of the first and the sixth line of the corresponding hyperfine group. The signs of the parameters determined in the present study are only relative and have been determined from the observed second order hyperfine shift, assuming hyperfine constant 'A' to be negative.[40,41] First, in the Eq. (II.13), we solve for the initial values of the parameters by considering only terms upto second order. Using these initial values of the parameters, an iterative procedure has been adopted to get the best-fit parameters. Adding Eqs. (II.13) and (II.14) we calculate the positions of the thirty lines of Mn^{2+} spectra and the root mean square deviation from the observed experimental values is calculated. A computer program has been used in which all the parameters are varied separately to minimize the root mean square deviation. In this procedure the higher order nonlinear terms are added one by one with the help of the computer program by an iterative procedure and finally the best-fit values of the parameters are taken.

In certain cases where the magnitude of the off-diagonal terms in the spin-Hamiltonian was rather large, the

perturbation approach used was not applicable. Therefore we used a method in which exact numerical diagonalization of the spin-Hamiltonian matrix has been performed with a simultaneous fitting of data corresponding to the magnetic field orientations along the Z and X axes. Here we only consider the fine structure part of the spin-Hamiltonian matrix i.e. 6 x 6 matrix for Mn^{2+} (the elements of this matrix are given in Table II-1). Another computer program has been made to get the best-fit parameters by exact diagonalization procedure. This program calculates all the five fine structure transition field positions for a given set of parameters and finds the root mean square deviation from the experimentally measured field positions. The fitting of the experimental data has been done by varying all the parameters. The initial values of the parameters have been taken to be those estimated from the perturbation expressions. Thus the set of best-fit parameters is obtained. All the calculations have been carried out using the IBM 7044 Computer.

Table II-1: Matrix elements of spin-Hamiltonian matrix for Mn^{2+} (S = 5/2)

	-5/2	-3/2	-1/2	+1/2	+3/2	+5/2
-5/2	(-5G/2+10D/3 +a/2)	0	E$\sqrt{10}$	0	a$\sqrt{5}$/2	0
-3/2	0	(-3G/2-2D/3 -3a/2)	0	3$\sqrt{2}$E	0	a$\sqrt{5}$/2
-1/2	E$\sqrt{10}$	0	(-G/2-8L/3+a)	0	3$\sqrt{2}$E	0
+1/2	0	3$\sqrt{2}$E	0	(G/2-8L/3+a)	0	E$\sqrt{10}$
+3/2	a$\sqrt{5}$/2	0	3$\sqrt{2}$E	0	(3G/2-2L/3 -3a/2)	0
+5/2	0	a$\sqrt{5}$/2	0	E$\sqrt{10}$	0	(5G/2+10D/3+a/2)

$g\beta H = G$

SECTION C

THEORY OF EPR OF Mn^{2+} IN PARAMAGNETIC SINGLE CRYSTALS

As mentioned in Chapter I, the main source of the width of paramagnetic resonance lines in magnetically concentrated materials is the dipolar interaction, which usually hampers the observation of EPR because of its significant broadening effect. Hence, to get sharp resonance lines, the effects of the dipolar interaction must either be eliminated, or at least reduced significantly. This reduction of the effective dipolar interaction can be accomplished either by motional effects, or by what is called spin quenching. The situation is same for the observation of EPR of a paramagnetic impurity in paramagnetic hosts. Only a handful of reports exist in the literature on the EPR of iron group and lanthanide metal ions doped in paramagnetic iron group or lanthanide ion lattices (upto date list is given in Appendix A). These generally show sharp EPR spectra and often unusual and anomalous linewidths. It will be the purpose of this section to review all these effects and come out with the criteria for determining when the sharp spectra of paramagnetic impurities will be observed in paramagnetic hosts. The two above mentioned

phenomena, employed for the reduction of the effective dipolar interaction, will be discussed separately and in detail. Before going to the particular cases of linewidths of impurity in paramagnetic hosts it will be useful to describe, in brief, the motional narrowing theory along the standard lines as its results will be needed in the latter discussion.

MOTIONAL NARROWING THEORY.[+]

Motional narrowing reduces the effective magnitude of the dipolar interaction by its rapid modulation. The cases where the modulating motion results from coordinate motion or electron exchange are well known.[42,43] The physical nature of the phenomenon can be understood from the fact that only interactions of magnetic nature, such as dipolar, spin-orbit and hyperfine, are capable of affecting the magnetic moment of the spin directly and hence are responsible for the time dependence of the magnetic moment which determines the linewidth. However, these interactions are controlled by non-magnetic interactions, which can not affect the magnetic moment directly, and this control produces the narrowing. The control is brought about because the magnetic interactions are dependent on the positions of the electrons and atoms which in turn are controlled by the non-magnetic interactions as these are much larger than

[+] The description of motional narrowing closely follows the theory given by Dr. St. John in his thesis.

the magnetic interactions. The magnetic interactions will then show a time dependence controlled by the electronic or atomic motion resulting in their time averaging. In cases of sufficiently rapid motion, the averaged effect becomes much smaller than otherwise.

Now the motional narrowing process will be described quantitatively and various important and useful results will be derived from this description. The system under consideration can be described in terms of the Hamiltonian $\mathcal{H}$, which can be divided in three parts as follows:

$$\mathcal{H} = \mathcal{H}_o + \mathcal{H}_m + \mathcal{H}_d \qquad \text{(II.15)}$$

Here $\mathcal{H}_o$ is the unperturbed spin-Hamiltonian giving rise to the positions of spectral lines and is the Zeeman interaction of a system of spins with an applied field, $\mathcal{H}_m$ is unspecified and is the modulating Hamiltonian and $\mathcal{H}_d$ is the time-dependent perturbation, taken to be the dipolar interaction. For narrowing to occur, the following assumptions are made:

$$\text{(1)} \qquad i\hbar\,\dot{\mathcal{H}}_d = [\mathcal{H}, \mathcal{H}_d] = [\mathcal{H}_o + \mathcal{H}_m, \mathcal{H}_d] \approx [\mathcal{H}_m, \mathcal{H}_d] \qquad \text{(II.16)}$$

This assumption emphasizes two facts: first, that $\mathcal{H}_m$ does not commute with $\mathcal{H}_d$ and thus it does cause a time variation of $\mathcal{H}_d$; and second, that we leave out, at least for the time being, the time variation due to $\mathcal{H}_o$; this is only justifiable

on the basis of later assumption (3) which throws away all the off-diagonal terms of $\mathcal{H}_d$ to $\mathcal{H}_o$ as non-secular perturbations.

(2) $$[\mathcal{H}_m, \mathcal{H}_o] = 0 \qquad \text{(II.17)}$$

$$[\mathcal{H}_m, M_x] = 0 \qquad \text{(II.18)}$$

where $\vec{M}$ is the magnetic moment of resonating spins. This assumption expresses the fact that $\mathcal{H}_m$ causes narrowing rather than broadening, since it can not directly change the unperturbed energies (by Eq. (II.17)) or interrupt the radiation in any way (by Eq. (II.18)).

(3) $\mathcal{H}_d$ is so small as to have no important matrix elements connecting different unperturbed states of $\mathcal{H}_o$, or $\mathcal{H}_d$ only causes a change in the resonance condition without causing any transitions.

To begin with, the line-shape for the determination of linewidth is taken to be that given by the Fourier transform of the relaxation function, G(t), defined as:[44]

$$G(t) = \mathrm{Tr}\,[M_x(t)\, M_x] \qquad \text{(II.19)}$$

where $$M_x(t) = \exp(i\mathcal{H}t/\hbar)\, M_x \exp(-i\mathcal{H}t/\hbar) \qquad \text{(II.20)}$$

and obeys the equation of motion

$$\frac{\hbar}{i}\frac{dM_x}{dt} = [\mathcal{H}, M_x(t)] = [\mathcal{H}_o + \mathcal{H}_d , M_x(t)] \qquad (II.21)$$

This equation is usually solved by using the so called 'interaction picture', using an operator $M_x^*(t)$, defined as:

$$M_x^*(t) = \exp(-i(\mathcal{H}_o + \mathcal{H}_m)\, t/\hbar)$$

$$\times M_x(t) \exp(i(\mathcal{H}_o + \mathcal{H}_m)\, t/\hbar) \qquad (II.22)$$

where the star indicates that operator is in interaction picture. From Eqs. (II.20) and (II.22) it is clear that if $\mathcal{H}_d$ is absent, $M_x^*(t)$ is just M_x and is time-independent. Therefore, if $\mathcal{H}_d$ is small, it is reasonable to expect the variation of $M_x^*(t)$ to be slow. Thus the equation of motion becomes:

$$\frac{\hbar}{i}\frac{dM_x^*}{dt} = [\mathcal{H}_d^*, M_x^*]$$

$$= [\exp(-i\mathcal{H}_o t/\hbar)\, \mathcal{H}_d(t) \exp(i\mathcal{H}_o t/\hbar), M_x^*] \qquad (II.23)$$

where $\mathcal{H}_d^* = \exp(-i(\mathcal{H}_o + \mathcal{H}_m)\, t/\hbar)\, \mathcal{H}_d \exp(i(\mathcal{H}_o + \mathcal{H}_m)t/\hbar)$

$$= \exp(-i\mathcal{H}_o t/\hbar)\, \mathcal{H}_d(t) \exp(i\mathcal{H}_o t/\hbar)$$

with $\mathcal{H}_d(t) = \exp(-i\mathcal{H}_m t/\hbar)\, \mathcal{H}_d \exp(i\mathcal{H}_m t/\hbar)$ (II.24)

Using eigenfunctions of $\mathcal{H}_0$ and the matrix notation, Eq. (II.23) becomes,

$$-i\hbar \frac{d(M_x^*)_{ij}}{dt} = \sum_k [(\mathcal{H}_d)_{ik} (M_x^*)_{kj} \exp(i(E_k - E_i)t/\hbar) - (M_x^*)_{ik} (\mathcal{H}_d)_{kj} \exp(-i(E_k - E_j)t/\hbar)] \quad \text{(II.25)}$$

Since the variation of M_x^* is slow, it is reasonable to assume that the contribution of terms with rapidly varying exponents, $\exp(-i(E_i - E_k)t/\hbar)$, averages approximately to zero when integrated over a sufficiently long time, and can be neglected in comparison with the secular terms for which $E_k = E_j$ or $E_k = E_i$. Thus the equation of motion reduces to,

$$-i\hbar \frac{d(M_x^*)_{ij}}{dt} = [(\mathcal{H}_d)_{ii} - (\mathcal{H}_d)_{jj}] (M_x^*)_{ij} = \hbar \Delta\omega_{ij}(t) (M_x^*)_{ij} \quad \text{(II.26)}$$

with the solution,

$$(M_x^*)_{ij} = (M_x^*)^o_{ij} \exp\left(i \int_o^t \Delta\omega_{ij}(t')\, dt'\right) \quad \text{(II.27)}$$

The quantity $\Delta\omega_{ij}(t)$ is taken to be a random function of time and depends on the values of the diagonal elements of $\mathcal{H}_d$ which change in a random way at a rate governed by $\mathcal{H}_m$, via Eq.(II.16). Thus the relaxation function (II.19) becomes,

$$G(t) = \sum_{i,j} \exp\left[i\,(E_i - E_j)\,t/\hbar\right] \left|\langle i\,|M_x|\,j\rangle\right|^2 \exp\left[i \int_0^t \Delta\omega_{ij}(t')\,dt'\right]. \qquad \text{(II.28)}$$

Considering only a well defined transition of $\mathcal{H}_o$ with $E_i - E_j = \hbar\,\omega_o$ and taking $|\langle i\,|M_x|\,j\rangle|^2$ as weighting function for the exponential terms, G(t) becomes,

$$G(t) = \exp(i\,\omega_o\,t) \int_{-\infty}^{+\infty} dx\,P(x) \exp(iX(t))$$

$$= \exp(i\,\omega_o\,t) \langle \exp(iX(t)) \rangle \qquad \text{(II.29)}$$

where $X(t) = \int_0^t \Delta\omega_{ij}(t')\,dt'$

and $P(x)$ = Probability distribution for $\exp(i\,X(t))$

Now the problem reduces to finding distribution law $P(x)$ for $X(t)$ and then to calculate $\langle \exp(i\,X(t)) \rangle$. For this the following model is chosen: (i) the random function $\Delta\omega_{ij}(t)$ is stationary and Gaussian and (ii) the mean square value $\langle \omega^2 \rangle$ of $\Delta\omega_{ij}(t)$ is the same as in the absence of any motion. Now if $\Delta\omega_{ij}(t)$ is a Gaussian random function, it is completely characterized, aside from its mean square magnitude, by its reduced correlation function,

$$g_\omega(\tau) = \langle \Delta\omega_{ij}(t)\,\Delta\omega_{ij}(t+\tau) \rangle / \langle \omega^2 \rangle \qquad \text{(II.30)}$$

where $\langle \omega^2 \rangle$ is the mean squared dipolar fluctuation and

$g_\omega(0) = 1$. Also, from the assumption of Gaussian character of $\Delta\omega_{ij}(t)$, $X(t)$ also comes out to be Gaussian with,

$$P(x) = \frac{1}{\sqrt{2\pi\langle X^2\rangle}} \exp\left(-\frac{1}{2} X^2/\langle X^2\rangle\right) \qquad \text{(II.31)}$$

Hence we get,

$$\langle \exp(-i X(t))\rangle = \frac{1}{\sqrt{2\pi\langle X^2\rangle}} \int_{-\infty}^{+\infty} \exp\left(-\frac{1}{2} x^2/\langle X^2\rangle\right) \times \exp(-i x(t))\, dx$$

$$= \exp\left(-\langle X^2\rangle/2\right) \qquad \text{(II.32)}$$

and thus the relaxation function becomes,

$$G(t) = \exp(i\omega_o t) \exp\left(-\langle X^2\rangle/2\right) \qquad \text{(II.33)}$$

Using Eq. (II.30), $\langle X^2\rangle$ becomes,

$$\langle X^2\rangle = \left\langle \int_o^t dt' \int_o^t dt'' \Delta\omega_{ij}(t') \Delta\omega_{ij}(t'')\right\rangle$$

$$= \langle\omega^2\rangle \int_o^t dt' \int_o^t dt''\, g_\omega(t'' - t')$$

Next the substitution of,

$$\tau = t'' - t'$$

$$\tau' = t'' + t'$$

as new variables in $\langle X^2 \rangle$ leads to,

$$\langle X^2 \rangle = 2 \langle \omega^2 \rangle 2 \int_0^t d\tau \, g_\omega(\tau) \int_\tau^{2t-\tau} d\tau' \left| \frac{\partial(t', t'')}{\partial(\tau, \tau')} \right|$$

$$= 2\left(\frac{1}{4}\right) \langle \omega^2 \rangle 2 \int_0^t d\tau \, g_\omega(\tau) \, (2t - 2\tau)$$

$$= 2 \langle \omega^2 \rangle \int_0^t d\tau \, (t - \tau) \, g_\omega(\tau) \qquad \text{(II.34)}$$

Hence,

$$G(t) = \exp(i \omega_o t) \exp\left[-\langle \omega^2 \rangle \int_0^t d\tau \, (t - \tau) \, g_\omega(\tau)\right] \qquad \text{(II.35)}$$

From this Eq. (II.35), it is possible to describe the effects of the random modulation $\Delta\omega_{ij}(t)$. Before making any explicit assumption about $g_\omega(\tau)$, first we will consider two extreme cases viz. those of slow and fast motion.

Case I:

$\Delta\omega_{ij}(t)$ varies slowly or the correlation time τ_c† is so long that $\langle \omega^2 \rangle \tau_c^2 \gg 1$. Then, for $\tau < \tau_c$ $g_\omega(\tau)$ can be replaced by unity, giving,

$$G(t)_I \cong \exp(i \omega_o t) \exp\left[-\langle \omega^2 \rangle \int_0^t (t - \tau) \, d\tau\right]$$

$$= \exp(i\omega_o t) \exp(-\langle \omega^2 \rangle t^2/2) \qquad \text{(II.36)}$$

---

† $g_\omega(\tau) = \exp(-\tau/\tau_c)$

Eq. (II.36) represents the relaxation function, termed as rigid-lattice relaxation function, and gives an important result that in the absence of rapid motion the lineshape is Gaussian with the linewidth given by

$$\Delta\omega = \sqrt{\langle\omega^2\rangle} \qquad \text{(II.37)}$$

Case II:

$\Delta\omega_{ij}(t)$ varies rapidly, i.e. τ_c is so short that $\langle\omega^2\rangle\ \tau_c^2 \ll 1$. Then, for $t \gg \tau_c$ the reduced correlation function $g_\omega(\tau)$ falls rapidly to zero before $G(t)$ has a chance to decay and the integral in the exponential factor can be extended to infinity with the result,

$$G(t)_{II} \cong \exp(i\omega_o t)\exp\left(-\langle\omega^2\rangle\, t \int_o^\infty g_\omega(\tau)\, d\tau\right)$$

$$= \exp(i\omega_o t)\exp\left(-\langle\omega^2\rangle\, t\, \tau_c'\right) \qquad \text{(II.38)}$$

where τ_c' ($= \int_o^\infty g_\omega(\tau)\, d\tau$) is some characteristic time related to how fast the correlation function falls off, and is related to the inverse of the frequency of modulation of the dipolar interaction, ω_m,

$$\tau_c' = \int_o^\infty g_\omega(\tau)\, d\tau = 1/\omega_m \qquad \text{(II.39)}$$

Hence under the narrowing condition of fast modulation the relaxation function becomes,

$$G(t)_{II} = \exp(i\omega_o t) \exp(-\langle\omega^2\rangle t/\omega_m) \qquad (II.40)$$

The relaxation function, $G(t)_{II}$, describes a Lorentzian lineshape. The important result is that the linewidth in the presence of rapid motion is given by,

$$\Delta\omega = \langle\omega^2\rangle / \omega_m \qquad (II.41)$$

The presence of $\langle\omega^2\rangle$ in both Eqs. (II.37) and (II.41) supports the original assumption that the width depends on the size of dipolar fluctuations.

At this point it is necessary to make a comment as the treatment given above is very simplified. When the modulating motion is very rapid such that the modulating frequency is greater than the resonance frequency i.e. $\omega_m >> \omega_o$, the contribution of non-secular terms can not be neglected. These introduce a numerical factor of 10/3 in Eq. (II.41) with the dipolar and modulating frequency dependences remaining unchanged.[45] This is called the spin-lattice relaxation or '10/3' effect and causes further broadening. With this description of the theory of motional narrowing, we will switch over to the special cases of doped paramagnetic hosts, i.e. host spin-lattice relaxation narrowing and spin quenching.

HOST SPIN-LATTICE RELAXATION NARROWING:

From the discussion of the theory of the motional effects, it comes out that the presence of an appropriate fast motion of some sort in the system may reduce the dipolar interaction to a large extent resulting in the motional narrowing of the resonance lines. The question arises whether or not any appropriate motional effects are operative for the observation of the EPR of impurity ions, with sufficiently large spin-lattice relaxation times, in paramagnetic hosts.

A well known application of the motional narrowing theory is the exchange narrowing in the magnetic resonance.[46] Here the exchange interaction in the pure and mixed materials has been discussed as a motional Hamiltonian causing narrowing of the resonance lines, which is termed as 'exchange narrowing'. In the case of impurity doped paramagnetic hosts, exchange between unlike spins (i.e. impurity and host spins) will be of interest. Exchange effects among unlike spins are more complicated than those among like spins and do not result in narrowing of resonance lines but contribute to their broadening. The reason being, the exchange Hamiltonian of unlike spins does not commute with M_x, the x component of the magnetic moment of resonating spins and thus contributes to its time dependence through Eq. (II.21).[44]

temperature. At temperatures as high as room temperature ($\sim$ 300 K), these systems meet the requirement that the hosts are fast relaxing and impurity T_1 is long enough that it is not the source of its own line broadening. The primary candidates for the observation of this narrowing are the well known slow relaxing S-state ions Gd^{3+} and Mn^{2+}. In lanthanide group all the trivalent ions, except Gd^{3+}, are fast relaxing due to Orbach mechanism and therefore are suitable as hosts for the observation of this narrowing in the EPR spectrum of Gd^{3+}. However, in iron group the fast relaxing hosts are those for which the orbital angular momentum is not quenched, as for example Co^{2+}. Since the present study is confined only to Mn^{2+} doped iron group host lattices, we will restrict ourselves to iron group metal ions. In what follows, we show that Co^{2+} ions are suitable host ions for this narrowing to occur in Mn^{2+} spectra.

Since this narrowing effect is not well understood, it will be worthwhile to show that the requirements of the earlier section for motional narrowing to occur are met for Mn^{2+} doped cobalt salts. The schematic diagram, showing the relation among the systems involved in Mn^{2+} line narrowing mechanism at 300 K due to rapid relaxing Co^{2+} ions, is given in Fig. II-2. The total spin-Hamiltonian of the system can be written as a sum of three parts:

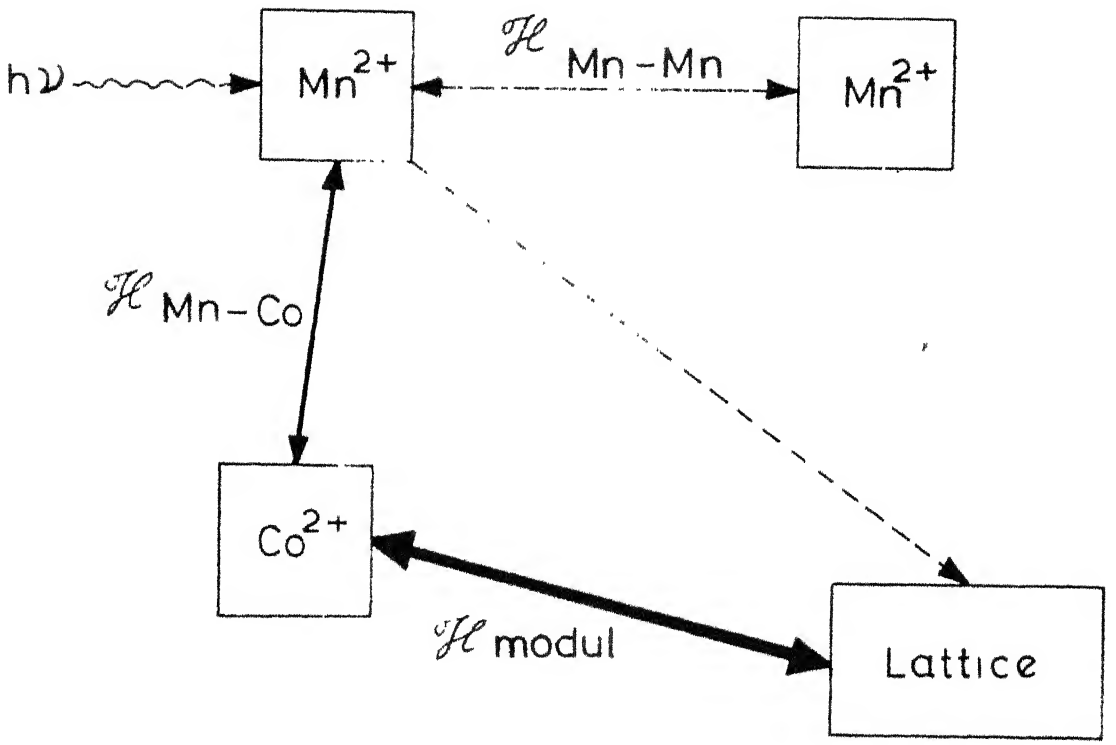

Fig.II-3: Schematic diagram showing the relation among the systems involved in the Mn^{2+} line narrowing mechanism due to rapid relaxing Co^{2+} ions.

$$\mathcal{H} = \mathcal{H}_o + \mathcal{H}_m + \mathcal{H}_d$$

Here $\mathcal{H}_o$ is the unperturbed spin-Hamiltonian which gives rise to the positions of spectral lines (Zeeman interaction mainly). $\mathcal{H}_m$ is the Hamiltonian, which causes the modulation of dipolar and exchange interactions between host and impurity and is identified by the spin-lattice coupling of the host i.e. mainly superposition of host spin-orbit and orbit-lattice coupling. $\mathcal{H}_d$ is the time dependent perturbation taken to be the host-impurity dipolar and exchange interactions and is the sum of $\mathcal{H}_{Mn-Mn}$ and $\mathcal{H}_{Co-Mn}$ as shown in Fig. II-2. Further $\mathcal{H}_o$ and M_x (x component of the magnetic moment of resonating spins) contain only impurity spin operators, the commutation relations,

$$[\mathcal{H}_o, \mathcal{H}_m] = 0 \quad \text{and} \quad [\mathcal{H}_m, M_x] = 0$$

hold. $\mathcal{H}_d$ does not commute with $\mathcal{H}_m$ because $\mathcal{H}_d$ contains both host and impurity spin operators and $\mathcal{H}_d$ will obtain a time dependence from $\mathcal{H}_m$ by Eq. (II.16). It remains to show that $\mathcal{H}_m$ can be greater than $\mathcal{H}_d$ and that no large matrix elements of $\mathcal{H}_d$ connect the states of $\mathcal{H}_o$. As $\mathcal{H}_d$ is typically ~ 0.01 cm^{-1} (i.e. $10^7 - 10^8$ Hz in frequency units), the host spin-lattice relaxation time T_1 should be faster than $\sim 10^{-9}$ sec (i.e. 10^9 Hz) for narrowing to occur. In most of the cobalt salts it is certainly true at higher

temperatures ($\sim$ 300 K) and the condition $\mathcal{H}_m >> \mathcal{H}_d$ can be fulfilled. Further, with the conventional spectrometers (X-band in our case), the dipolar interaction is always smaller than the Zeeman splitting, which meets the second condition that no large matrix elements of $\mathcal{H}_d$ connect the states of $\mathcal{H}_o$. Thus the conditions for the observation of sharp EPR spectrum of Mn^{2+} in cobalt salts at $\sim$ 300 K due to host spin-lattice relaxation narrowing are fulfilled. The confirmation of the fact that this narrowing is only due to host spin-lattice relaxation narrowing, and not due to the exchange narrowing, can be made by lowering the temperature of the crystal from 300 K. In the case of exchange narrowing, there will be almost no temperature dependence of the impurity linewidth until one goes much below 77 K. While for host spin-lattice relaxation narrowing, the widths of impurity resonance lines should increase on lowering the temperature because the host T_1 should increase on lowering the temperature and will then be not able to average out the dipolar interaction as effectively. Earlier unexplained data regarding broadening of impurity resonance lines on lowering the temperature, as in Cu^{2+} doped $K_2Co(SO_4)_2.6H_2O$,[49] Mn^{2+} doped $(NH_4)_2 Co(SO_4)_2.6H_2O$,[50] and Gd^{3+} doped in many lanthanide ethylsulphates,[51] can be satisfactorily explained

by host spin-lattice relaxation narrowing theory. Mitsuma[47] has earlier explained his results of Cr^{3+} doped $K_3Fe(CN)_6$ on the same lines.

Besides, when the conditions for host spin-lattice relaxation narrowing are in effect, the impurity linewidth will reflect the host T_1. In the absence of any rigorous formulation of the lineshape when narrowing is present, it will be a very satisfactory approximation to take the width given by Eq. (II.41) i.e. $\langle\omega^2\rangle/\omega_m$, where $\langle\omega^2\rangle$ is the mean squared width in the absence of narrowing and ω_m is the average rate at which the broadening interactions are modulated, which here will be the inverse of host T_1. Now, as the exchange between unlike spins also adds to the broadening, the contribution to $\langle\omega^2\rangle$ will be from both dipolar and exchange interactions, where the latter is generally unknown. However, for an estimation of the order of host T_1, the following approximation for $\langle\omega^2\rangle$ in field units can be made:[43]

$$H_d^2 = 5.1\,(g\beta n)^2\,S\,(S+1) \qquad \text{(II.42)}$$

where all the terms pertain to the host and n is the density of host spins per c.c., which can be calculated from the crystallographic data. This value of H_d^2 will be the lower limit of $\langle\omega^2\rangle$ as we have neglected exchange contribution. Thus the formula of host T_1 can be written as:[47]

$$T_1(\text{host}) = (h/g_{host}\,\beta) \times (3/20) \times (\Delta H_{imp}/H_d^2) \qquad \text{(II.43)}$$

Here the contribution due to non-secular terms has been taken into account by using the factor (10/3). From the observed linewidth ΔH of impurity, one can estimate host T_1. These studies, may thus be utilized to estimate the extremely fast spin-lattice relaxation times at higher temperatures.

SPIN QUENCHING:

Another process which produces sharp EPR spectra of impurity ions in paramagnetic hosts is spin quenching. In spin quenching, the host-impurity dipolar interaction is reduced by an actual decrease in the magnetic moment of host ions (e.g. Ni^{2+} ions). It is known from motional narrowing theory (described earlier) that the linewidths with or without narrowing are $\langle\omega^2\rangle / \omega_m$ or $\sqrt{\langle\omega^2\rangle}$, respectively, where $\langle\omega^2\rangle$ is the mean squared dipolar fluctuation, and that linewidth is a function of the magnetic moment size in both cases. Further the reduction of the magnetic moment results from the quenching of the spin by crystal field and spin-orbit coupling through complete removal of the degeneracy. Here two cases may arise depending upon whether the spin is completely or partially quenched. The

complete spin quenching occurs for non-Kramers host ions with very low site symmetry, i.e. rhombic or lower. This makes the magnetic moment of host ions entirely of second order, causing an acute reduction of the mean squared dipolar fluctuation, $\langle \omega^2 \rangle$. At temperatures greater than the zero field splittings of host ions (in temperature units), the susceptibility measurements do not indicate, whether the spin is quenched or not, because eventhough the magnetic moments of the host ions are reduced, the increased splittings between the energy states result in the increase of the population difference causing the susceptibility to be basically the same. Therefore, the only way of seeing spin quenching at high temperatures, due to low site symmetry is the observation of sharp EPR spectra of an impurity ion in such a paramagnetic sample.

From the above discussion, Ni^{2+} ions come out to be suitable examples for spin quenching because these are commonly occurring non-Kramers ions and in many compounds, such as nickel Tutton salts,[52] $Ni(CH_3COO)_2.4H_2O$,[53] $NiSO_4.7H_2O$[54] and $Ni(OH_2)_6.(NO_3)_2$,[55] are known to have rhombic site symmetry.

Using the expressions of the energy states for Ni^{2+} in an orthorhombic crystalline field,[52] the instantaneous magnetic moment of Ni^{2+} can be written as:

$$\mu_{ins} = -\frac{\partial W_n}{\partial H} = 0, \pm \frac{g^2\beta^2 H}{(A_{cr}^2 + g^2\beta^2 H^2)^{1/2}}$$

$$= 0, \pm \frac{g\beta}{[1 + (A_{cr}/g\beta H)^2]^{1/2}} \qquad \text{(II.44)}$$

where W_n is the energy of state n and A_{cr} contains the crystal field parameters of Ni^{2+} and its value depends upon the orientation of the magnetic field, H. Above expression for μ_{ins} shows the values between which the Ni^{2+} magnetic moments fluctuate, and which are responsible for mean squared dipolar fluctuation, $\langle\omega^2\rangle$. When zero field term $A_{cr} >> g\beta H$, the magnetic moment of Ni^{2+} and hence $\langle\omega^2\rangle$ will be reduced by a sizable factor. This will give sharp spectra of impurity, which, as implied by the expression (II.44), will show anisotropic and field dependent linewidths. In the earlier studies[56-58] of Mn^{2+} doped nickel salt single crystals, these features of impurity linewidth have been observed. Now we will first discuss and explain them more convincingly in terms of spin quenching idea. Upreti[58] observed a large anisotropy of Mn^{2+} linewidth in the EPR of Mn^{2+} doped potassium and ammonium Tutton salts. In both the cases Mn^{2+} spectra were almost broadened out for H along the Z-axis of one set of equivalent Mn^{2+} complexes, while sharp spectra were observed for H along the X-axis. Upreti[58] explained

this complete broadening and disappearance of spectra due to cross-relaxation between Mn^{2+} and Ni^{2+} ions. But it seems more convincing to explain the above observation in terms of spin quenching idea. The values of A_{cr} for H along the Z, X and Y axes are E, (D+E)/2 and (D-E)/2, respectively, where D and E are the crystal field parameters of Ni^{2+} in these salts. When H is along the Z-axis, one set of ions in unit cell has A_{cr} = E and |E| is not much larger than Zeeman energy, $g\beta H$ (~ 0.3 cm^{-1}), in both Tutton salts (see Table II-2). This causes an increase of Ni^{2+} magnetic moment and consequent increase of linewidth along the Z-axis. At the same time, when H is along the X-axis, A_{cr} = (D+E)/2 for the above set of ions and H for other set of ions lies nearly along the Y-axis which gives an A_{cr} value of (D-E)/2. Both A_{cr} values are much larger than the Zeeman energy and hence the consequent narrowing of Mn^{2+} lines for H along the X- and Y-axis. Further, as the magnetic moment of Ni^{2+}, μ_{ins}, is a function of field orientation, so will be the linewidth of Mn^{2+}. Thus there will be a linewidth anisotropy. Also it is noticed, from the comparison of the EPR spectra of Mn^{2+} for H along the Z-axis in the two Tutton salts, that the Mn^{2+} lines are narrower in potassium salt than those in ammonium salt. This is, what is demanded by the above discussion as the magnitude of 'E' of Ni^{2+} in potassium salt is greater than that in the ammonium salt.

Table II-2

Spin-Hamiltonian parameters of Ni^{2+} in various nickel salt single crystals.

Crystal	Temp. °K	D (cm^{-1})	E (cm^{-1})	g	Ref.
		Orthorhombic Site Symmetry			
$(NH_4)_2Ni(SO_4)_2.6H_2O$	290	-2.24	-0.38	2.25	(52)
$K_2Ni(SO_4)_2.6H_2O$	290	-3.5	-0.55	2.25	(52)
$(NH_4)_2Ni(SeO_4)_2.6H_2O$	290	-1.89	-0.79	2.25	(52)
$K_2Ni(SeO_4)_2.6H_2O$	290	-3	-1	2.25	(52)
$Tl_2Ni(SO_4)_2.6H_2O$	290	-2.65	-0.10	2.25	(52)
$Ni(CH_3COO)_2.4H_2O$+	1.3-20	-5.61	-0.83	2.24	(53)
$NiSO_4.7H_2O$	290	-3.56	-1.5	2.2	(54)
$NiCl_2.6H_2O$	77	-1.2	0.15	2.2	(64)
$Ni(NO_3)_2.6H_2O$+	1.3-20	-6.07	-1.86	2.25	(55)
		Trigonal Site Symmetry			
$NiSiF_6.6H_2O$	290	-0.5	0	2.3	(65)
$NiSnCl_6.6H_2O$	4.2	+0.455	0	2.3	(66)
$La_2Ni_3(NO_3)_{12}.24H_2O$(X)	77	$-0.03\pm.02$	0	2.24	(67)
$La_2Ni_3(NO_3)_{12}.24H_2O$(Y)	77	$-2.20\pm.02$	0	2.24	(67)

+ From studies other than paramagnetic resonance.

Now we will discuss the field dependence of Mn^{2+} linewidths in nickel salts as observed earlier.[56-58] It is an expected result since the magnetic moment of Ni^{2+} μ_{ins}, given by Eq. (II.44), is field dependent. The field dependence of linewidth adds to the information, whether or not a narrowing process is operative. By coupling the expression for μ_{ins} with the expressions for linewidths with or without narrowing, i.e. $\langle\omega^2\rangle / \omega_m$ or $\sqrt{\langle\omega^2\rangle}$, the field dependences are found to be quadratic with narrowing and linear without narrowing. Moriya et al.[59] obtained the same results in a more rigorous way. This way the information about the narrowing process can be made available, if the quadratic dependence is observed. In many of Ni^{2+} compounds, listed in Table II-2, the EPR of Ni^{2+} is observed at room temperature implying their spin-lattice relaxation ~~narrowing~~ would be too slow for host spin-lattice relaxation narrowing to be operative. Thus, in these salts if there is any narrowing of impurity (e.g. Mn^{2+}) resonance lines other than that due to spin quenching, it would be due to exchange interaction. Earlier field dependent linewidth data of Mn^{2+} doped in $Ni(CH_3COO)_2.4H_2O$,[56] and $NiSO_4.7H_2O$,[57] were fitted to both linear and quadratic forms with the result that neither fit the data very well, implying the existence of some intermediate case.

Besides, the linewidth of impurity also reflects the zero field splitting of the host ions and the anisotropy of the linewidth results as a consequence of the changes in the energy level pattern of the host. In principle, the zero field (or crystal field) parameters of the host could be determined from the angular dependence of the linewidth of impurity, but in practice, factors like the extreme line broadening and the presence of more than one ion per unit cell would make their determination unreasonable, and hence other methods are preferred. In conclusion, eventhough many linewidth effects are observable, only little quantitative information can be easily extracted from these.

Further for such systems, the impurity linewidth is expected to show very little temperature dependence until temperatures low enough to be comparable with energy separations of spin states (in temperature units) are reached. The temperature dependence can be explained by observing that μ_{ins} will be unchanged, but their weights in the average for the mean squared dipolar fluctuations will change. However, for temperatures greater than the energy separations (in temperature units), the weights will be effectively equal, but when temperatures are smaller than the energy separations (in temperature units), the average will depend on the statistical weights. Thus in the temperature range (300 K to 77 K)

no appreciable change in linewidths of Mn^{2+} in nickel salts is expected as the former condition holds. The same results were also obtained by Moriya et al.[59] from a rigorous mathematical formulation.

Fe^{2+} ions in low symmetry crystalline fields are the only other iron group ions where spin quenching is expected to be operative. These are different from Ni^{2+} ions because the host spin-lattice relaxation narrowing is operative here alongwith spin quenching and it is expected that a combined effect of the two processes will be observed. Further Fe^{2+} ions have large ZFS, and this leads to the quenching of magnetic moments very effectively. Thus one would expect little or no influence of temperature on impurity linewidth. This is what has been observed in earlier studies on $(NH_4)_2Fe(SO_4)_2.6H_2O:Mn^{2+}$ [60] and $FeSiF_6.6H_2O:Ni^{2+}$ [61]. However, the width of Cu^{2+} in $(NH_4)_2Fe(SO_4)_2.6H_2O$ [62] broadens on lowering the temperature, with a maximum at 13 K. Details about Mn^{2+} doped Fe^{2+} Tutton salts will be discussed in Chapter V.

Another case of partial quenching arises when the symmetry of the crystal field is not low enough to remove the host ion spin-degeneracy completely. Further, where the singlet lies lowest, the situation of complete quenching can be achieved by populating this singlet exclusively by thermal means i.e. by lowering the temperature. Also this thermal

restriction to a singlet state will diminish the fluctuations between states and thus there will remain no temperature dependence of the dipolar field. Here again the non-Kramers ions will give singlet ground state. This sort of ions, which can be used as hosts, are usually found in lanthanide group because their singlet ground states are separated from first excited states by the energies of the order of the spin-orbit coupling i.e. 10^2-10^3 cm^{-1}. With this much of energy separation, to populate only the ground singlet by thermal means is relatively easy and may only require temperature in liquid nitrogen range ($\sim$ 77 K). But in the case of iron group ions this separation is about 0.1 - 20 cm^{-1}, and liquid helium temperatures are required to populate only the ground singlet. Various iron group ion impurities have been studied in α-$NiSO_4.6H_2O$ and $NiSeO_4.6H_2O$,[63] which belong to the latter case.

REFERENCES

1. B. Bleaney and D.J.E. Ingram, Proc. Phys. Soc. A65, 953 (1952).

2. H. Watanabe, J. Phys. Chem. Solids 25, 1471 (1964).

3. A. Abragam, Phys. Rev. 79, 534 (1950); A. Abragam and M.H.L. Pryce, Proc. Roy.Soc.(London) A205, 135 (1951).

4. A. Abragam and B. Bleaney, 'Electron Paramagnetic Resonance of Transition Ions', Chap. 17, Clarendon Press, Oxford (1970).

5. A.J. Freeman and R.E. Watson, 'Magnetism', Vol.II A (Ed. G.T.Rado and H.Suhl), p. 167, Acad.Press, New York (1965); R.E. Watson and A.J.Freeman,'Hyper Interactions', (Ed.A.J.Freeman and R.B.Frankel), p.53, Acad. Press, New York (1967).

6. J.H.van Vleck and W.Q. Penney, Phil. Mag. 17, 961 (1934).

7. M.H.L. Pryce, Phys. Rev. 80, 1107 (1950).

8. R. Bersohn and T.P. Das, Bull. Am. Phys. Soc. 1, 397 (1956).

9. H. Watanabe, Prog. Theor. Phys. 18, 405 (1957).

10. J.Kondo, Prog. Theor. Phys. 23, 106 (1960) and 28, 1026 (1962).

11. M.Blume and R.Orbach, Phys. Rev. 127, 1587 (1962).

12. G.D.Watkins and E.Feher, Bull. Am.Phys.Soc. 7, 29 (1962).

13. N.S.Shiren, ibid. 7, 29 (1962).

14. E.R.Feher, Phys. Rev. 136, A 145 (1964).

15. R.R.Sharma, T.P.Das and R.Orbach (Unpublished).

16. R.Orbach, T.P.Das and R.R.Sharma, Proc.Int.Conf. on Magnetism, p. 330, Nottingham (1964).

17. R.M.Sternheimer and H.M. Foley, Phys. Rev. 102, 731 (1956).

18. R.E.Watson, Phys. Rev. 118, 1036 (1960).

19. R.R.Sharma, T.P.Das and R.Orbach, ibid 149, 257 (1966).

20. M.Tinkham, Proc. Roy, Soc. (London) A236, 535 (1956).

21. A.M.Clogston, J.P. Gordon, V.Jaccarino, M.Peter and L.R.Walker, Phys. Rev. 117, 1222 (1960).

22. R.R.Sharma, T.P.Das and R.Orbach, Phys. Rev. 155, 338 (1967) and 171, 378 (1968).

23. J.E.Lowther, Phys. Stat. Sol.(b) 58, 293 (1973).

24. J.E.Lowther, ibid. 52, 639 (1972).

25. V.J.Folen, Phys. Rev. B7, 2771 (1973).

26. P.A. Narayana, Phys. Rev. B10, 2676 (1974).

27. H.Watanabe, Phys. Rev. Letters 4, 410 (1960).

28. R.R.Sharma, J.Appl.Phys. 42, 1572 (1971).

29. A.van Heuvelen, J.Chem.Phys. 46, 4903 (1967).

30. B.G.Wybourne, ibid 43, 4506 (1965).

31. W.E.Hagston and J.E.Lowther, J.Phys. Chem.Solids 34, 1773 (1973).

32. R.A.Serway, Phys. Rev. B3, 608 (1971).

33. P.Schlottmann and M.C.G.Passeggi, Phys. Stat.Sol(b) 52, K 107 (1972).

34. R.Chatterjee and D. Van Ormondt, Phys. Lett 33A, 147 (1970).

35. D.J.Newman and W.Urban, Advances in Phys. 24, 793 (1975).

36. R.Chatterjee, M.R.Smith and H.A.Buckmaster, Can.J. Phys. 54, 1224 (1976).

37. C.Marti, R.Romestain and R.Visocekas, Phys. Stat.Sol. 28, 97 (1968).

38. B.Bleaney and R.S.Rubins, Proc.Phys.Soc. 77, 103 (1961).

39. S.D.Pandey and G.C.Upreti, Ferroelectrics 2, 155 (1971).

40. R.E.Watson and A.J.Freeman, Phys. Rev. 123, 2027 (1961).

41. R.J.Richardson, S.Lee and T.J.Menne, ibid. B2, 2295 (1970).

42. N.Bloembergen, E.M.Purcell and R.V.Pound, ibid. 73, 679 (1948).

43. P.W.Anderson and P.R. Weiss, Rev. Mod. Phys. 25, 269 (1953).

44. A.Abragam, 'The Principles of Nuclear Magnetism,' Clarendon Press, Oxford (1961).

45. R.Kubo and K.Tomita, J.Phys. Soc. Japan 9, 888 (1954).

46. P.W. Anderson, J.Phys. Soc. Japan 9, 316 (1954).

47. T.Mitsuma, J.Phys. Soc. Japan 17, 128 (1962).

48. B.Bleaney, R.J.Elliot and H.E.D. Scovil, Proc.Phys. Soc. A64, 933 (1951).

49. B.A. Sastry and G.S. Sastry, J.Chem. Phys. 59, 6419 (1973) and Physica 74, 151 (1974).

50. G.C. Upreti, Chem. Phys. Letters 18, 120 (1973).

51. R.E.Gerkin and D.L.Thorsell, J.Chem.Phys. 57, 2665 (1972).

52. J.H.E.Griffiths and J.Owen, Proc. Roy.Soc. (London) A213, 459 (1952).

53. R.B.Flippen and S.A.Friedberg, Phys.Rev. 121, 1591 (1961).

54. K.Ono, J.Phys. Soc. Japan 8, 802 (1953).

55. L. Berger and S.A. Friedberg, Phys. Rev. 136, A158 (1964).

56. R.Janakiraman and G.C.Upreti, J.Chem.Phys. 54, 2336 (1971)

57. R.Janakiraman and G.C. Upreti, Phys. Stat. Sol.(b) 47, 679 (1971).

58. G.C. Upreti, J.Magn. Resonance 14, 274 (1974).

59. T.Moriya and Y.Obata, J.Phys. Soc. Japan 13, 1333 (1958).

60. R.Janakiraman and G.C.Upreti, Chem.Phys. Letters 4, 550 (1970).

61. R.S.Rubins, J.Chem.Phys. 60, 4189 (1974).

62. J.C.Gill and P.A.Ivey, J.Phys. C. 7, 1536 (1974).

63. Michael R.St.John, Ph.D. Thesis, Univ. of California, Berkeley (1975).

64. M.Date and M.Motokawa, J.Phys. Soc. Japan 22, 165 (1967).

65. R.P.Penrose and K.W.H.Stevens, Proc.Phys. Soc. A63, 29 (1950).

66. Y.Ajiro, N.S.Vanderven and S.A.Friedberg, Bull.Am.Phys. Soc. 17, 262 (1972).

67. R.T.Dixon and J.W.Culvahouse, Phys.Rev.B3, 2279 (1971).

GENERAL REFERENCES

1. G.E.Pake and T.L.Estle,'The Physical Principles of Electron Paramagnetic Resonance', 2nd Ed., Benjamin, London (1973).

2. J.W.Orton, 'Electron Paramagnetic Resonance', Iliffe, London (1968).

3. W.Low, 'Paramagnetic Resonance in Solids', Solid State Physics, Supplement 2, Acad. Press, New York (1964).

4. J.C. Gill, Rept. Progr. Phys. 38, 91 (1975).

CHAPTER III

EXPERIMENTAL

ABSTRACT

A brief description of the experimental set up used in the EPR studies - Varian V-4502 X-band EPR spectrometer fitted with V-4540 variable temperature accessory, a crystal rotator and a quartz dewar used for studies at liquid nitrogen temperature (77 K) - is given. The growing of doped single crystals from aqueous solutions is also discussed.

EPR SPECTROMETER:

The experimental EPR studies were carried out on a Varian V-4502 EPR spectrometer[+] operating at X-band microwave frequency ($\sim$ 9.5 GHz) and provided with a 100 kHz field modulation. Fig. III-1 shows the simplified block diagram of the spectrometer. The Varian V-4540 variable temperature accessory (range 77 K to 570 K) was used with the spectrometer to carry out the temperature variation studies. An all quartz dewar, suitable for use with liquid nitrogen, was used for studies at 77 K. A 9 inch Varian electromagnet, rotatable about the vertical axis and equipped with 'Fieldial' magnetic field regulator, was used. It provides a very homogeneous magnetic field in the air gap (2.625 inches) and the field can be varied from near zero to about 10 kG. DPPH, with g = 2.0036, was used as the standard field marker by fixing a small speck of DPPH on to the sample. The magnetic field at DPPH resonance was measured by proton resonance using a Varian F-8A flux meter and a Systronics Counter-timer Type 701 (Sr. No. 016). The EPR spectra were recorded using a Varian G-14 strip chart recorder. A Varian V-4531 multipurpose rectangular cavity operating in the TE_{102} mode was used.

+ 'V-4502 EPR Spectrometer System Manual' Varian Associates, California.

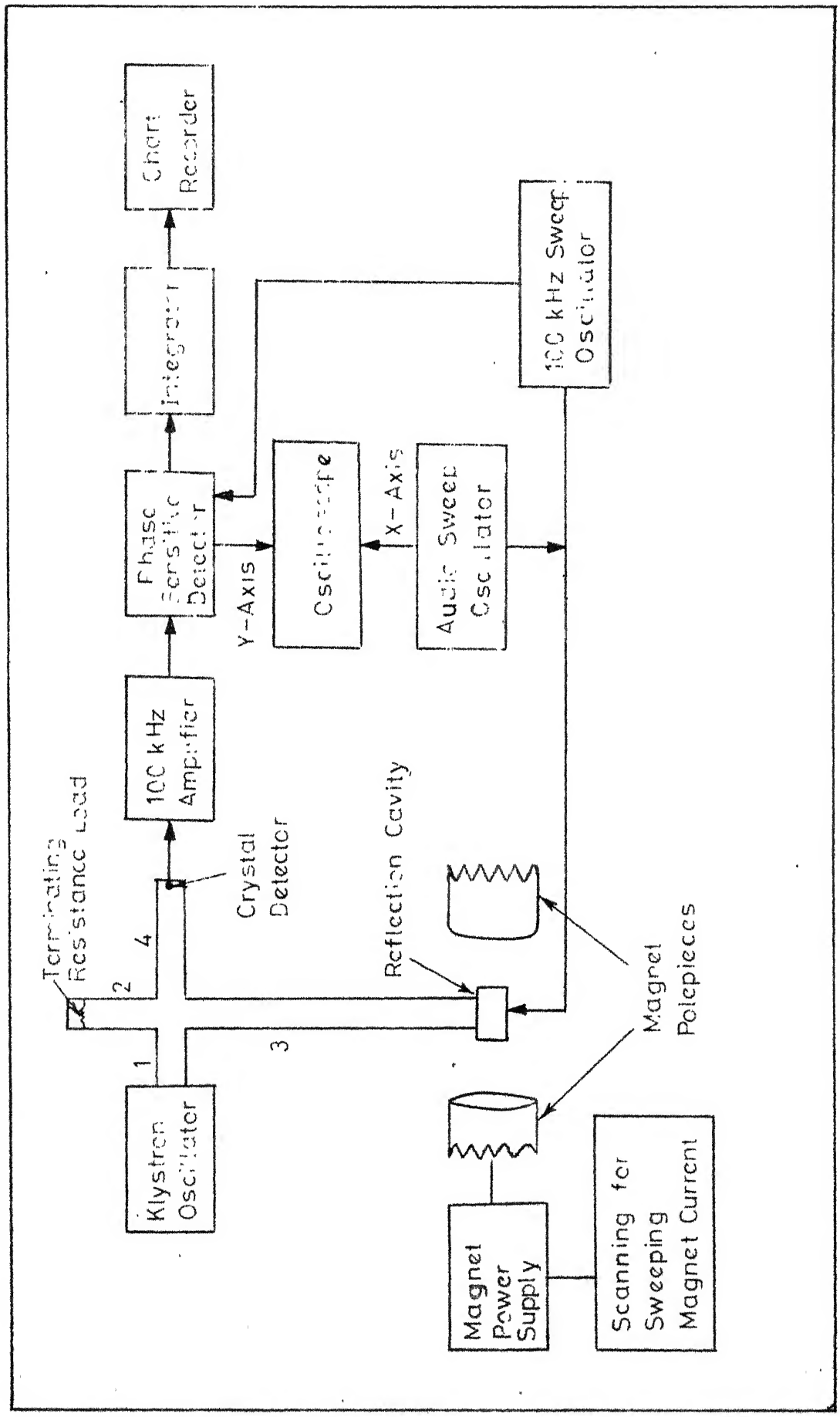

Fig. III-1. Block diagram of the EPR spectrometer.

CRYSTAL ROTATOR AND DETERMINATION OF AXES:

Angular variation EPR studies of the doped crystals were carried out using a Varian E-229 goniometer sample rotator, which rotates the crystal in increments of 0.5^{o} by means of a gear drive about a vertical axis. This goniometer is physically attached to the multipurpose cavity. In addition, for spatial orientations a crystal holder, shown in Fig. III-2, was employed. This provides the rotation of the crystal within the cavity about a horizontal and a vertical axis without removing it from the cavity. This facilitates the alignment of any desired axis of the crystal along the Zeeman field direction. Here the rotation of the crystal about a horizontal axis was achieved by means of a thread and shaft arrangement (also called string drive method).

The directions of the crystal field axes (X, Y, Z) were determined from the angular variation of the EPR spectra employing the following method: the crystal was rotated independently about a horizontal and a vertical axis and the direction of maximum spread of the fine structure of Mn^{2+} EPR spectra was obtained. This direction is termed as the Z-axis. Then the crystal was rotated in a plane perpendicular to the Z-axis and the directions of maximum and minimum spreads of the spectra in this plane were determined, which are called the X- and the Y-axis, respectively.

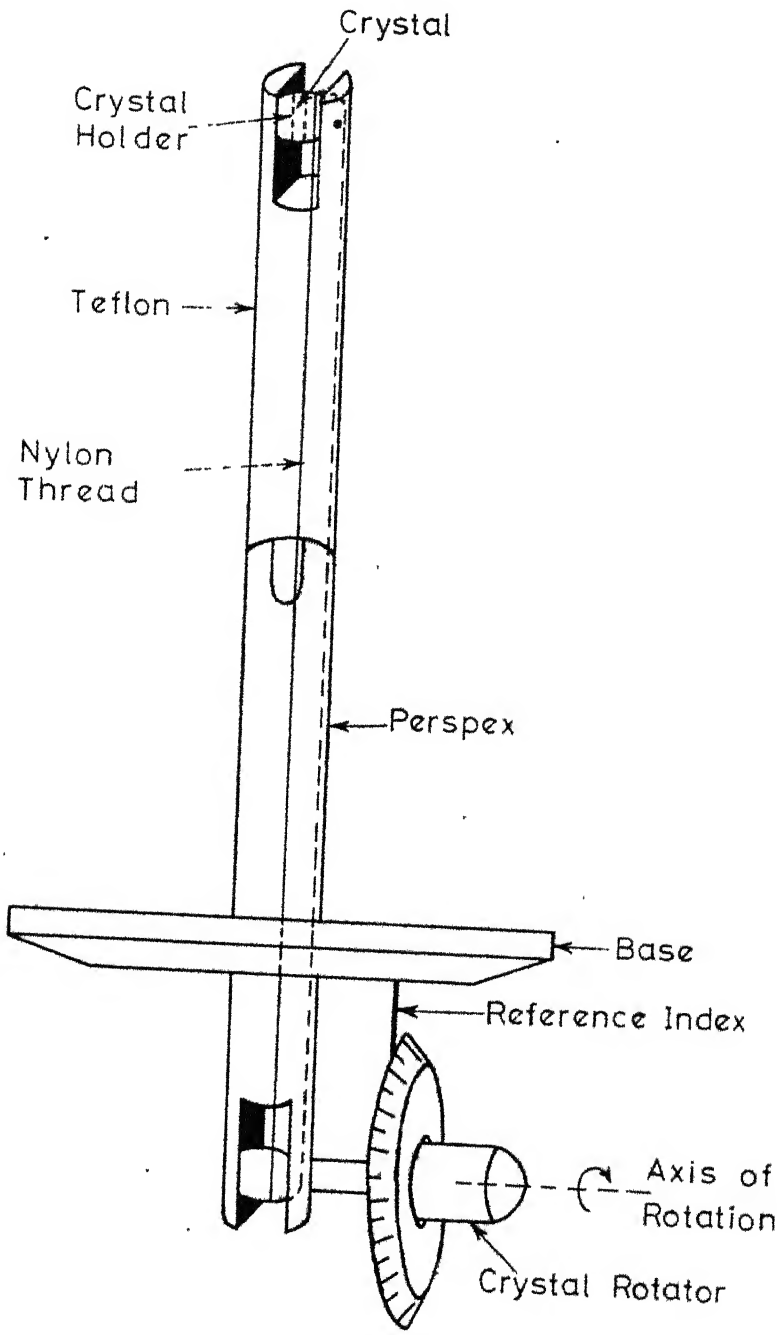

Fig. III-2: Device to rotate the single crystal inside the cavity about a horizontal axis.

CRYSTAL GROWING:

The doped single crystals of all the compounds, studied in the present thesis, were grown by slow evaporation at constant temperature of the saturated distilled water solution of the particular salt containing ~1% of the corresponding manganese salt by weight. All the chemicals used in growing the crystals were of AR grade. Potassium Tutton salts of cobalt, ferrous, magnesium and zinc were prepared by taking equimolar K_2SO_4 and the corresponding metal sulphate heptahydrate ($MSO_4.7H_2O$) salts and the grown crystals were analysed for the percentage of hydrogen to make sure that the grown crystals are hexahydrates only. $NiSeO_4.6H_2O$ crystals were crystallized from aqueous solution of nickel selenate, prepared by the reaction of selenic acid with $NiCO_3$. These, on mixing with equimolar $(NH_4)_2SeO_4$ and on preparing saturated distilled water solution for slow evaporation, give $(NH_4)_2Ni(SeO_4)_2.6H_2O$ crystals. In case of highly hygroscopic hexaquometal nitrate crystals the aqueous saturated solutions were kept inside a dessicator over anhydrous $CaCl_2$ or H_2SO_4 and left for slow evaporation. In the case of $CoSO_4.7H_2O$ crystals, two types of doped crystals were obtained, which are morphologically different and were also found to grow in two different temperature ranges about the room temperature. The crystals of Type I (CoSH(I))

grew by slow evaporation at room temperature in winters which is below 298 K. These crystals were prismatic with hexagonal bases and were found to dehydrate readily on exposure to atmosphere. In summer, CoSH(I) crystals were grown by keeping the growth solution in a refrigerator maintaining temperatures below 298 K. These crystals of type II (CoSH (II)) were grown by slow evaporation at room temperature in summers which is higher than 298 K. These crystals were rectangular needles and were more stable towards exposure to atmosphere than CoSH(I). All the crystals, which are either hygroscopic or dehydrate readily on exposure to atmosphere, were protected against exposure to atmosphere by coating them with petroleum jelly and paraffin oil mixed in ratio 1:1. A good quality nailpolish was also found to work nicely for the protection of these crystals against exposure to atmosphere.

CHAPTER IV

ELECTRON PARAMAGNETIC RESONANCE STUDY OF Mn^{2+} DOPED IN MAGNESIUM, COBALT AND NICKEL ACETATE TETRAHYDRATE SINGLE CRYSTALS†

ABSTRACT

A comparative EPR study of Mn^{2+} doped in isomorphous single crystals of tetrahydrate acetates of magnesium, cobalt and nickel has been carried out from 400 K to 77 K to study the effects of the paramagnetic host ions on the EPR of Mn^{2+} ions. Mn^{2+} is found to substitute for the divalent metal ion and exhibits two inequivalent magnetic complexes corresponding to the bimolecular unit cell of the three isomorphous crystals. The observed differences in the EPR of Mn^{2+} in dia- and paramagnetic hosts are attributed to the magnetic interaction between Mn^{2+} and the paramagnetic host ions. In addition, the use of impurity probe (i.e. Mn^{2+}), to measure the extremely fast T_1 of host (Co^{2+}) ions at high temperatures, is demonstrated by estimating Co^{2+} T_1 at different temperatures.

---

† The contents of this chapter have been published in J. Magn. Resonance 20, 39 (1975).

INTRODUCTION:

There are early reports of EPR studies of undiluted and Zn^{2+} diluted $Mn(CH_3COO)_2.4H_2O$.[1,2] Later studies[3-5] are reported on EPR of Co^{2+}, Cu^{2+}, Mn^{2+} and VO^{2+} doped in $Mg(CH_3COO)_2.4H_2O$ single crystals. Janakiraman et al.[6] studied EPR of Mn^{2+} in $Ni(CH_3COO)_2.4H_2O$ at room temperature. A number of other studies, such as magnetic susceptibility[7-11] and specific heat measurements[12] at low temperatures and optical absorption studies,[13,14] were carried out in the tetrahydrate acetates of Ni^{2+} and Co^{2+}. These studies have revealed very pronounced anisotropy of the magnetic moments of Ni^{2+} and Co^{2+} which may be attributed to a structural peculiarity evident from X-ray studies.[15] This is that each metal ion in these substances is surrounded by an octahedron composed of four water molecules and two oxygens of different acetate groups. The two later oxygens are at opposite vertices of the octahedron and this arrangement could contribute a sufficiently strong rhombic component to the crystalline electric field at each magnetic ion and account for the anisotropy. From the single crystal magnetic studies Mookherji et al.[10,11] have shown that the crystal field splittings in tetrahydrate acetates of Ni^{2+} and Co^{2+} are much higher than those in the corresponding Ni^{2+} and Co^{2+} Tutton salts with divalent ions octahedrally surrounded with

six water molecules and that spin-orbit coupling in $Co(CH_3COO)_2.4H_2O$ is weaker compared to the anisotropic crystal field. Low temperature heat capacity measurements[12] in $Ni(CH_3COO)_2.4H_2O$ between 0.43 and 10.75 K have revealed a schottky anomaly at 1.98 K and the presence of a small interaction between Ni^{2+} ions which can be described by an antiferromagnetic molecular field constant $A/k = + 0.08$ K, largely of dipolar origin. In this chapter we describe our results of a comparative EPR study, from 400 K to 77 K, on Mn^{2+} doped single crystals of tetrahydrate acetates of magnesium, cobalt and nickel, hereafter to be referred to as MgAc, CoAc and NiAc, respectively.

CRYSTAL STRUCTURE:

The crystal structure of MgAc has been determined by Shankar et al.[16] Van Niekerk and Schoening[15] have determined the crystal structure of CoAc and NiAc. Later Downie et al.[17] have reported slight modifications in the crystal structure of NiAc. The crystals of MgAc, CoAc and NiAc are isomorphous. The unit cell is monoclinic and contains two molecules related by the operation of the space group $P2_1/c$. The unit cell dimensions are given in Table IV-1. For the space group $P2_1/c$, the positions of the atoms are,

(0,0,0) and (0, 1/2, 1/2)

Table IV-1

Crystal structure parameters of tetrahydrate acetates of magnesium, cobalt and nickel.

	a Å	b Å	c Å	β	M-O(W_1) Å	M-O(W_2) Å	M-O (carboxyl)	Refs.
MgAc	4.75	11.79	8.52	94°54'	2.07	2.08	2.11	(16)
CoAc	4.77	11.85	8.42	94°30'	2.06	2.11	2.12	(15)
NiAc+	4.75	11.77	8.44	96°36'	2.06	2.11	2.12	(15)
	(4.746)	(11.711)	(8.425)	(93°36')	(2.048)	(2.081)	(2.067)	

+ Parameters in parentheses are from Ref. (17).

for Ni, Co or Mg atoms, and

$\pm$ (x, y, z ; x, 1/2-y, z + 1/2)

for other atoms and molecules.

The monoclinic structure of $M(CH_3COO)_2.4H_2O$ (M=Mg,Co or Ni), projected along its a-axis, is shown in Fig. IV-1. In this structure each cation, M^{2+}, is surrounded by a distorted octahedron of four water molecules and two oxygens of the two different carboxyl groups. The distances of these six oxygen ligands are given in Table IV-1 alongwith the unit cell dimensions.

RESULTS AND DISCUSSION:

Angular variation studies of the EPR spectra of Mn^{2+} in single crystals of MgAc, CoAc and NiAc show that Mn^{2+} ions occupy the two magnetically inequivalent Mn^{2+} sites. The principal axes of the two inequivalent complexes have been obtained by getting the extrema in fine structure spreads. The EPR spectra at 300 K and at 77 K for the Zeeman field, H, along the Z-axis of one set of equivalent M^{2+} complexes in MgAc are shown in Fig. IV-2. The corresponding spectra in NiAc and in CoAc at 300 K and 77 K are shown in Figs. IV-3 and 4, respectively. The observed angular variation of the spectra can be described by an orthorhombic spin-Hamiltonian. The EPR spectra have been analysed for spin-Hamiltonian

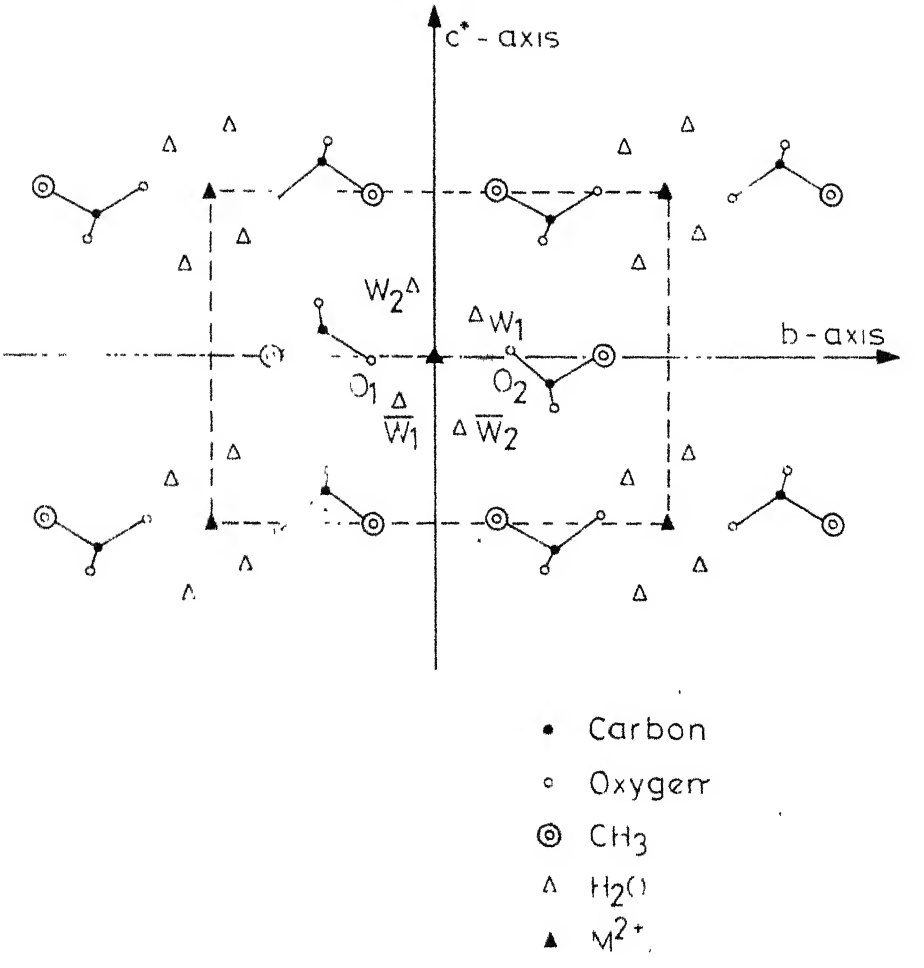

Fig IV.1: Projection of the atoms in the bc* plane for crystals of tetrahydrate acetates of Mg, Co and Ni. Here c*-axis is perpendicular to both a-and b-axes. W_1, W_2, $\overline{W}_1$ and W_2 are the water molecules and O_1 and O_2 are the oxygens of the two acetate groups.

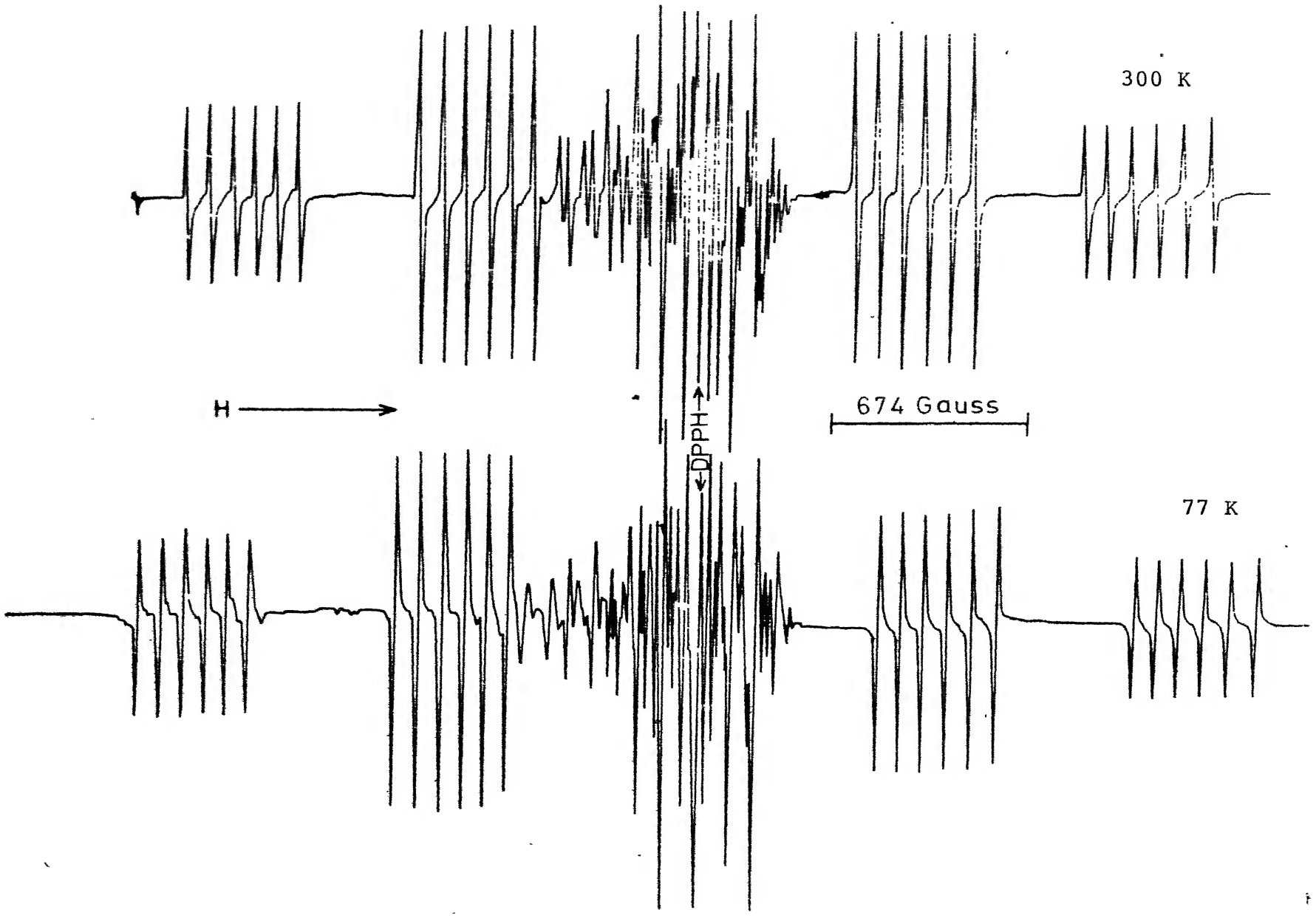

Fig.IV-2: The EPR spectra of Mn^{2+} in $Mg(CH_3COO)_2.4H_2O$ at 300 K and at 77 K for H along the Z-axis of one set of equivalent Mn^{2+} complexes.

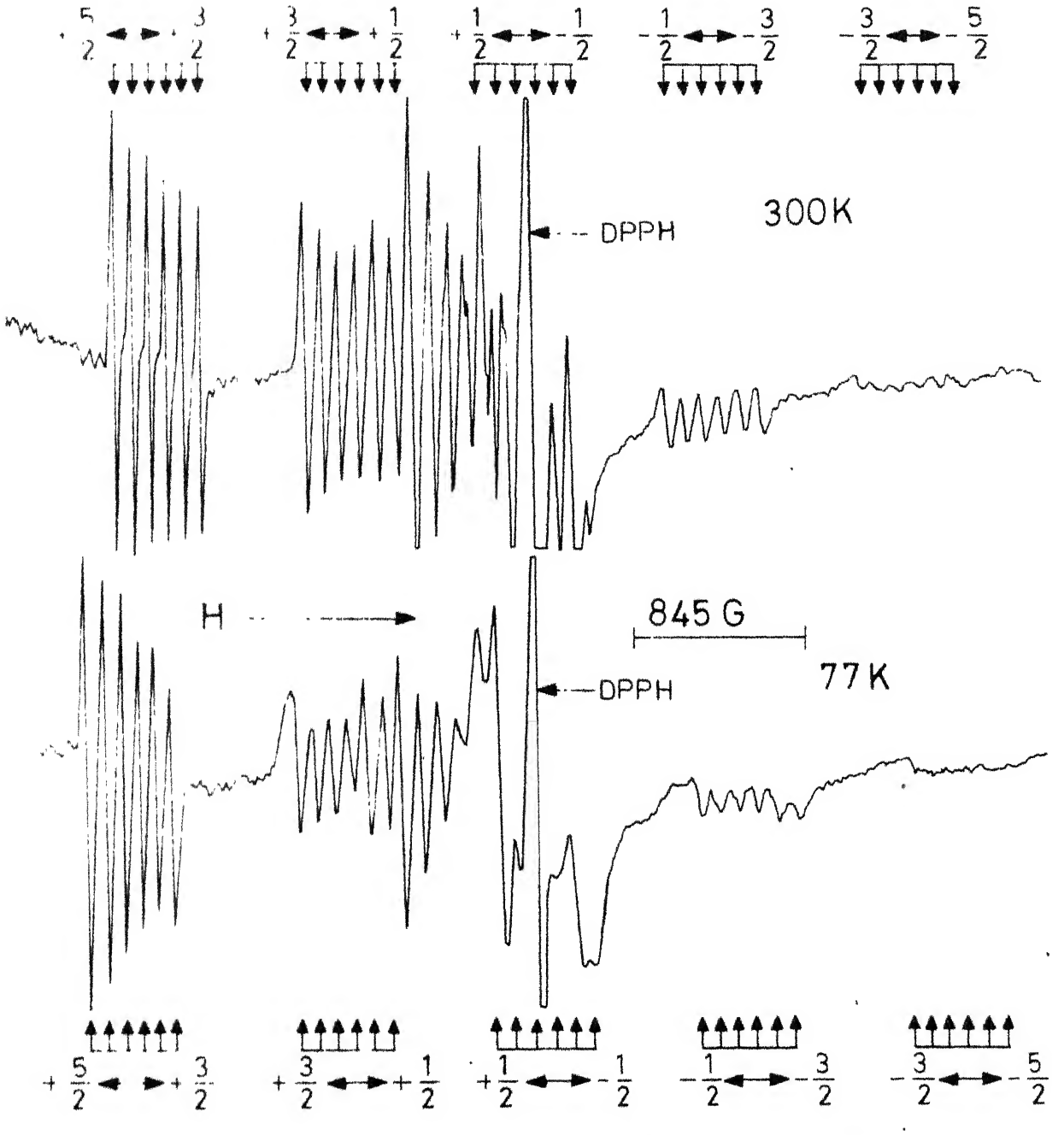

Fig. IV-3: The EPR spectra of Mn^{2+} in $Ni(CH_3COO)_2 \cdot 4H_2O$ at 300K and at 77K for H along the Z-axis of one set of equivalent Mn^{2+} complexes.

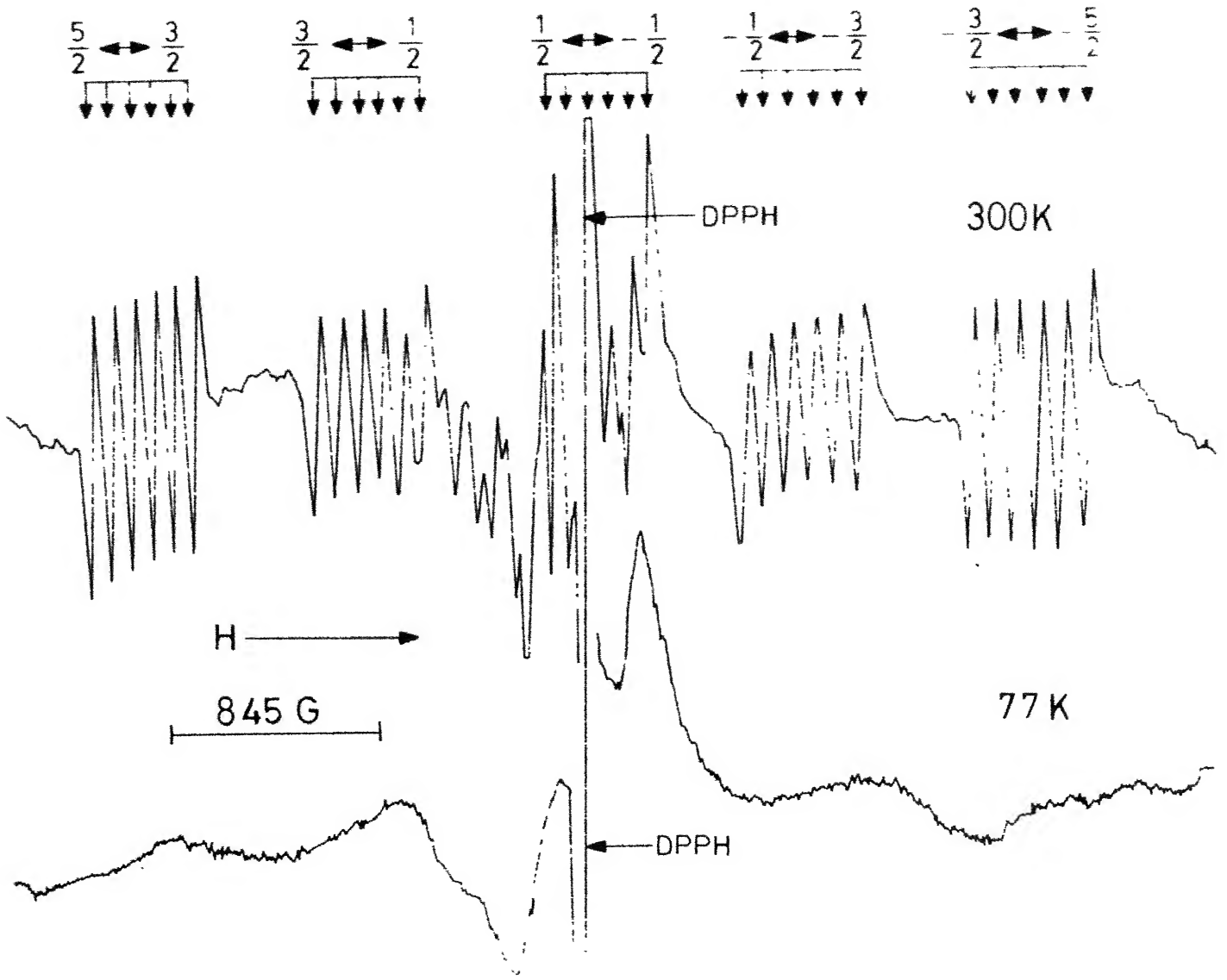

Fig. IV_4: The EPR spectra of Mn^{2+} in $Co(CH_3COO)_2 \cdot 4H_2O$ at 300K and at 77K for H along the Z-axis of one set of equivalent Mn^{2+} complexes.

parameters (the details of analysis are given in Chapter II-B) and the best-fit parameters, thus obtained, are listed in Table IV-2.

A comparative study of the EPR spectra of Mn^{2+} doped in MgAc, CoAc and NiAc reveals no appreciable differences in the general properties of the Mn^{2+} complexes, like the strength and symmetry of the crystal field at Mn^{2+} site, the angle between the Z-axes of the two inequivalent complexes, etc. As the crystal field parameters and the angles between the Z axes of the two inequivalent complexes are very nearly the same in the three hosts, it can be concluded that the ligand coordination around the divalent cation is almost the same in MgAc, CoAc and NiAc. Also it has been found that Mn-W_1 (see Fig. IV-1) forms the Z-axis of the distorted octahedron of four water molecules and two oxygens surrounding the Mn^{2+} ions substituting for M^{2+} ions.

On going down to 77 K the dominant crystal field parameter 'D' is found to increase by about the same amount in all the three hosts, due likely to the shrinkage of lattice at lower temperatures. On going above 300 K, no appreciable change is observed till only a six line spectrum is observed at $\sim$ 400 K due to dehydration of the crystals. A decrease in the leakage current and an imbalance in the AFC meter are observed at $\sim$400 K due to change in the Q of the cavity resulting from the dehydration of the crystals.

Table IV-2

Spin-Hamiltonian parameters (non-Zeeman parameters are in units of $10^{-4}cm^{-1}$) of Mn^{2+} in single crystals of tetrahydrate acetates of magnesium, cobalt and nickel at X-band.

Crystal	Temperature	g_z	L	|E|	a	A	B	Ref.
MgAc	300 K	2.0069±0.003	-403±2	63±10	-8±1	-85±1	-90±2	(4)
		2.003 ±0.003	+401±2	65±10	-6.5±1	-84±1	-89±10	(PW)
	77 K	1.9986±0.005	-448±3	77±14	-12 ±1	-84±1	-90±2	(4)
		2.000 ±0.005	+447±4	75±10	-10 ±1	-83±1	-89±10	(PW)
NiAc	300 K	1.996 ±0.005	431±5	84±10	-	-84±5	-84±10	(6)
		1.997 ±0.005	423±5	56±10	6.5±2	-83±5	-84±10	(PW)
	77 K	1.980 ±0.005	466±5	46±10	7.4±2	-82±5	-83±10	(PW)
CoAc	300 K	1.998 ±0.005	417±5	55±10	7.5±2	-83±5	-84±10	(PW)
	77 K	The spectrum gets completely broadened out leaving a band at the center.						(PW)

(PW) = Present Work

In addition to the aforesaid similarities, there are certain distinct features observed in the EPR of Mn^{2+} in CoAc and NiAc. These additional features are a negative shift in the g_z-value and typical linewidth variations. We will now discuss these features in CoAc and NiAc separately.

$Ni(CH_3COO)_2.4H_2O:Mn^{2+}$

Janakiraman and Upreti[6] reported the EPR of Mn^{2+} doped in NiAc at 300 K. They observed a negative shift in the Mn^{2+} g_z-value from the free spin value and a monotonic increase in the width+ of Mn^{2+} resonance lines with the intensity of the Zeeman field. We have carried out the EPR studies of Mn^{2+} doped in NiAc at 300 K and at 77 K. In addition we have carried out a temperature variation study from ~ 400 K down to 77 K. We found that the linewidths and their behavior remain unchanged on going to lower temperatures upto 77 K. However, the negative shift in the g_z-value gets enhanced at 77 K (see Table IV-2). The observed features can be explained to be due to the magnetic interactions between Mn^{2+} and the host Ni^{2+} ions following Moriya et al.[18] and Hutchings et al.[19] alongwith the spin quenching idea, discussed in Chapter II-C. There is no appreciable change on going above 300 K till the dehydration temperature.

+ Width or linewidth in the present thesis is used for the peak-to-peak width of the first derivative resonance lines.

linewidths in paramagnetic CoAc. Same type of linewidth variation has been reported by Sharma[21] in the EPR spectra of Gd^{3+} (S-state ion like Mn^{2+}) doped in some paramagnetic rare earth trifluorides at 300 K.

In principle, the study of widths and shapes of EPR lines can be used to understand the interactions between the various ions involved. For a multilevel ion, like Mn^{2+}, it is theoretically expected that the lineshapes will depend in a complicated way upon the relaxation transition probabilities between various levels.[22] Further, Mn^{2+} has hyperfine structure, so it is difficult to interpret Mn^{2+} lines precisely. However, there are two features of Mn^{2+} lines in CoAc distinct from those in MgAc at 300 K viz. much larger linewidths and the increase of linewidths as one goes from outer fine structure groups $\pm 5/2 \leftrightarrow \pm 3/2$ towards the central group $+1/2 \leftrightarrow -1/2$. The presence of a net magnetic moment on Co^{2+} at 300 K is known from other magnetic studies.[7-10] The large width of Mn^{2+} resonance lines is due likely to the fluctuating magnetic field created by the Co^{2+} magnetic moment. The unusual variation in Mn^{2+} linewidths with various fine structure groups may be due to an unequal influence of exchange interaction upon various $\Delta M = \pm 1$ transitions of Mn^{2+}.

On lowering the temperature of the crystal, it is found that the linewidths of all the Mn^{2+} fine structure groups increase so rapidly that the well resolved spectrum of Mn^{2+} completely broadens out at 135 ± 5 K leaving just a broad band at the centre (See Fig. IV-4). On raising the temperature again the well resolved spectrum reappears indicating that the smearing out of the spectrum is due to increased linewidths. This has further been confirmed by lowering the temperature in steps and measuring the linewidths (See Table IV-3). For Mn^{2+} severe line broadening and its striking temperature dependence due to the presence of Co^{2+} ions have also been observed in the paramagnetic state of $RbMnF_3$.[23] Co^{2+} ion being a fast relaxing one as compared to Mn^{2+} or Ni^{2+} ions appears to be responsible for the highly temperature dependent linewidth effects.

This unusual temperature dependence of linewidths can also be described, following Mitsuma[24], assuming narrowing at 300 K by a model similar to that used in the case of narrowing by exchange interaction.[25] The model (as described in Chapter II-C) is that the interactions between Mn^{2+} and Co^{2+} ions (dipolar interaction, exchange interaction etc.) are randomly modulated by rapid spin-lattice relaxation of Co^{2+} ions. At 300 K the spin-lattice relaxation time (T_1) of Co^{2+} host ions is fast enough to average out the dipolar interaction resulting in the narrowing of Mn^{2+} lines. On

Table IV-3

Widths of EPR lines and corresponding estimated values of $T_1(Co^{2+})$ at various temperatures for Mn^{2+} doped in single crystals of $Co(CH_3COO)_2.4H_2O$.

Temperature K	$\pm 5/2 \longleftrightarrow \pm 3/2$ Linewidths in gauss	fine group $T_1(Co^{2+})$ 10^{-12}sec.	$\pm 3/2 \longleftrightarrow \pm 1/2$ Linewidths in gauss	fine group $T_1(Co^{2+})$ 10^{-12}sec.
373	22.5±2	6.5±0.6	33.0±2	9.5±0.6
353	22.5±2	6.5±0.6	34.0±2	9.7±0.6
333	24.5±2	7.0±0.6	35.0±2	10.0±0.6
300	27.5±2	7.9±0.6	36.0±2	10.3±0.6
273	30.0±2	8.6±0.6	38.0±2	10.9±0.6
253	33.0±2	9.5±0.6	41.0±2	11.7±0.6
233	34.0±2	9.7±0.6	42.0±3	12.0±0.9
213	37.0±3	10.6±0.9	45.5±4	13.0±1.1
193	42.0±3	12.0±0.9	50.0±5	14.3±1.4
173	43.0±4	12.3±1.1	53.0±5	15.2±1.4

lowering the temperature Co^{2+} T_1 increases and, therefore, is not able to average out the dipolar interaction as effectively as at higher temperatures. This will result in a broadening of Mn^{2+} lines. The increase of linewidth with decreasing temperature and consequent complete broadening of the spectrum at $\sim$135 K are what we have observed in Mn^{2+} doped CoAc. This temperature dependence of linewidths is the identifying feature of the host spin-lattice relaxation narrowing effect in Mn^{2+} doped CoAc. Further, when the conditions for the narrowing are in effect, the impurity linewidth reflects the host T_1 (here Co^{2+}). Using Mitsuma's formula, as described in Chapter II-C by Eq. (II.43), we have calculated T_1 of Co^{2+} in CoAc at various temperatures. Taking g-value of Co^{2+} in CoAc to be 4.5,[8,9] and calculating n, the density of spins per c.c., from the crystallographic data,[15] H_d is calculated to be 305 G. Using this value of H_d, the calculated T_1 values of Co^{2+} at various temperatures are listed in Table IV-3 alongwith the linewidths of Mn^{2+}.

The magnitude of the g-value of Mn^{2+} in CoAc along the principal Z-axis is less than the free spin g-value. In the case of EPR of Mn^{2+} in MgAc[4] at 300 K the g_z-value was observed to be 2.0069, larger than the free spin-value. CoAc is isomorphous with MgAc, and one expects the same magnitude of zero field splitting of Mn^{2+} in this case also

(which is really the case) and a corresponding positive shift in the g_z-value. The negative shift in the g_z-value is, most probably, due to Co^{2+}, which produces a local static magnetic field at Mn^{2+} ions. Hence, if we assume that the shift in the g_z-value in CoAc from that in MgAc is purely due to Co^{2+}, the local field at Mn^{2+} is $\sim$12 G for Zeeman field along the Z-axis of one set of equivalent Mn^{2+} complexes.

REFERENCES

1. H. Abe and H. Morigaki, 'Paramagnetic Resonance', (Ed.W.Low) Vol. 2, p. 567, Academic Press, New York (1963).

2. D.J.E. Ingram, Proc. Phys. Soc. A66, 412 (1953).

3. J.A. Cowen and G.T. Johnston, J. Chem. Phys. 44, 2217 (1966).

4. T.J. Manakkil, Ph.D. Thesis, New Mexico State University Las Cruces (1967).

5. M.V. Krishnamurthy, Z. Phys. Chemie, Leipzig 254, 17 (1973)

6. R. Janakiraman and G.C. Upreti, J.Chem. Phys. 54, 2336 (1971).

7. B.C. Guha, Nature 184, 50 (1959).

8. R.B. Flippen and S.A. Friedberg, Phys. Rev. 121, 1591 (1961).

9. S.A. Friedberg and J.T. Schriempf, J.Appl.Phys. 35, 1000 (1964).

10. A. Mookherji and S.C. Mathur, Physica 31, 1547 (1965).

11. A. Mookherji and S.C. Mathur, ibid. 31, 1540 (1965).

12. L.G. Polgar and S.A. Friedberg, Phys. Rev. B6, 3497 (1972).

13. P.A. Narayana, A. Mehra and P. Venkateswarlu, Can.J. Phys. 46, 1705 (1968).

14. P.A. Narayana, A. Mehra and P. Venkateswarlu, ibid, 46, 325 (1968).

15. J.N. van Niekerk and F.R.L. Schoening, Acta Crystallogr. 6, 609 (1953).

16. J. Shankar, P.G. Khubchandani and V.M. Padmanabhan, Proc. Indian Acad. Sci. A 45, 117 (1957).

17. T.C. Lownie, W. Harrison, E.S. Raper and M.A. Hepworth, Acta Crystallogr. B27, 706 (1971).

18. T. Moriya and Y. Obata, J. Phys. Soc. Japan 13, 1333 (1958).

19. M.T. Hutchings and W.P. Wolf, Phys. Rev. Lett. 11,187 (1963).

20. W.B. Mims and R. Gillen, Phys. Rev. 148, 438 (1966).

21. V.K. Sharma, J. Chem. Phys. 54, 496 (1971).

22. See, for example, A.E. Siegman, 'Microwave Solid State Masers', p. 171 ff, McGraw-Hill, New York (1964).

23. J.E. Gulley and V. Jaccarino, Phys. Rev. B6, 58 (1972).

24. T. Mitsuma, J. Phys. Soc. Japan 17, 128 (1962).

25. P.W. Anderson and P.R. Weiss, Rev. Mod. Phys. 25,269 (1953) R. Kubo and K. Tomita, J. Phys. Soc. Japan 9, 888 (1954).

CHAPTER V

ELECTRON PARAMAGNETIC RESONANCE OF Mn^{2+} IN SOME TUTTON SALTS

ABSTRACT

EPR investigations have been carried out in Mn^{2+} doped isomorphous single crystals of $MK_2(SO_4)_2 \cdot 6H_2O$, Tutton salts, where M = Co, Fe, Mg and Zn, at 300 K and at 77 K and at X-band. In addition, EPR of Mn^{2+} doped single crystals of $Ni(NH_4)_2(SeO_4)_2 \cdot 6H_2O$ has also been studied at 300 K. Mn^{2+} has been found to substitute for divalent cations exhibiting two magnetically inequivalent complexes. The EPR spectra have been analysed using a spin-Hamiltonian of orthorhombic symmetry. The additional features observed in the EPR spectra of Mn^{2+} in paramagnetic hosts have been attributed to the magnetic interactions between Mn^{2+} and the paramagnetic host ions.

INTRODUCTION:

Tutton salts have been studied by EPR since the early days[1,2] mainly in salts with Ni^{2+} and Cu^{2+} divalent cations[3-6] and in Mn^{2+} doped single crystals of ammonium Tutton salts, viz. $M(NH_4)_2(SO_4)_2.6H_2O$ where M = Mg,Zn,Co,Fe,Ni and potassium nickel Tutton salt, $NiK_2(SO_4)_2.6H_2O$.[7-14] In addition, a number of other transition ions, such as Cu^{2+}, VO^{2+}, V^{2+}, Cr^{3+} and Co^{2+}, have also been studied by doping these in various Tutton salts.[15-19] This chapter contains the results of our EPR studies on Mn^{2+} doped single crystals of four potassium-metal Tutton salts, $MK_2(SO_4)_2.6H_2O$, where M = Co,Fe,Mg and Zn, hereafter to be referred to as CPSH, FPSH, MPSH and ZPSH, respectively and ammonium nickel selenate Tutton salt, $Ni(NH_4)_2(SeO_4)_2.6H_2O$, abbreviated as NASeH.

CRYSTAL STRUCTURE:

CPSH, FPSH, MPSH, ZPSH and NASeH belong to a family of isomorphous compounds, known as Tutton salts. The general chemical formula of a Tutton salt is of the form $M''M'_2(XO_4)_2.6H_2O$, where M'' is a divalent cation (Mn^{2+}, Fe^{2+}, Co^{2+}, Ni^{2+}, Cu^{2+}, Zn^{2+}, Mg^{2+} or Cd^{2+}), M' is a monovalent ion (NH_4^+, K^+, Rb^+, Cs^+ or Tl^+) and X is S or Se. The unit cell of the Tutton salts is monoclinic and contains two molecules related by the space group operation $P2_1/a$.[20-21] The

projection of the unit cell of one of the Tutton salts, viz. $Mg(NH_4)_2(SO_4)_2.6H_2O$, along its c_o axis is shown in Fig. V-1. The divalent cations are situated at the positions (0,0,0) and (1/2, 1/2, 0) in the unit cell, while the other atoms and molecules are at $\pm$ (x,y,z) and $\pm$ $(x + \frac{1}{2}, \frac{1}{2} - y, z)$. The divalent cation is surrounded by a distorted octahedron of six water molecules. Of the many compounds of this family, the detailed crystal structure has been studied only for a few members. To the best of our knowledge no detailed crystal structure studies are available for these particular members, viz. CPSH, FPSH, MPSH, ZPSH and NASeH. Among these the unit cell dimensions of only MPSH, given below, are available.[20]

$a = 9.06$ Å $\quad b = 12.26$ Å $\quad c = 6.107$ Å and

$\beta = 104^{\circ}48'$

RESULTS AND DISCUSSION:

The observed spectra of Mn^{2+} and their angular variation in CPSH, FPSH, MPSH, ZPSH and NASeH single crystals show that Mn^{2+} ions substitute the two magnetically inequivalent metal ion sites in the unit cell. The principal axes of the two identical, but differently oriented, Mn^{2+} complexes have been found by obtaining the extrema in the fine structure spreads. The EPR spectra at 300 K for Zeeman field, H, along the Z-axis of one set of equivalent Mn^{2+} complexes in CPSH,

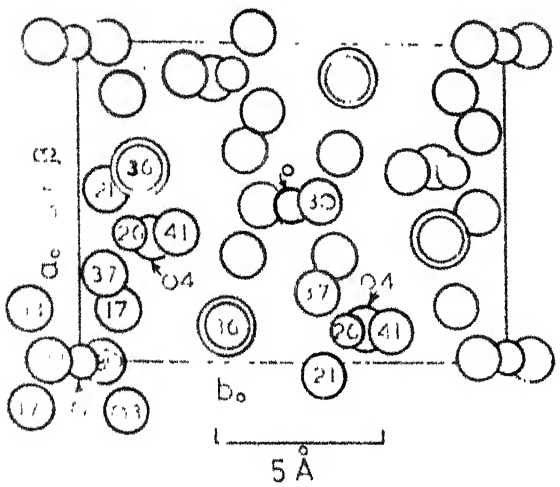

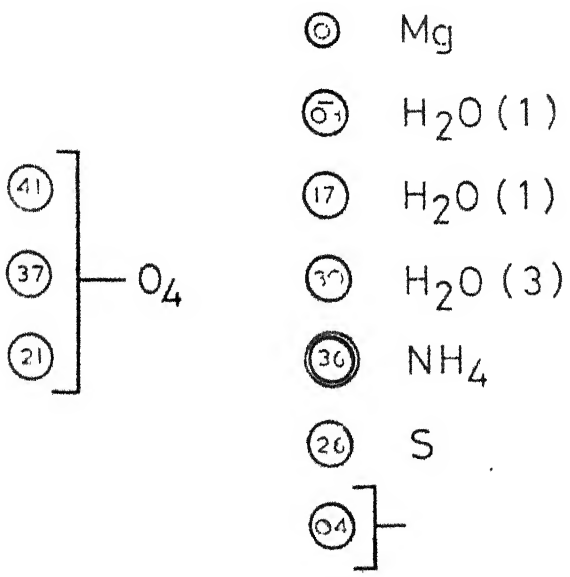

Fig. V-1 The monoclinic crystal structure of $Mg(NH_4)_2(SO_4)_2 \cdot 6H_2O$ projected along its c_o axis. The numbers inside the circles represent the positions of the atoms or molecules along the c_o axis in units of the unit cell dimension along the c_o axis (100 = 6.11 Å). For the other molecule of the unit cell, the positions of Mg and $H_2O(3)$ are given.

FPSH and MPSH are shown in Fig. V-2. The corresponding spectra at 77 K are shown in Fig. V-3. Fig. V-4 shows the corresponding spectra of Mn^{2+} at 300 K and 77 K in ZPSH, while Fig. V-5 shows the Mn^{2+} spectra in NASeH at 300 K for H along and at different angles from the Z-axis of one set of equivalent Mn^{2+} complexes. In all the cases, the Mn^{2+} spectra and their angular variation can be described by a spin-Hamiltonian of orthorhombic symmetry. All the EPR spectra have been analysed and the best-fit parameters, thus obtained, are listed in Table V-1 alongwith those for some other Tutton salts for comparison. Now we will describe our results and their discussion on these five Tutton salts in two parts. First part will contain the comparative EPR study of Mn^{2+} doped single crystals of four potassium-metal Tutton salts, viz. CPSH, FPSH, MPSH and ZPSH, while in the second part we discuss our EPR results of Mn^{2+} doped NASeH single crystals.

(a) Comparative EPR Study of Mn^{2+} Doped CPSH,FPSH,MPSH and ZPSH

A comparison of the EPR results of Mn^{2+} in CPSH, FPSH, MPSH and ZPSH single crystals reveals no appreciable differences in the general properties of the magnetic complexes, viz. the strength and symmetry of the crystalline field at Mn^{2+} sites, the angle between the Z axes of the two magnetically inequivalent complexes etc. From these nearly same general

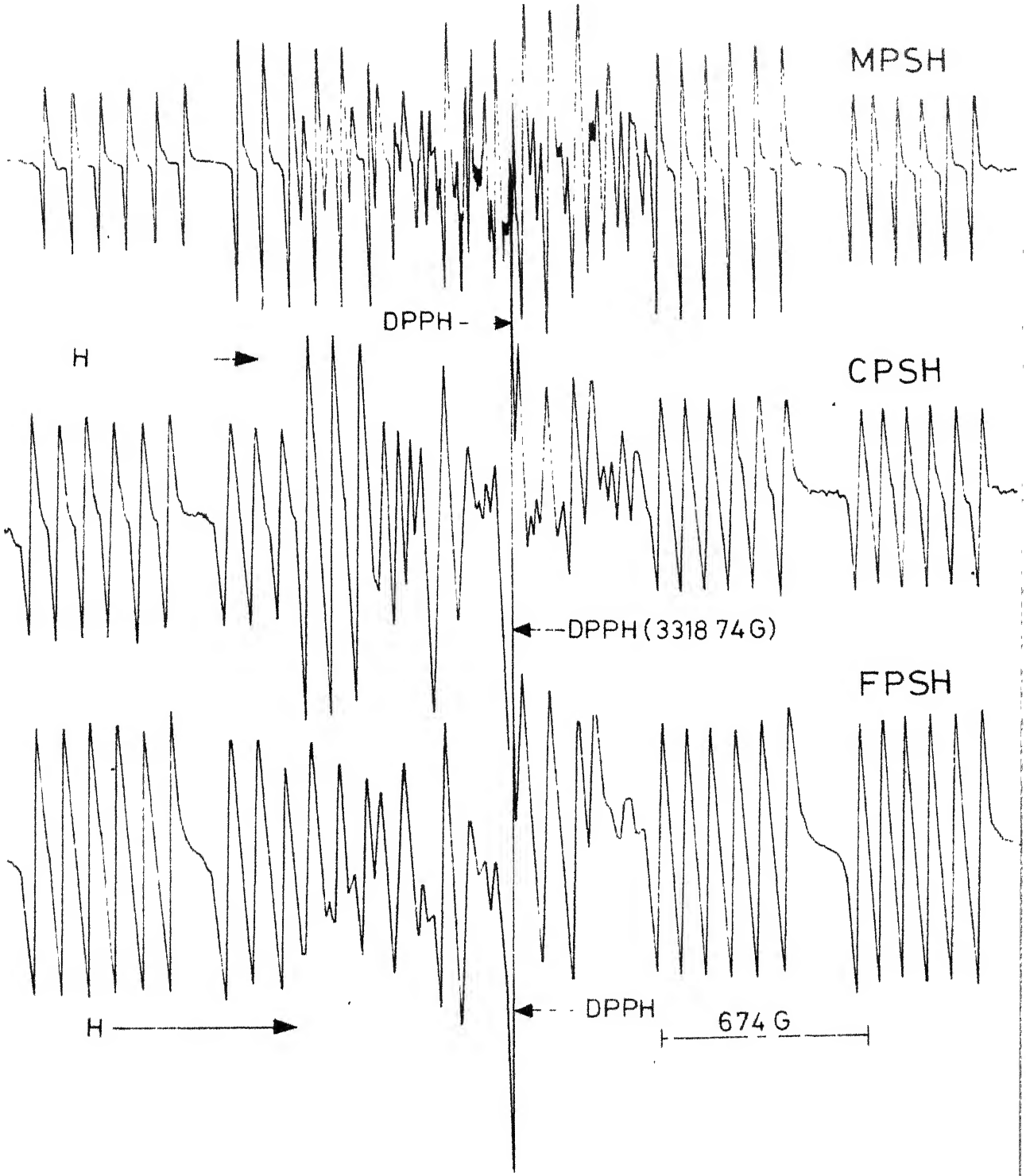

Fig.V-2: The EPR spectra of Mn^{2+} IN MPSH, CPSH and FPSH at 300 K for H along the Z-axis of one set of equivalent Mn^{2+} complexes.

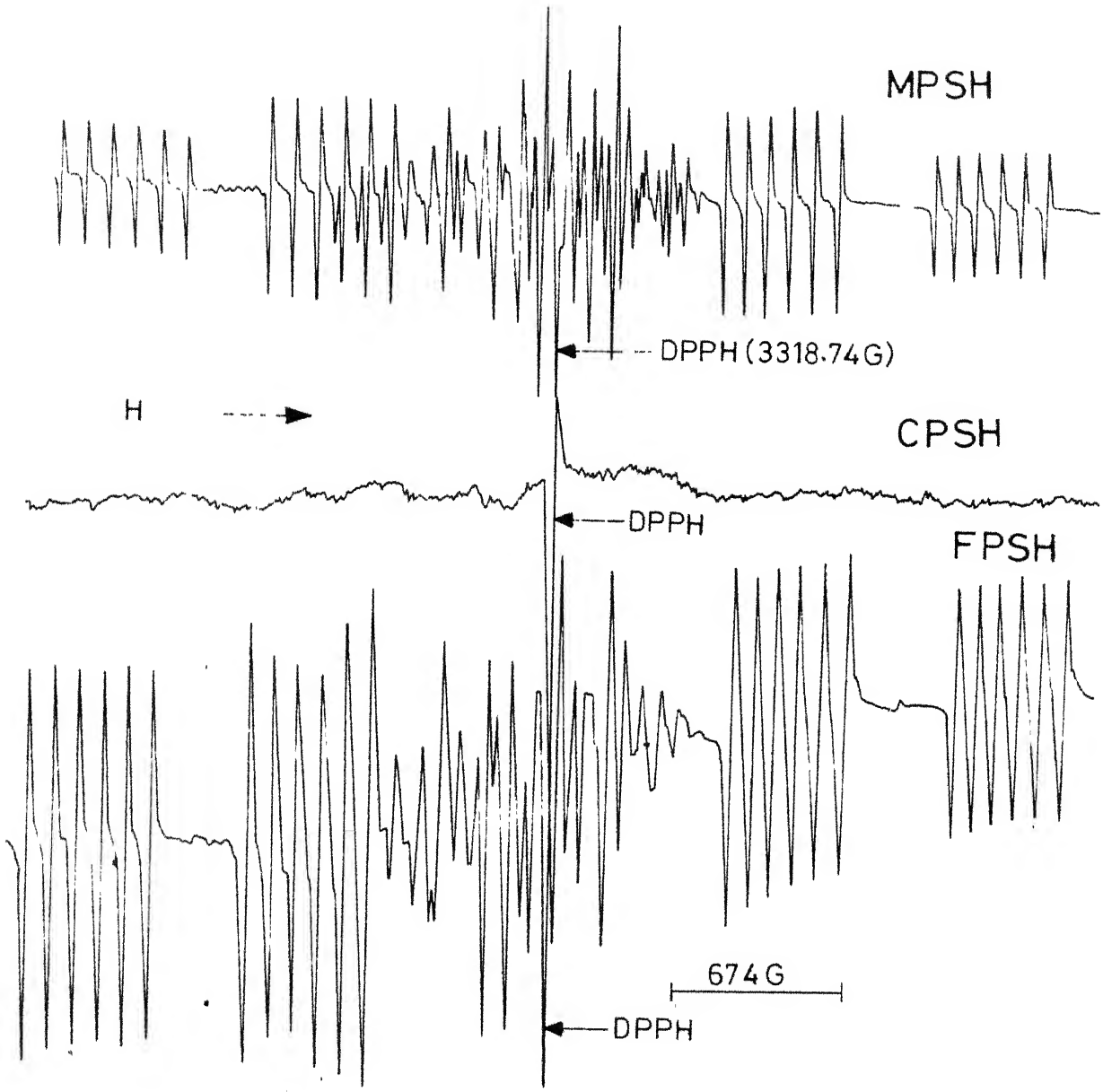

Fig.V-3: The EPR spectra of Mn^{2+} in MPSH, CPSH and FPSH at 77 K for H along the Z-axis of one set of equivalent Mn^{2+} complexes.

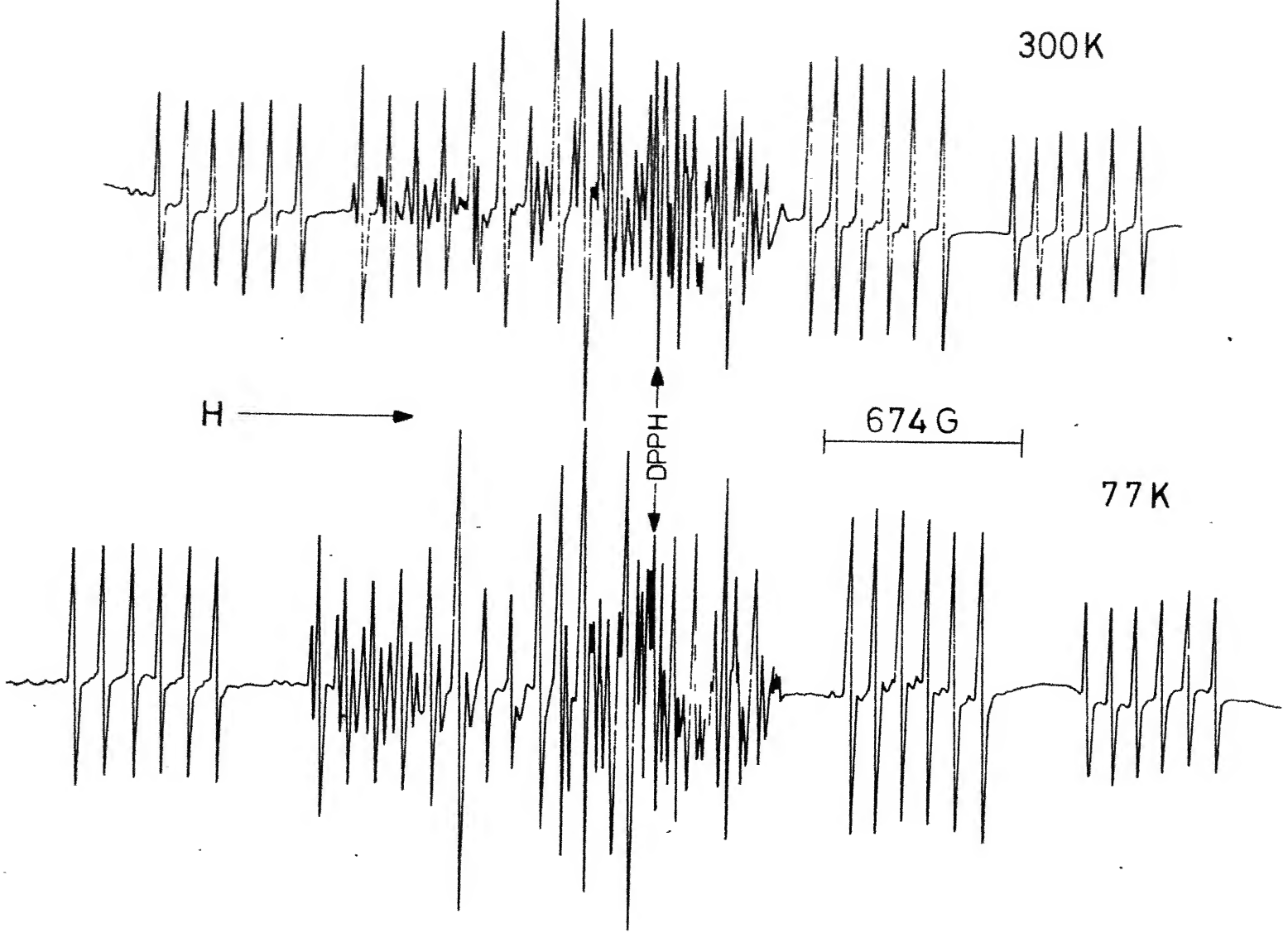

Fig. V-4 : The EPR spectra of Mn^{2+} in ZPSH at 300K and at 77K for H along the Z-axis. of one set of equivalent Mn^{2+} complexes.

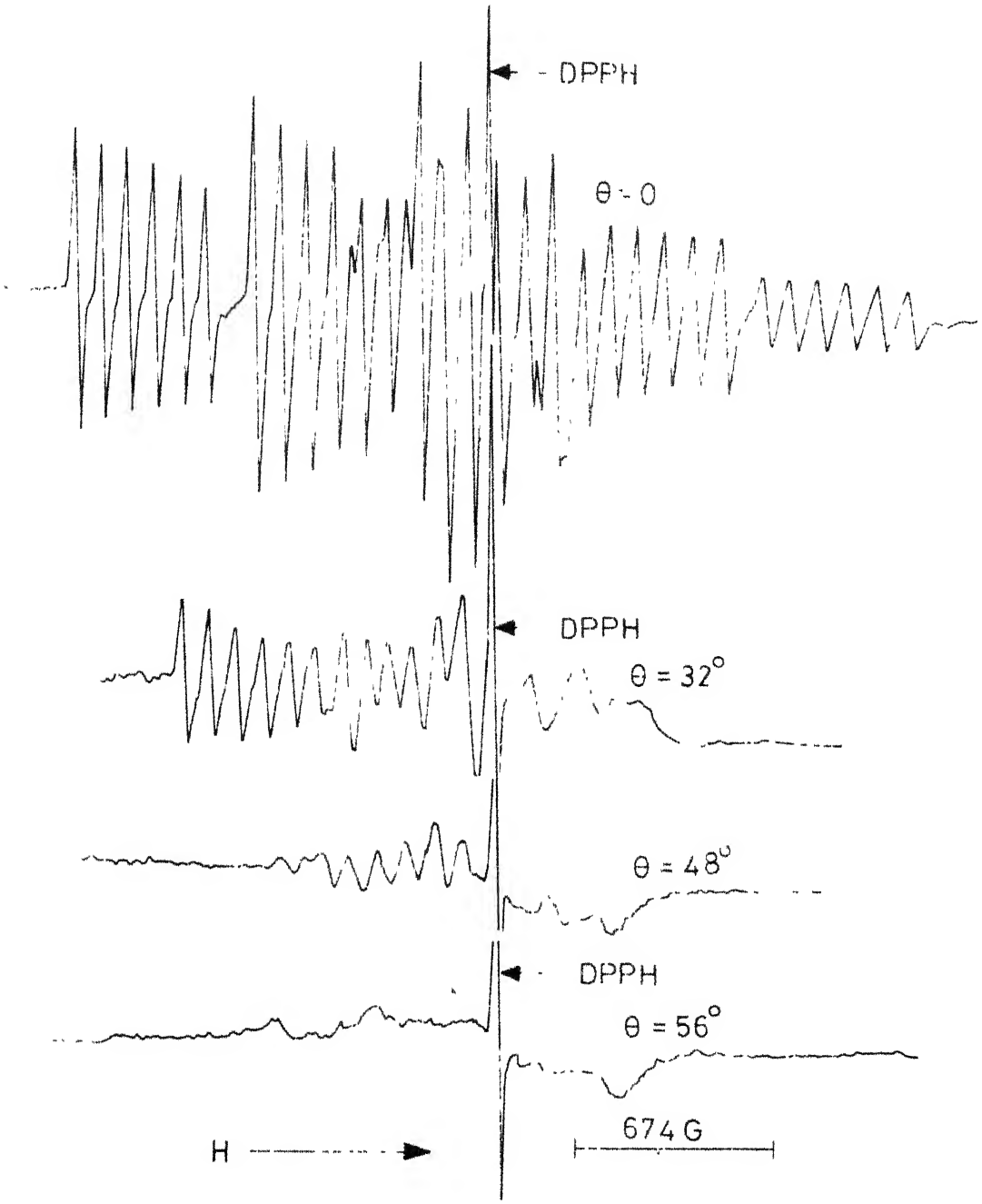

Fig.V-5: The EPR spectra of Mn^{2+} in $Ni(NH_4)_2(SeO_4)_2.6H_2O$ at 300 K for H along and at different angles from the Z-axis of one set of equivalent Mn^{2+} complexes.

Table V-1

Spin-Hamiltonian parameters (non-Zeeman parameters are in units of 10^{-4} cm^{-1}) of Mn^{2+} in single crystals of some potassium and ammonium tutton salts.

Crystal	Temp.	g_z	D	A	a	F	B	Ref.
$MgK_2(SO_4)_2.6H_2O$	300 K	2.001±0.003	-343±3	-87±2	11±1	62±10	-86±5	(PW)
	77 K	2.004±0.003	-410±3	-88±2	12±1	52±10	-86±5	(PW)
$ZnK_2(SO_4)_2.6H_2O$	300 K	2.005±0.003	-348±3	-87±2	10.3±1	47±10	-87±5	(PW)
	77 K	1.998±0.003	-411±3	-87±2	10.3±1	56±10	-86±5	(PW)
$CoK_2(SO_4)_2.6H_2O$	300 K	2.004±0.003	-350±3	-87±2	10.3±1	40±10	-86±5	(PW)
	77 K	The spectrum gets completely broadened out.						(PW)
$FeK_2(SO_4)_2.6H_2O$	300 K	2.003±0.003	-349±3	-87±2	10.3±1	40±10	-89±5	(PW)
	77 K	2.004±0.003	-435±3	-87±2	11.2±1	56±10	-89±5	(PW)
$Fe(NH_4)_2(SO_4)_2.6H_2O$	300 K	2.004±0.001	-232.5 ±0.5	-87.8 ±0.5	-	45±5	-90.8±5	(12)
$Co(NH_4)_2(SO_4)_2.6H_2O$	300 K	2.005±0.001	-231.2 ±1	-86±1	-	65.5±1	-90.3±1	(13)
$Zn(NH_4)_2(SO_4)_2.6H_2O$	290 K	2.000±0.005	238	91	5	70	-	(9)
	90 K	-	275±5	-89±1	7±1	70±10	-	(7)

Crystal	Temp.	g_z	D	A	a	E	B	Ref.
$Mg(NH_4)_2(SO_4)_2.6H_2O$	290 K	-	231±2	90±2	3	60	-	(8)
$NiK_2(SO_4)_2.6H_2O$	300 K	g_x=1.976 ±0.002	-422.5	-	-	38.7	A_x = -88.6	(14)
$Ni(NH_4)_2(SO_4)_2.6H_2O$	300 K	g_x=1.992 ±0.002	-309.7	-	-	45.6	A_x = -89.3	(14)
$Ni(NH_4)_2(SeO_4)_2.6H_2O$	300 K	1.996±0.001	274±2	-86±2	5.6±2	-42±5	-87±5	(PW)
$Zn(NH_4)_2(SeO_4)_2.6H_2O$	300 K	2.005±0.001	264.9 ±4	-88.6±2	5.28	-51.4±5	-86.6±2	(28)
$Mg(NH_4)_2(SeO_4)_2.6H_2O$	300 K	2.002±0.001	248.6 ±4	-87.8±2	5.79	-60.8±5	-87.5±2	(28)
$MgRb_2(SeO_4)_2.6H_2O$	300 K	2.006±0.001	-296.5 ±2	-88±2	8.61	68±5	-86.8±2	(28)
$ZnRb_2(SeO_4)_2.6H_2O$	300 K	2.005±0.001	-301.6 ±2	-88.8±2	9.06	63±5	-89±2	(28)

(PW) = Present Work

properties of Mn^{2+} complexes, it can be qualitatively concluded that the ligand coordination around the divalent cation is almost the same in all the four systems. Further on lowering the temperature of the crystals down to 77 K, the dominant crystal field parameter 'D' is found to increase by about the same amount in all the four hosts. This behavior of 'D' can be described in part due to the lattice shrinkage as well as assuming coupling with a dominant vibrational mode. The relative importance of the contributions due to thermal expansion and to lattice vibrations can not be assessed in the absence of hydrostatic pressure data and detailed data on temperature variation of 'D'. An interesting observation is a larger 'D' value for potassium salts than that for the corresponding ammonium salts (see Table V-1). At present we do not have any plausible explanation for this consistent observation. A detailed crystal structure study should provide complete information on the $M(H_2O)_6^{2+}$ octahedra in these Tutton salts, which may be helpful in understanding this observation.

On the other hand there are certain interesting but distinct features observed in the EPR of Mn^{2+} in CPSH and FPSH, where the host ions are rapid-relaxers (to the lattice). These additional features are unusual and typical widths of Mn^{2+} resonance lines at 300 K and at 77 K. We will now discuss the Mn^{2+} linewidths in ZPSH, MPSH, CPSH and FPSH.

$MgK_2(SO_4)_2.6H_2O:Mn^{2+}$ and $ZnK_2(SO_4)_2.6H_2O:Mn^{2+}$:

EPR studies in Mn^{2+} doped MPSH and ZPSH at 300 K as well as at 77 K show the usual features of Mn^{2+} spectra in diamagnetic hosts. Here the Mn^{2+} linewidths at 300 K and 77 K are ∿11G and ∿9 G, respectively. This linewidth is mainly due to the local magnetic fields of the proton nuclear moments in water molecules surrounding the magnetic ion in the form of a distorted octahedron. The EPR studies in some hydrated crystals have shown that this linewidth can be reduced by a factor of about 1/3 in deuterated crystals.[22] Further the intensity ratio among the different fine structure groups is found to be in accord with what is demanded by theory i.e. 5:8:9:8:5.

$CoK_2(SO_4)_2.6H_2O:Mn^{2+}$:

EPR investigation of Mn^{2+} doped CPSH single crystals has been carried out to observe the effect of the rapidly relaxing paramagnetic host Kramers Co^{2+} ions on the EPR of Mn^{2+}. From a comparison of the EPR results of Mn^{2+} in CPSH with those in isomorphous diamagnetic MPSH and ZPSH hosts, following differences have been observed:

(1) The widths of Mn^{2+} resonance lines in CPSH are much larger (∿20 G) than those encountered in ZPSH and MPSH hosts (∿ 11 G).

(2) A comparison at 300 K of the EPR spectrum of Mn^{2+} in CPSH with that in MPSH or ZPSH shows that the linewidths associated with various fine structure groups show an unusual variation (see Fig. V-2). Table V-2 lists the linewidths of various fine structure groups of the EPR spectrum of Mn^{2+} in CPSH for the Zeeman field, H, along the Z-axis of one set of equivalent Mn^{2+} complexes. It is clear from the above data that the linewidths increase as we go from outer fine structure groups towards the central group. The linewidths for the central group ($+ 1/2 \leftrightarrow -1/2$) could not be measured accurately due to the overlap of the spectrum due to the second magnetic complex. However, these have been estimated to be larger than the widths for the $\pm 3/2 \leftrightarrow \pm 1/2$ fine structure groups.

(3) In CPSH the widths of all the Mn^{2+} resonance lines increase rapidly on lowering the temperature of the crystal and a completely broadened out spectrum of Mn^{2+} is observed at 77 K (see Fig. V-3). On raising the temperature again the well resolved spectrum reappears indicating that the smearing out of the spectrum is due to increased linewidths on lowering the temperature.

Similar observations have also been reported in Mn^{2+} doped $Co(CH_3COO)_2.4H_2O$ single crystals[23] (see Chapter IV also). As explained earlier the large linewidths are due likely to the fluctuating magnetic field created by the cobalt magnetic

Table V-2

Linewidths of various fine structure groups of Mn^{2+} Complex, for which H||Z, in $CoK_2(SO_4)_2.6H_2O$ and $FeK_2(SO_4)_2.6H_2O$ Tutton salt single crystals at 300 K.

Crystal	Linewidths in gauss for $\pm 5/2 \leftrightarrow \pm 3/2$ fine groups	Linewidths in gauss for $\pm 3/2 \leftrightarrow \pm 1/2$ fine groups
CDSH	18 ± 2	22 ± 3
FDSH	22 ± 2	26 ± 3

moments. Further, the unusual variation of linewidths with various fine structure groups may be due to an unequal influence of exchange interaction upon the various $\Delta M = \pm 1$ transitions of Mn^{2+}. The highly temperature dependent behavior can be ascribed to the presence of fast relaxing Co^{2+} ions. The characteristic increase of Mn^{2+} resonance linewidths on lowering the temperature in CPSH indicates that host spin-lattice relaxation narrowing is operative. As a consequence, the spin-lattice relaxation time T_1 of the host Co^{2+} ions can be calculated from the linewidth of the impurity, Mn^{2+}. Using the expression (II.43), $T_1(Co^{2+})$ in CPSH is estimated to be $\sim 10^{-11}$ sec, of the same order as for Co^{2+} in other salts.[24,25] The linewidth of Mn^{2+}, used for these calculations, has been taken as the average of linewidths of all the fine structure groups for H along the Z-axis and the g-value of Co^{2+} is taken to be 4. As the unit cell parameters for CPSH are not known, those for MPSH have been used for the calculation of n.

$FeK_2(SO_4)_2.6H_2O:Mn^{2+}$:

EPR of Mn^{2+} in FPSH single crystals has been studied for the first time at 300 K and at 77 K to observe the effect of the rapidly relaxing paramagnetic host non-Kramers Fe^{2+} ions on the paramagnetic resonance of Mn^{2+}. Furthermore the Fe^{2+} ions in FPSH are accessible to study by microwave resonance only through their effect on impurity spectra because

their study by EPR has been discouraged due to large crystal field splittings.[26] From a comparison of the EPR results of Mn^{2+} in FPSH with those in isomorphous diamagnetic MPSH or ZPSH hosts at 300 K and at 77 K, the following differences have been observed:

(1) The widths of Mn^{2+} resonance lines at 300 K in FPSH are larger ($\sim$ 28 G) than those encountered in ZPSH and MPSH hosts ($\sim$ 11 G).

(2) The linewidths associated with various fine structure groups, for H along the Z-axis, increase as we go from outer fine structure groups towards the central group (see Table V-2). Here again the linewidths of the central group could not be measured accurately due to the overlap of the spectrum due to the second complex. However, these have been estimated to be larger than those for the $\pm 3/2 \leftrightarrow \pm 1/2$ fine structure groups.

(3) The widths of Mn^{2+} resonance lines on lowering the temperature of the crystal are found to decrease from $\sim$28 G at 300 K to $\sim$20 G at 77 K.

(4) The linewidths of Mn^{2+} at 77 K show magnetic field dependence. A monotonic increase of linewidths with the Zeeman field can be seen in Fig. V-3 (see also Table V-3).

Table V-3

The Zeeman-field intensity (H) and the corresponding linewidth (ΔH) of Mn^{2+} resonance lines for H || Z in $FeK_2(SO_4)_2 \cdot 6H_2O$ at 77 K.

H (gauss)	ΔH (gauss)
1324	13 ± 2
1526	14 ± 2
2105	15 ± 2
2436	18 ± 2
3356	19 ± 2
4047	21 ± 2
4404	21.5 ± 2
4935	22 ± 2
5275	23 ± 2

The above observations in Ferrous host have been reported for the first time. No such observations were reported in an earlier EPR study of Mn^{2+} doped in $Fe(NH_4)_2(SO_4)_2 \cdot 6H_2O$ (FASH) single crystals.[12] The reason may be the small value of 'D' due to which there will be a large overlap of the lines due to the two complexes even along the Z-axis. A careful study of Mn^{2+} spectrum along the Z-axis in FASH reveals the presence of feature (2) of FPSH. However, the Mn^{2+} linewidths in FASH are quite small ($\sim$ 10 G at 300 K) and show practically no magnetic field and temperature dependence from 300 K to 77 K.

There may be two causes for the observed resolved EPR spectrum of Mn^{2+} in FPSH: (1) rapid spin-lattice relaxation of Fe^{2+} ions and/or (2) large initial splitting of Fe^{2+} ions. Cause (1) can explain narrow lines at 300 K for Mn^{2+} in FPSH just as explained above for CPSH and earlier in Chapter II-C under host spin-lattice relaxation narrowing. However, on lowering the temperature the spin-lattice relaxation of Fe^{2+} must become slower and should result in an increase of Mn^{2+} linewidths. But our observations show that the Mn^{2+} lines in FPSH become narrower as one goes from 300 K ($\sim$28 G) to 77 K ($\sim$ 20 G). Therefore, either there is no appreciable change in Fe^{2+} T_1 on going upto 77 K or cause (1) is not effective in FPSH. For cause (2) the theory has been

elaborated by Moriya et al.[27] They have considered those paramagnetic host ions (e.g. Ni^{2+} and Fe^{2+}) for which the degeneracy of the spin-multiplet is completely lifted in the presence of an orthorhombic crystalline field and the spin moments are 'quenched' in the absence of the external magnetic field. Further the spin operator has no diagonal elements and thus there is no contribution to the linewidth of foreign ion (i.e. Mn^{2+}). On the switching of the external magnetic field, magnetic moments are induced on the ions owing to the polarization effect. These moments will contribute to the linebroadening of the foreign ion. This also yields the field dependence of the linewidth. However, the temperature dependence of Mn^{2+} linewidth in FPSH is expected only below liquid helium temperature, whereas an appreciable narrowing ($\sim$8 G), with decrease of temperature from 300 K down to 77 K, has been observed in our experiments. The width of Mn^{2+} resonance lines in the corresponding diamagnetic hosts decreases from $\sim$ 11 G at 300 K to $\sim$9 G at 77 K. The decrease in linewidths due to freezing of thermal vibrations on going to 77 K is thus expected to be only $\sim$ 2 G and can not explain the observed decrease of $\sim$8 G in FPSH. Thus the cause for this narrowing of lines on lowering the temperature is not clear. In addition our experiments in FPSH doped Mn^{2+} show a monotonic increase of linewidth with applied

field at 77 K. We have also reinvestigated FASH doped Mn^{2+} single crystals at 77 K to check this field dependence of linewidth. Practically no field dependence has been observed in FASH.

It is thus clear that the mechanisms, discussed above, are insufficient to explain all the observations regarding linewidths in Mn^{2+} doped FPSH single crystals. However, it is certain that these mechanisms contribute to linewidths but the discrepancies in the experimental and the theoretical results suggest the presence of some other mechanism contributing to the linewidth of Mn^{2+} in FPSH which should explain the narrowing of Mn^{2+} resonance lines on going from 300 K to 77 K.

(b) Mn^{2+} in $Ni(NH_4)_2(SeO_4)_2.6H_2O$(NASeH):

EPR of Mn^{2+} has been studied in NASeH crystals for the first time. A comparison of our EPR results of Mn^{2+} in NASeH with those in diamagnetic and isomorphous $Zn(NH_4)_2(SeO_4)_2.6H_2O$ and $Mg(NH_4)_2(SeO_4)_2.6H_2O$ single crystals[28] reveals no appreciable differences in the general properties of the Mn^{2+} complexes. From these nearly same general properties of the Mn^{2+} complexes, it can be qualitatively concluded that the ligand coordination around the divalent cations is almost the same in all the three cases.

The additional features observed in the EPR of Mn^{2+} in NASeH from those in other diamagnetic Tutton salts[7-9,28] can be summarized as follows:

(1) The widths of Mn^{2+} resonance lines show a magnetic field dependence. A monotonic increase of linewidths with the Zeeman field can be seen in Fig. V-5. Table V-4 lists the Zeeman field intensity and the corresponding width of Mn^{2+} resonance lines in NASeH.

(2) A large anisotropy in Mn^{2+} linewidth is observed in the EPR of Mn^{2+} in NASeH. In addition, a complete broadening and disappearance of Mn^{2+} spectrum is observed for Zeeman field, H, making an angle of $56^{\circ} \pm 5^{\circ}$ from the Z-axis in the ZX plane, as can be seen in Fig. V-5.

(3) The g_z-value of Mn^{2+} in NASeH shows a negative shift from its value in diamagnetic Tutton salts, where it is either equal to or greater than the free spin value.[8,9,28]

Observations (1) and (2) regarding the linewidths can be explained qualitatively in terms of the spin quenching idea. As described in Chapter II-C about spin-quenching and Ni^{2+} hosts, NASeH crystal is suitable host for the study of EPR of Mn^{2+} and the observation of the sharp EPR spectrum of Mn^{2+} in NASeH at 300 K indicates that Ni^{2+} spins are quenched. Further the field dependence of Mn^{2+} linewidths

Table V-4

The Zeeman-field intensity (H) and the corresponding linewidth (ΔH) of Mn^{2+} resonance lines for $H||Z$ in $Ni(NH_4)_2(SeO_4)_2.6H_2O$ at 300 K.

H (gauss)	ΔH (gauss)
1988	15.0 ± 2
2070	16.0 ± 2
2250	16.5 ± 2
2684	17.5 ± 2
3050	19.0 ± 2
3341	20.0 ± 2
3730	21.0 ± 2
4103	23.0 ± 3
4433	26.0 ± 3
4623	27.0 ± 3
4836	28.0 ± 3

is obvious since the magnetic moment of Ni^{2+}, given by μ_{ins} in Chapter II-C and Eq. (II.44), is field dependent. In principle, the field dependence should give the information whether or not a narrowing process is operative because the field dependence should be quadratic with narrowing and linear without narrowing. But our data of Mn^{2+} linewidth could not fit very well to either of the two forms, implying the existence of some intermediate case.

The anisotropy of Mn^{2+} linewidth (observation (2)) is a result of the fact that the magnetic moment of Ni^{2+}, μ_{ins}, is a function of field orientation. This anisotropy has been described in detail in Chapter II-C for the case of Mn^{2+} doped NASH and NPSH Tutton salts.

Finally we describe g_z-shift (observation (3)). It can be explained to be due to the internal magnetic field at the site of Mn^{2+} ions, caused by the moments induced on Ni^{2+} spins due to the polarization by Zeeman field. This additional field shifts the resonance from its 'isolated' value, i.e. the value in the absence of Ni^{2+} spins.[28] Similar observations have also been discussed elsewhere.[23,29]

In conclusion, all the additional features in the EPR of Mn^{2+} in NASeH can be attributed to Ni^{2+} hosts.

REFERENCES

1. K.D. Bowers and J.Owen, Rept. Progr.Phys. 18, 304 (1955).

2. S.A. Al'tshuler and B.M. Kozyrev, 'Electron Paramagnetic Resonance' Chap. 4, Academic Press, New York (1964).

3. J.H.E. Griffiths and J.Owen, Proc. Roy.Soc. (London) A 213, 459 (1952).

4. B. Bleaney, R.P. Penrose and B.I.Plumpton, ibid. A 198, 406 (1949).

5. D.M.S. Bagguley and J.H.E. Griffiths, Proc. Phys.Soc. A 65, 594 (1952).

6. F.E.Mabbs and J.K. Porter, J.Inorg.Nucl.Chem.35, 3219 (1973).

7. B.Bleaney and D.J.E. Ingram, Proc. Roy.Soc.(London) A 205, 336 (1951).

8. D.J.E. Ingram, Proc. Phys. Soc. A 66, 412 (1953).

9. I. Hayashi and K. Ono, J. Phys. Soc. Japan 8, 270 (1953).

10. B. Brovetts, G. Cini and S. Ferroni, Il Nuovo Cimento 10, 1325 (1953).

11. K. Ono and I. Hayashi, J.Phys. Soc. Japan 8, 561 (1953); H. Kumagai, Proc. Int. Conf. Theoret. Phys. (Kyoto and Tokyo) p. 791 (1953).

12. T. Ohtsuka, H.Abe and E.Kanda, Sci.Rep. Res. Inst. Tohuku Univ. 9A, 476 (1957); R. Janakiraman and G.C.Upreti Chem. Phys. Lett. 4, 550 (1970).

13. G.C. Upreti, Chem. Phys. Letters 18, 120 (1973).

14. G.C. Upreti, J. Magn. Resonance 14, 274 (1974).

15. B.Bleaney, K.D. Bowers and D.J.E. Ingram, Proc. Roy. Soc. (London) A 228, 147 (1955).

16. R.H. Borcherts and C. Kikuchi, J. Chem. Phys. 40, 2270 (1964).

17. S.Kasthurirengan and R.R. Navalgund, J.Magn.Resonance 19, 357 (1975).

18. E.D. Arkhangel'skaya, M.M. Zaripov, Yu.E.Pol'skii, V.G. Stepanov, G.K. Chirken and L.Ya. Shekun, Sov. Phys. - Solid State 4, 1855 (1963).

19. B.Bleaney and D.J.E. Ingram, Proc. Roy. Soc. (London) A 208, 143 (1951).

20. R.W.G. Wyckoff, 'Crystal Structures', Vol. 3, p. 821, Interscience, New York (1965).

21. A.E.H. Tutton, 'Crystallography and Practical Crystal Measurements', Chap. 17, p. 258, Today and Tomorrow's Book Agency, New-Delhi-5 (1964).

22. A. Abragam and B. Bleaney, 'Electron Paramagnetic Resonance of Transition Ions,', Chap. 4, p. 217, Clarendon Press, Oxford (1970).

23. R.S. Saraswat and G.C. Upreti, J. Magn. Resonance 20, 39 (1975).

24. G.M.Zverev and N.G. Petelina, Sov. Phys. JETP 15, 820 (1962).

25. M.H.L. Pryce, Proc. Roy. Soc. (London) A 283, 433 (1965).

26. D.M.S. Bagguley, B.Bleaney, J.H.E. Griffiths, R.P.Penrose and B.I. Plumpton, Proc. Phys. Soc. 61, 551 (1948).

27. T.Moriya and Y. Obata, J.Phys.Soc. Japan 13, 1333 (1958).

28. V.K. Jain, Ph.D. Thesis, I.I.T. Kanpur (1976).

29. M.T. Hutchings and W.P. Wolf, Phys. Rev. Lett. 11, 187 (1963).

CHAPTER VI

ELECTRON PARAMAGNETIC RESONANCE STUDY OF Mn^{2+} IN $ZnSO_4.7H_2O$† AND $CoSO_4.7H_2O$ SINGLE CRYSTALS

ABSTRACT

EPR of Mn^{2+} doped in $ZnSO_4.7H_2O$ and $CoSO_4.7H_2O$ single crystals has been studied. EPR study of Mn^{2+} in $ZnSO_4.7H_2O$ at 300 K shows the presence of four magnetically inequivalent Mn^{2+} complexes corresponding to the tetramolecular unit cell of $ZnSO_4.7H_2O$. In the case of Mn^{2+} doped $CoSO_4.7H_2O$ two different types of crystals have been obtained, which grow in two different temperature ranges about 298 K. The two types of crystals exhibit different numbers of magnetically inequivalent Mn^{2+} complexes. Further the spin-Hamiltonian parameters for the Mn^{2+} complexes in the two types of crystals are different. The spectra in both types of crystals show unusual linewidth variations and g-shift which are attributed to fast relaxing Co^{2+} ions. To illustrate the use of impurity probe to measure extremely fast spin-lattice relaxation time, T_1 of Co^{2+} in $CoSO_4.7H_2O$ is estimated from the observed linewidth of the EPR spectrum of Mn^{2+} in single crystals of $CoSO_4.7H_2O$.

† The study on $ZnSO_4.7H_2O$ is to appear in Phys. Stat. Sol. (b) 78 No. 2 (Dec. 1976).

INTRODUCTION:

Heptahydrate sulphates of Zn^{2+}, Mg^{2+}, Ni^{2+}, Co^{2+} and Fe^{2+} do not form an isomorphous series of crystals. Out of these, heptahydrate sulphates of Zn^{2+}, Mg^{2+} and Ni^{2+} are orthorhombic and isomorphous, while heptahydrate sulphates of Co^{2+} and Fe^{2+} are monoclinic but not isomorphous. EPR studies of $ZnSO_4.7H_2O$ crystals doped with Co^{2+} and Cu^{2+} were reported by Bleaney et al.[1] and Kasthurirengan et al.[2], respectively. Date[3] observed the EPR of Mn^{2+} in $CoSO_4.7H_2O$ and reported a shift in the resonance lines. Janakiraman et al.[4] studied Mn^{2+} doped $NiSO_4.7H_2O$ and $MgSO_4.7H_2O$ crystals by EPR technique. Sukle et al.[5] reported the EPR of Mn^{2+} in anhydrous $ZnSO_4$ crystals. EPR studies of pure $CoSO_4.7H_2O$ and $NiSO_4.7H_2O$ crystals were carried out by Bleaney et al.[1] and Ono[6], respectively. In this chapter we present the results of our EPR studies of Mn^{2+} doped in $ZnSO_4.7H_2O$ and $CoSO_4.7H_2O$ single crystals.

CRYSTAL STRUCTURE:

The crystals of $ZnSO_4.7H_2O$, $MgSO_4.7H_2O$ and $NiSO_4.7H_2O$ are isomorphous with orthorhombic unit cell symmetry.[7] The unit cell contains four formula units related by the space group operation $P2_12_12_1$. The unit cell dimensions for the sulphate heptahydrates of zinc, magnesium and nickel are,[7]

$ZnSO_4.7H_2O$: a = 11.779 Å b = 12.050 Å c = 6.822 Å

$MgSO_4.7H_2O$: a = 11.91 Å b = 12.02 Å c = 6.87 Å

$NiSO_4.7H_2O$: a = 11.86 Å b = 12.08 Å c = 6.81 Å

For the space group operation $P2_12_12_1$, the atoms and molecules are in the general positions:

(x,y,z); $(\bar{x},\bar{y},\bar{z} + 1/2)$; $(x+1/2, 1/2-y, z)$;

$(1/2 - x, y + 1/2, 1/2 - z)$

Each divalent cation is surrounded by six water molecules, $H_2O(1)$ - $H_2O(6)$, at distances ranging from, in case of $NiSO_4.7H_2O$, 1.93 - 2.40 Å.[7] The seventh water molecule, $H_2O(7)$, is not coordinated with the cation, but instead fills what would otherwise be a void in the structure.

To the best of our knowledge the detailed crystal structure data for $CoSO_4.7H_2O$ is not available. Preliminary work has shown that the unit cell of $CoSO_4.7H_2O$ is monoclinic (space group C_{2h}^6) with sixteen molecules.[1] However, the unit cell dimensions are not given. Also Donnay et al.[8] mention other possible structures with different number of molecules per unit cell. Ananthanarayanan[9] has indicated the presence of fairly strong hydrogen bonding in $CoSO_4.7H_2O$ by observing the lowering of O-H Raman frequencies from the traditional value of 3650 cm^{-1} to 3050 cm^{-1}. In his thesis, he mentions, based on the preliminary and unpublished work of Mani, that

$CoSO_4.7H_2O$ belongs to monoclinic class, space group C_{2h}^6 or C_{2h}^5, having eight molecules per unit cell with a = 14.05 Å, b = 12.85 Å, c = 11.04 Å and $\beta = 105^o24'$. EPR results of Bleaney et al.[1] in undiluted $CoSO_4.7H_2O$ showed the presence of two inequivalent Co^{2+} sites per unit cell.

The crystals of $ZnSO_4.7H_2O:Mn^{2+}$ grew as prismatic needles along the c-axis with prominent faces m(110) and m'($1\bar{1}0$), consistent with the morphology reported in the literature.[1] In the case of $CoSO_4.7H_2O$, two types of doped crystals were obtained, which were morphologically different and were found to grow in two different ranges about 298 K. Type I (CoSH(I)) crystals grew at temperatures below 298 K and were prismatic with hexagonal bases, while type II (CoSH(II)) grew as rectangular needles above 298 K. Once grown, the two forms of $CoSO_4.7H_2O$ crystals were found to be stable at temperatures both above and below 298 K and also did not transform from one form to the other.

RESULTS AND DISCUSSION:

EPR spectra of Mn^{2+} in heptahydrate sulphates of Zn^{2+} and Co^{2+} show no similarity and will, therefore, be discussed separately.

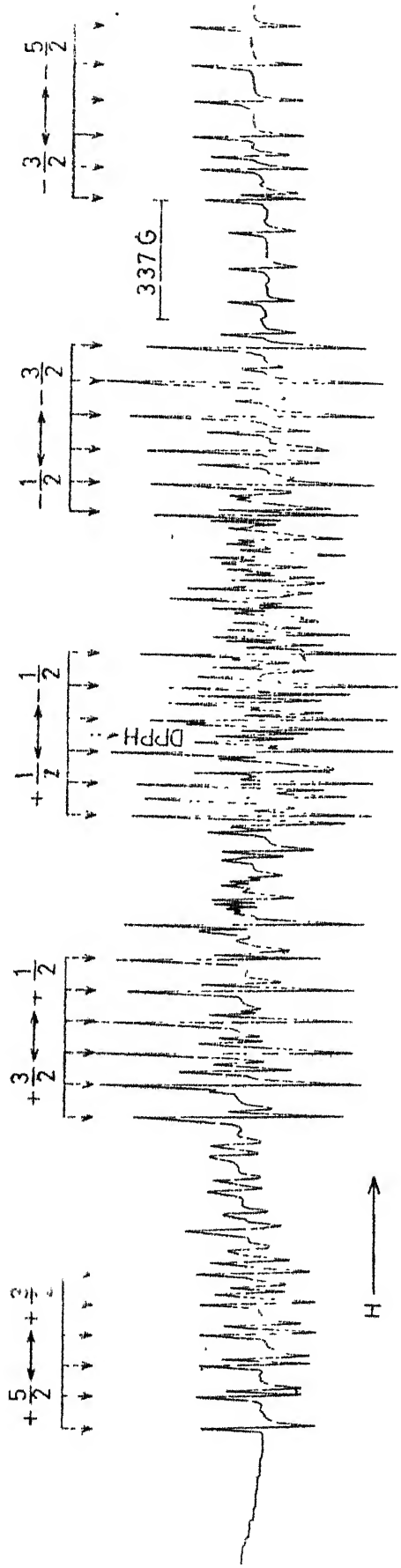

Fig.VI-1: The EPR spectrum of Mn^{2+} in $ZnSO_4 \cdot 7H_2O$ at 300 K for H along the Z-axis of one set of equivalent Mn^{2+} complexes.

Table VI-1

Spin-Hamiltonian parameters (non-Zeeman parameters are in units of 10^{-4} cm^{-1}) of Mn^{2+} in single crystals of heptahydrate sulphates of zinc, magnesium and nickel at 300 K and at X-band.

Crystal	g_z	D	E	a	A	B	Ref.
$ZnSO_4.7H_2O$	2.002±0.001	407±3	-65±10	5±2	-86±2	-84±5	(Present work)
$MgSO_4.7H_2O$	2.003±0.005	385±5	89±10	-	-86±5	82±10	(4)
$NiSO_4.7H_2O$	1.995±0.005	417±5	69±10	-	-85±5	81±10	(4)

$NiSO_4.7H_2O$ crystals reveals no appreciable differences in the general properties of the magnetic complexes, viz. the strength and the symmetry of the crystalline field at Mn^{2+} sites, the angles between the Z-axes etc. From the fact that the crystal field parameters, 'D' and 'E', in these three isomorphous crystals are nearly the same, it can be qualitatively concluded that the ligand coordination around the divalent cation is almost the same in all the three cases. The observed small differences in 'D' and 'E' may be due to the small differences in distances of water molecules from the cations in the three cases. Further, for the Mn^{2+} in $ZnSO_4.7H_2O$, the observed widths of Mn^{2+} resonance lines are $\sim$ 10 G. This linewidth is mainly due to the local magnetic fields of the proton nuclear moments in water molecules surrounding the magnetic ion in the form of a distorted octahedron.

$CoSO_4.7H_2O:Mn^{2+}$:

The angular variation studies of the EPR spectra of Mn^{2+} have been carried out in the doped crystals of CoSH(I) and CoSH(II) at 300 K. These studies in CoSH(I) crystals show the presence of two thirty line Mn^{2+} spectra indicating the presence of two magnetically inequivalent Mn^{2+} complexes per unit cell. Whereas, the angular variation studies in CoSH (II) crystals show only a single thirty line Mn^{2+}

spectrum, indicating that all the Mn^{2+} complexes in the unit cell are equivalent. The EPR spectra of Mn^{2+} in CoSH (I) crystals for H along the Z-axis at 300 K and 77 K are shown in Fig. VI-2. The corresponding spectra of Mn^{2+} in CoSH (II) crystals are shown in Fig. VI-3. The Mn^{2+} spectra in CoSH (II) at 300 K for H along the X and Y axes are shown in Fig. VI-4. In the case of CoSH (II): Mn^{2+} crystals, the Z-axis of Mn^{2+} spectrum has been identified to be along the needle axis. The Mn^{2+} spectra in CoSH (I) and CoSH (II) crystals can be described by a spin-Hamiltonian of orthorhombic symmetry. The best-fit parameters, obtained from the spin-Hamiltonian analysis of the spectra, are,

for CoSH (I) : Mn^{2+}

$g_z = 2.0008 \pm .001$ $\quad D = (458.8 \pm 2) \times 10^{-4}$ cm^{-1}

$E = (-133.6 \pm 4) \times 10^{-4}$ cm^{-1} $\quad a = (1.9 \pm 2) \times 10^{-4}$ cm

$A = (-85.9 \pm 2) \times 10^{-4}$ cm^{-1} $\quad B = (-87 \pm 2) \times 10^{-4}$ cm

and for CoSH (II) : Mn^{2+}

$g_z = 1.996 \pm .001$ $\quad D = (234 \pm 2) \times 10^{-4}$ cm^{-1}

$E = (-18.6 \pm 3) \times 10^{-4}$ cm^{-1} $\quad a = (-4.7 \pm 2) \times 10^{-4}$ cm

$A = (-85.7 \pm 2) \times 10^{-4}$ cm^{-1} $\quad B = (-86.7 \pm 2) \times 10^{-4}$ cm

The EPR spectra of Mn^{2+} in CoSH (I) and CoSH (II) crystals show some unusual and interesting features both at

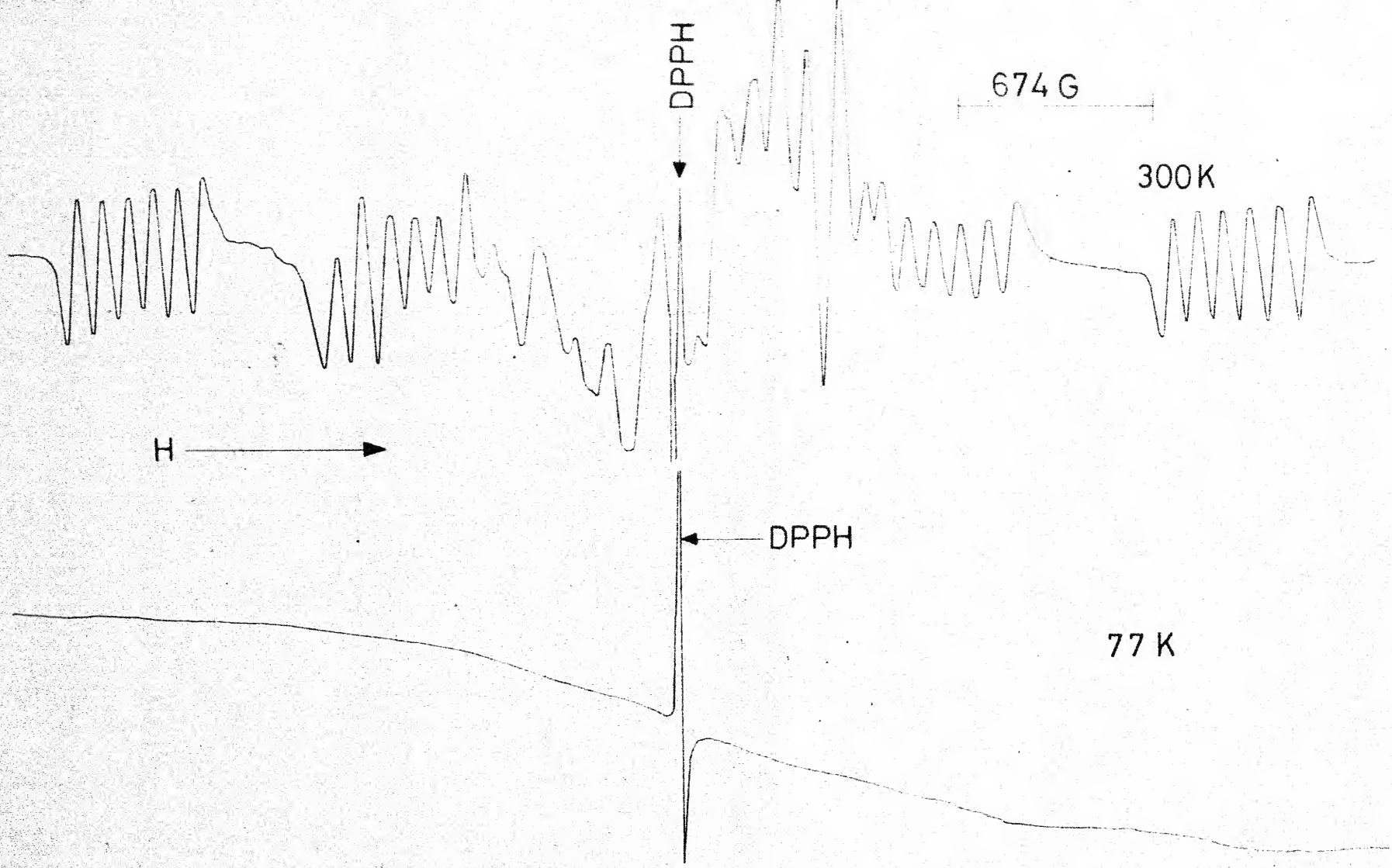

Fig.VI-2: The EPR spectra of Mn^{2+} IN $CoSO_4.7H_2O$(I) at 300 K and at 77 K for H along the Z-axis of one set of equivalent Mn^{2+} complexes.

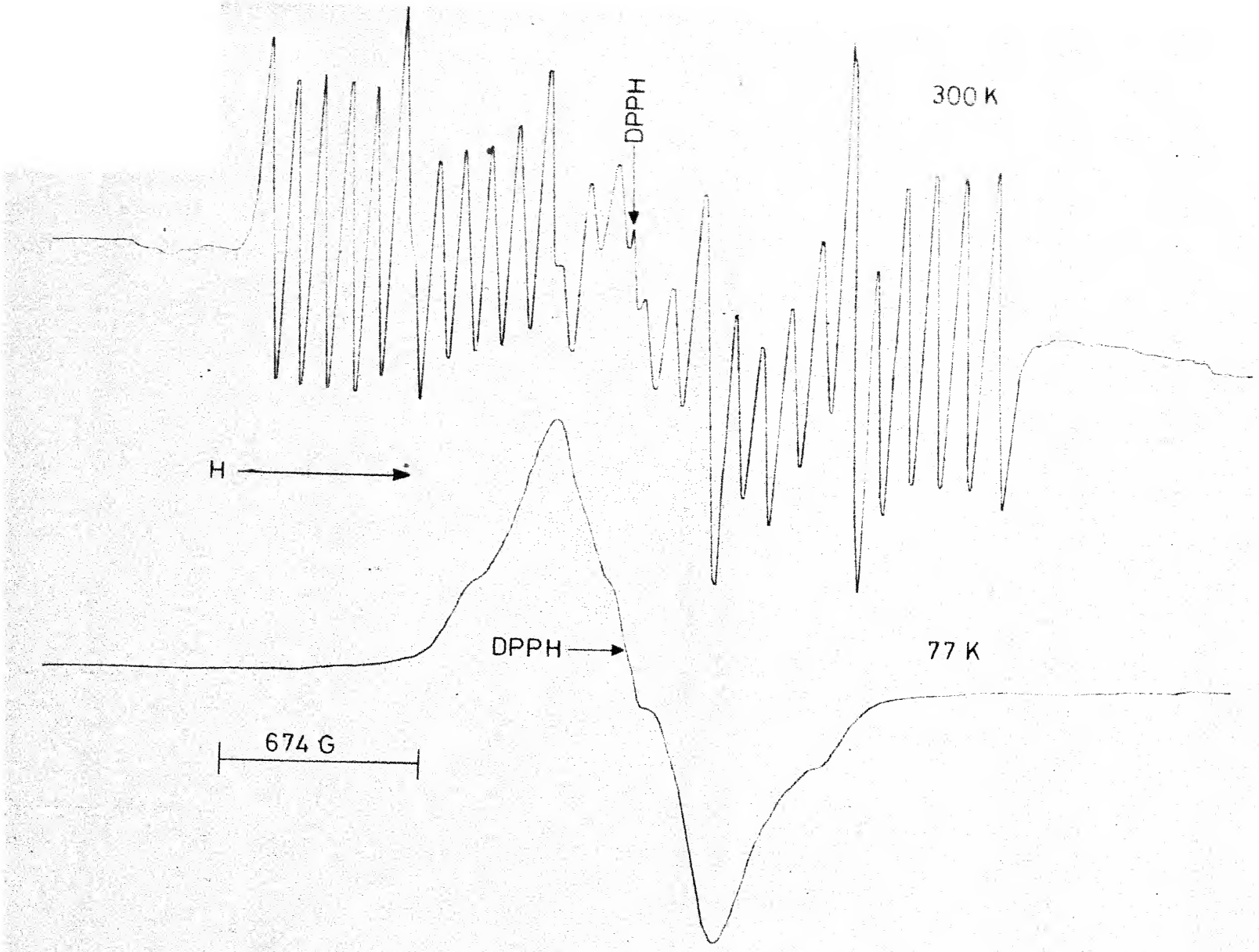

Fig.VI-3: The EPR spectra of Mn^{2+} in $CoSO_4.7H_2O$(II) at 300 K and at 77 K for H along the Z-axis.

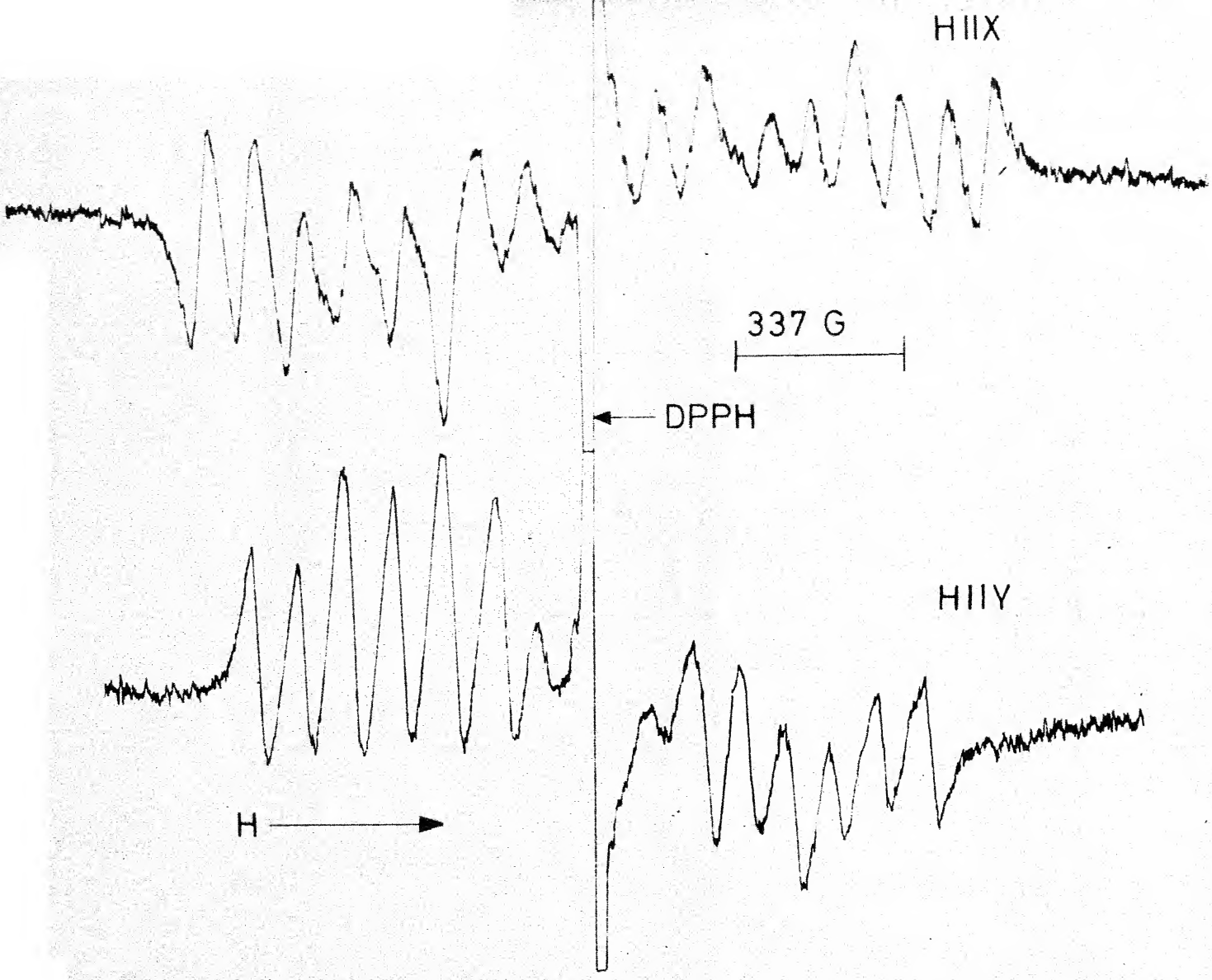

Fig.VI-4: The EPR spectra of Mn^{2+} in $CoSO_4.7H_2O$(II) at 300 K for H along the X and Y axes.

300 K and at 77 K. These features are same for both types of crystals and can be summarized as follows:

(1) At 300 K the linewidths of Mn^{2+} are larger ($\sim$ 36 G in CoSH (I) and $\sim$ 33 G in CoSH (II)) compared to those normally encountered in hydrated diamagnetic hosts e.g. $\sim$10 G in $ZnSO_4.7H_2O$.

(2) The widths of Mn^{2+} resonance lines associated with various fine structure groups show an unusual variation at 300 K as well as at lower temperatures. The linewidths of various fine structure groups for H along the Z-axis of Mn^{2+} complexes are given below in Table VI-2.

Table VI-2: Linewidths (in gauss) of various fine structure groups of Mn^{2+} complex, for which H||Z, in two forms of $CoSO_4.7H_2O$ at 300 K.

Fine groups	Linewidths in CoSH (I): Mn^{2+}	Linewidths in CoSH (II): Mn^{2+}
$\pm 5/2 \leftrightarrow \pm 3/2$	33 ± 3	28 ± 2
$\pm 3/2 \leftrightarrow \pm 1/2$	40 ± 3	34 ± 3
$+ 1/2 \leftrightarrow - 1/2$	-	38 ± 3

The linewidths increase on going from the outer fine structure groups towards the central group. In CoSH (I) the linewidths for the central group could not be measured accurately due to the overlap of the spectrum due to other

complex. However, these have been estimated to be larger than those for $\pm 3/2 \leftrightarrow \pm 1/2$ fine groups. In CoSH (II) the linewidths of the central group could be measured unambiguously because of the presence of a single complex and have been found to be larger than those for the outer fine structure groups.

(3) The widths of all the Mn^{2+} resonance lines increase rapidly on lowering the temperature of the crystals. The Mn^{2+} spectra get completely broadened out at 77 K. On raising the temperature to 300 K again the well resolved spectra reappear indicating that the smearing out of the spectra at 77 K is due to increased linewidths on lowering the temperature.

(4) The Mn^{2+} g_z-values show a negative shift from the value, which is generally observed in the case of diamagnetic hosts.

As described in general for Mn^{2+} in cobalt salts in Chapter II-C and for Mn^{2+} doped $Co(CH_3COO)_2.4H_2O$ and $CoK_2(SO_4)_2.6H_2O$ crystals in chapters IV and V, respectively, the observation of sharp EPR spectra of Mn^{2+} at 300 K in CoSH (I) and CoSH (II) crystals can be explained in terms of host spin-lattice relaxation narrowing process. In addition, this narrowing process also explains the increase of Mn^{2+} linewidths on lowering the temperature of crystals

(observation (3)). Besides, observation (3) also confirms that narrowing at 300 K is due to host spin-lattice relaxation narrowing. Further, as described in Chapter II-C and applied in Chapters IV and V for cobalt salts, the observed linewidth of Mn^{2+} in such a system, where host spin-lattice relaxation narrowing is in effect, can be utilized to estimate the host T_1. Thus using the expression for T_1 of Co^{2+} (Eq. II.43) and the observed linewidths of Mn^{2+}, T_1 of Co^{2+} in $CoSO_4.7H_2O$ has been estimated to be $\sim 1.1 \times 10^{-12}$ sec. In the absence of structure data for the two forms of $CoSO_4.7H_2O$, T_1 has been estimated by taking average value of Mn^{2+} linewidths for the two forms and n has been calculated using the unpublished data of Mani. The order of T_1 of Co^{2+} is found to be quite satisfactory, as on extrapolation to 300 K the data of Zverev et al.[10] for two Co^{2+} sites in Al_2O_3 give $T_1 = 3 \times 10^{-11}$ sec. and 3×10^{-12} sec. and the data of Pryce[11] for Co^{2+} in MgO give $T_1 = 1 \times 10^{-11}$ sec.

Next observation (2) about the unusual variation of Mn^{2+} linewidths with various fine structure groups may be due to the unequal influence of exchange interaction upon various $\Delta M = \pm 1$ transitions of Mn^{2+}.

In the end observation (4) regarding the shift in the g_z-value may be explained to be due to the local static magnetic field created at Mn^{2+} sites by the host Co^{2+} ions.

This causes the shift in Mn^{2+} g-value from its value when the diamagnetic divalent cations (e.g. Zn^{2+} or Mg^{2+}) are present in place of Co^{2+}.

In conclusion, two different types of crystals of $CoSO_4.7H_2O:Mn^{2+}$ have been obtained, which grow in two different temperature ranges about 298 K. The main differences in the Mn^{2+} EPR spectra in these two types of crystals are:

(1) A large value of the dominant crystal field parameter 'D' in CoSH (I) (458.8 x 10^{-4} cm^{-1}) compared to that in CoSH (II) (234 x 10^{-4} cm^{-1}). Also the magnitude of rhombic component 'E' is quite large in CoSH (I) (133.6 x 10^{-4} cm^{-1}) compared to that in CoSH (II) (18.6 x 10^{-4} cm^{-1}).

(2) A difference in the number of inequivalent Mn^{2+} complexes per unit cell.

These studies indicate the existence of two forms of $CoSO_4.7H_2O$ with different crystal structures. However, at present no such information is available in the literature.

REFERENCES

1. B. Bleaney and D.J.E. Ingram, Proc. Roy. Soc. (London) A 208, 143 (1951).

2. S. Kasthurirengan, R.R. Navalgund and L.C. Gupta, Phys. Stat. Sol. (b) 58, K 109 (1973).

3. M. Date, J.Phys. Soc. Japan 18, 912 (1963).

4. R. Janakiraman and G.C. Upreti, Phys. Stat. Sol (b) 47, 679 (1971).

5. L.J. Sukle and J.S. Wells, Phys. Rev. 180, 445 (1969).

6. K.Ono, J.Phys. Soc. Japan 8, 802, (1953).

7. R.W.G. Wyckoff, 'Crystal Structures', Vol.3, p.837, Interscience, New York (1965).

8. J.D.H. Donnay, G. Donnay, E.G.Cox, O.Kennard and M.V.King, 'Crystal Data Determinative Tables', No.5, American Crystallographic Association, Washington D.C. (1963).

9. V. Ananthanarayanan, Ph.D. Thesis, I.I.Sc. Bangalore (1961).

10. G.M. Zverev and N.G. Petelina, Sov. Phys. JETP 15, 320 (1962).

11. M.H.L. Pryce, Proc. Roy. Soc. (London) A 283, 433 (1965).

CHAPTER VII

ELECTRON PARAMAGNETIC RESONANCE STUDY OF Mn^{2+} DOPED IN HEXAQUONITRATES OF MAGNESIUM AND NICKEL

ABSTRACT

EPR study has been carried out in Mn^{2+} doped single crystals of hexaquonitrates of magnesium and nickel, $Mg(OH_2)_6.(NO_3)_2$ and $Ni(OH_2)_6.(NO_3)_2$, at 300 K and at X-band. Mn^{2+} substituting for Mg^{2+} in $Mg(OH_2)_6.(NO_3)_2$ exhibits two identical, but differently oriented, magnetic complexes, whose Z axes make an angle of $15^{\circ} \pm 1^{\circ}$ with each other in ZX plane. Besides the allowed ($\Delta M = \pm 1$, $\Delta m = 0$) transitions, forbidden hyperfine ($\Delta M = \pm 1$, $\Delta m = \pm 1$ and $\Delta m = \pm 2$) transitions have been observed for H along the K_1 and K_2 axes. From the doublet separations of the forbidden hyperfine transitions, the quadrupole coupling constants for Mn^{2+} in this system are calculated. However, Mn^{2+} doped $Ni(OH_2)_6.(NO_3)_2$ crystals exhibit only one single thirty line spectrum indicating the equivalency of two Mn^{2+} complexes per unit cell. The EPR spectra have been analysed using a spin-Hamiltonian of orthorhombic symmetry to get the best-fit parameters. These studies reveal that the two crystals are

not isomorphous and that the site symmetry at the cation sites is very low. Besides, EPR of Mn^{2+} in $Ni(OH_2)_6.(NO_3)_2$ shows additional features viz. g-value shift and anisotropic and field dependent linewidth of Mn^{2+}. These are attributed to the magnetic interactions between Mn^{2+} and Ni^{2+} ions.

INTRODUCTION:

Hexaquocations of divalent metals are the most common complexes considered in coordination-compound chemistry. One would expect ions of nearly similar size and properties such as Mg^{2+}, Mn^{2+}, Co^{2+}, Ni^{2+} and Zn^{2+} to form isomorphous series of compounds containing hexaquocations of these ions and a particular anion such as Cl^-, SO_4^{2-}, NO_3^-. The hexaquocations in these compounds are assigned octahedral structure, but small deviations from perfectly cubic symmetry are expected either because of the electronic configuration of the metal cation or because of the strains from the hydrogen bonds in the crystals. However, the nitrates of hexaquocations of Mg^{2+}, Mn^{2+}, Co^{2+}, Ni^{2+} and Zn^{2+} do not form an isomorphous series. It is not clear yet if the differences are due either to different types of bonding of water molecules with the metal ion, or to the packing strains, or to other causes such as thermal energy state of nitrato groups. Some recent structural studies[1-5] on these nitrates have been carried out to understand howfar this fact is related to the distortions in the octahedral arrangement of water molecules around the metal ion. However, the lack of mutual isomorphism of these nitrates has not been explained exactly. In addition, low temperature magnetic susceptibility[6] and specific heat[7] measurements have been

carried out on hexaquonickel nitrate and the magnetic and thermal data, thus obtained, can be successfully fitted to an orthorhombic spin-Hamiltonian for Ni^{2+} ions with $D = -6.07\ cm^{-1}$, $E = -1.86\ cm^{-1}$ and $g = 2.25$. This value of 'D' is higher than the values reported for other hexaquonickel salts and may be due to the lower symmetry environment around Ni^{2+} ions in hexaquonickel nitrate; most of the other nickel salts have an octahedral environment of water molecules of almost cubic symmetry around Ni^{2+} ion. The results of EPR study of Mn^{2+} in the hexaquonitrates of nickel and magnesium, $Ni(OH_2)_6.(NO_3)_2$ and $Mg(OH_2)_6.(NO_3)_2$ (hereafter to be referred to as HNiN and HMgN, respectively), are presented in this chapter with a view to get information about the symmetry and strength of the crystal field at the cation substituted Mn^{2+} sites and about the magnetic interactions between impurity Mn^{2+} and Ni^{2+} host ions.

CRYSTAL STRUCTURE:

The crystals of HMgN are monoclinic, space group $P2_1/c$ with unit cell constants: $a = 6.194$, $b = 12.707$, $c = 6.600$ Å; $\beta = 92.99^{\circ}$ and $Z = 2$.[2] The structure consists of hexaquomagnesium cations, which are centrosymmetric and nearly octahedral with the distances, $Mg-OH_2$, equal to 2.053, 2.061 and 2.063 Å and the angles, $H_2O-Mg-OH_2$, equal

to 91.3°, 90.7° and 90.4°, and the nitrato groups, which are not trigonally symmetric with N-O bond lengths 1.20, 1.25 and 1.26 Å. The $Mg(OH_2)_6^{2+}$ and NO_3^- ions are bound together by hydrogen bonds whose lengths range from 2.75 - 2.90 Å. The structure is shown in Fig. VII-1(a).

The HNiN crystals are triclinic, space group $P\bar{1}$ with unit cell constants: a = 7.694, b = 11.916, c = 5.817 Å; α = 102.3, β = 102.4, γ = 105.9° and Z = 2.[3] Here also the hexaquonickel cations and nitrato anions are joined by hydrogen bonds and form the network of the whole structure (see Fig. VII-1(b)). The symmetry of the cation is nearly octahedral, deformed by an orthorhombic bipyramid, with pairs of opposite distances, $Ni-OH_2$ = 2.03, 2.07 and 2.09 Å. The nitrato anions are not exactly trigonal; they have, in both the crystallographically independent anions, two short bonds with average N-O = 1.23 Å and one long bond with N - O = 1.28 Å.

The crystals of HMgN grew as prismatic needles along the c-axis, while those of HNiN grew as elongated plates with ab plane as the plate surface.[8]

RESULTS AND DISCUSSION:

EPR spectra of Mn^{2+} in HMgN and HNiN crystals have been studied at 300 K. As the EPR spectra in these two

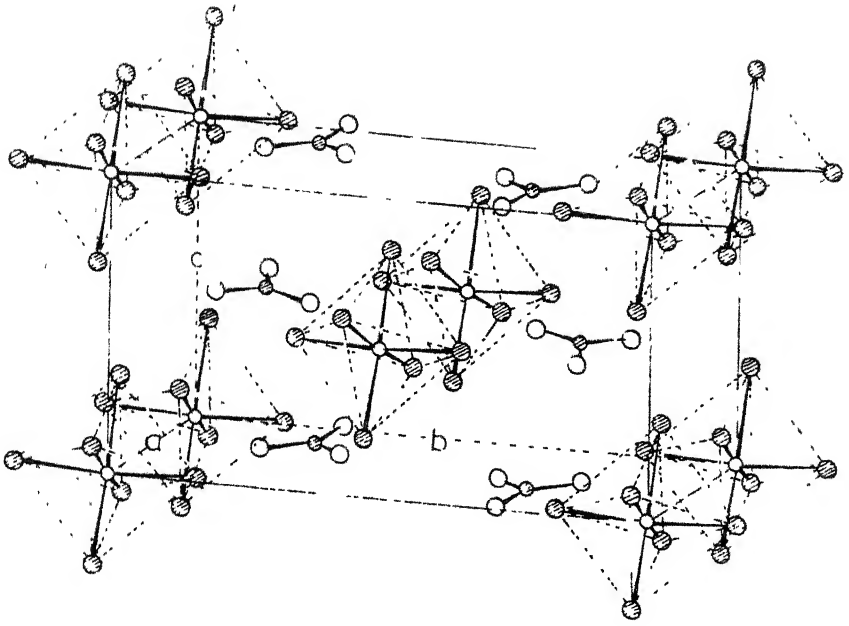

○Mg ○O ◍H_2O ◉ N

(a)

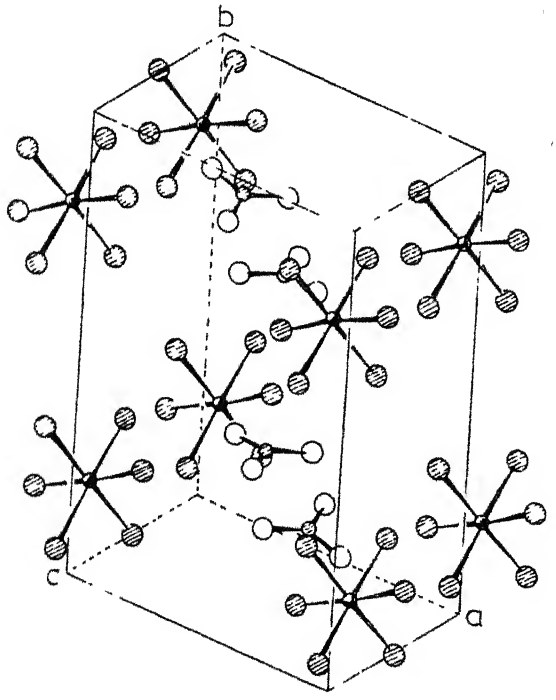

○ O ◍ H_2O ◉ N ● Ni

(b)

Fig. VII.1: The crystal structures of (a) $Mg(OH_2)_6.(NO_3)_2$ and (b) $Ni(OH_2)_6.(NO_3)_2$

crystals show different features, except for a large value of the rhombic spin-Hamiltonian parameter 'E', we will discuss them separately.

$Mg(OH_2)_6.(NO_3)_2:Mn^{2+}$:

From the angular variation studies of EPR spectra of Mn^{2+} in HMgN, it is observed that there are two identical, but differently oriented, Mn^{2+} complexes per unit cell. The principal axes of these two Mn^{2+} complexes have been found by obtaining the extrema in the fine structure spreads. The two Z axes and two X axes of the Mn^{2+} complexes have been found to be in a plane, perpendicular to the prismatic axis. The angle between the two Z or the two X axes have been determined to be 15 ± 1^{o}. The two Y axes are coincident and are along the prismatic axis. The EPR spectra of Mn^{2+} in HMgN for H along the Z-axis and the X-axis of one set of equivalent Mn^{2+} complexes are shown in Figs. VII-2 and 3 respectively. The observed angular variation of the Mn^{2+} spectra can be described by a spin-Hamiltonian of orthorhombic symmetry. The Mn^{2+} spectra along the principal axes have been analysed for the spin-Hamiltonian parameters using the method of exact diagonalization (described in Chapter II-B). The best-fit parameters, thus obtained, are as follows:

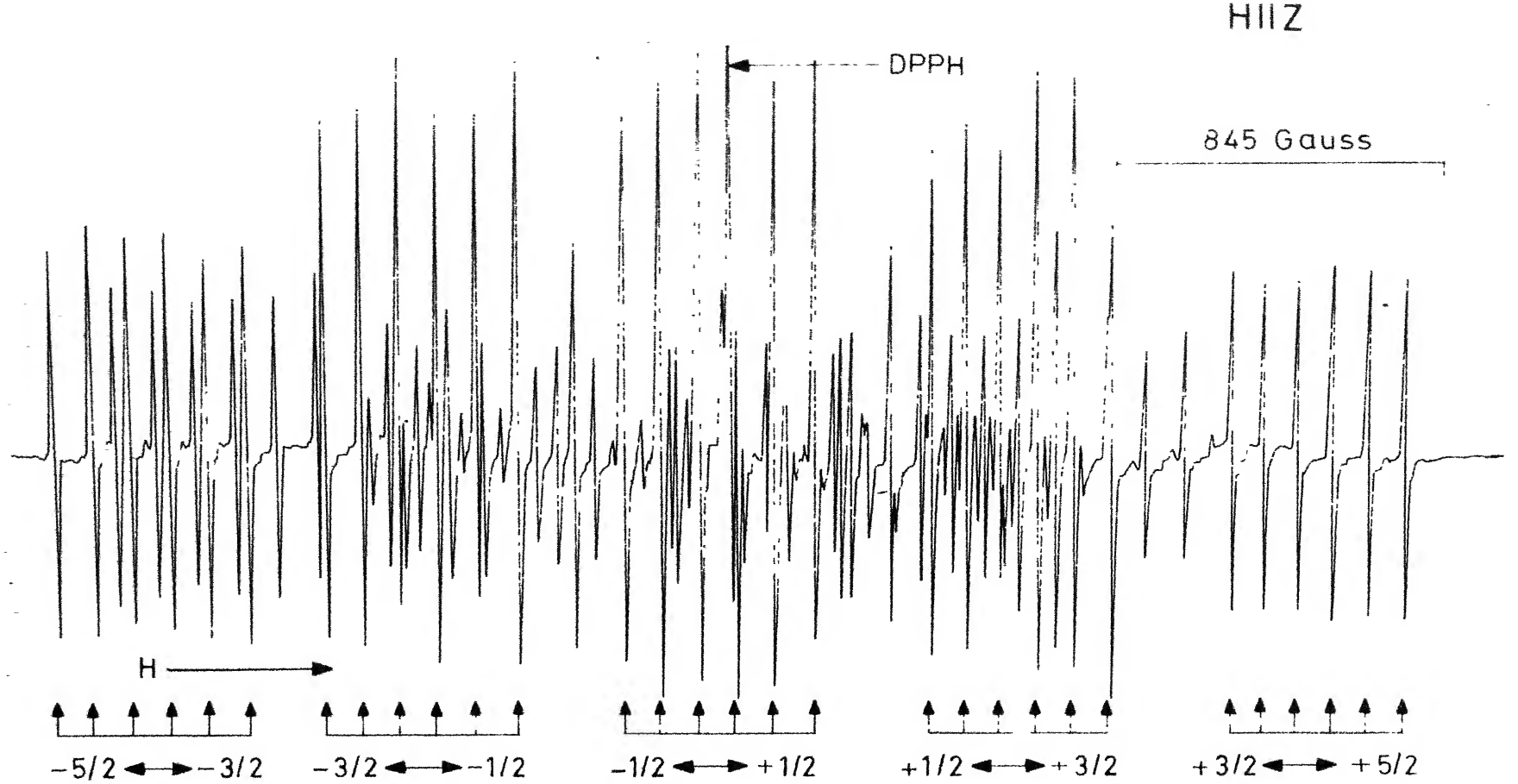

Fig.VII-2: The EPR spectrum of Mn^{2+} in $Mg(CH_3)_6(NO_3)_2$ at 30 K for H along the Z-axis of one set of equivalent Mn^{2+} complexes.

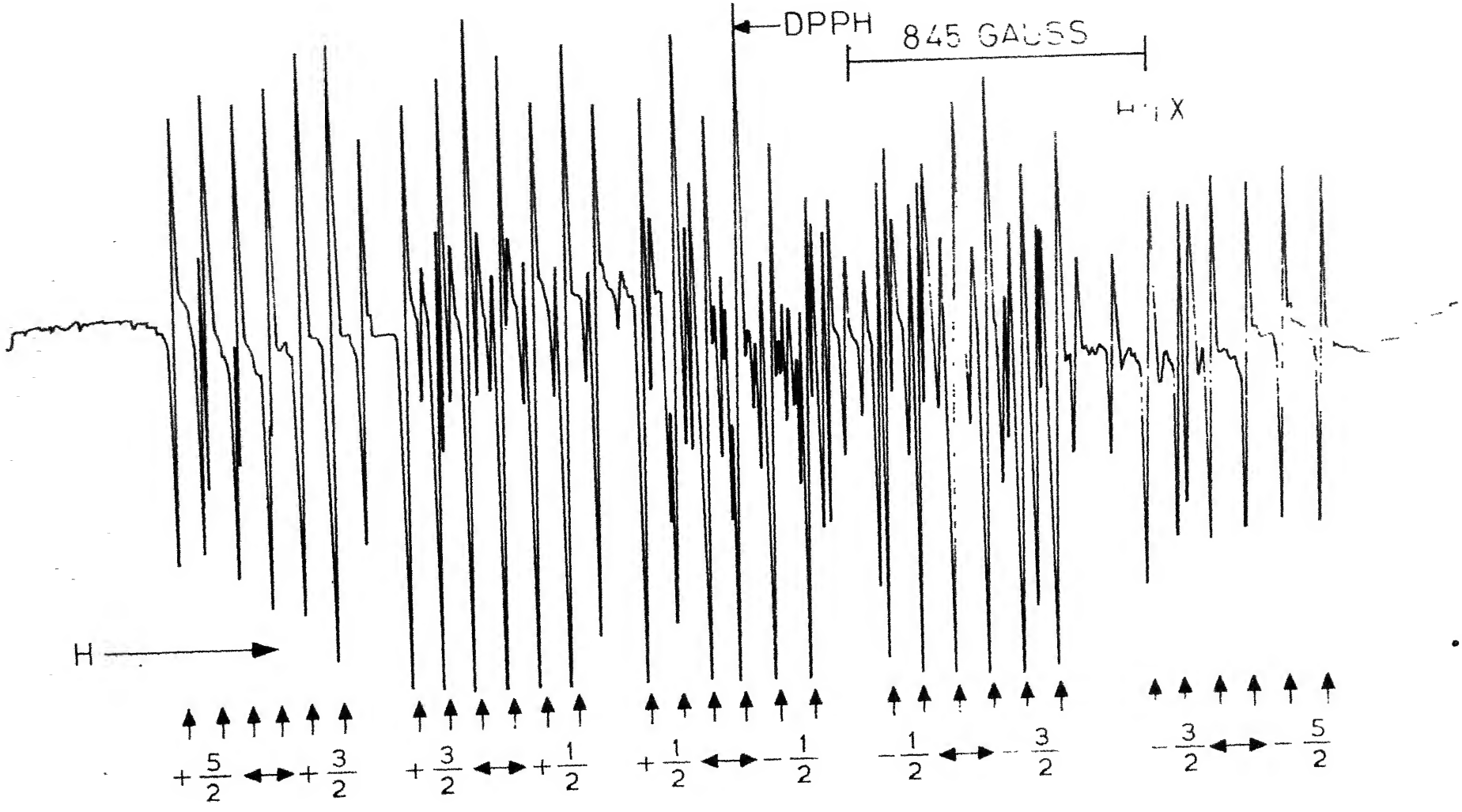

Fig.VII-3: The EPR spectrum of Mn^{2+} in $Mg(OH_2)_6 \cdot (NO_3)_2$ at 300 K for H along the X-axis of one set of equivalent Mn^{2+} complexes.

$g_z = 2.002 \pm 0.001$, $g_x = 2.003 \pm 0.001$

$D = (-359 \pm 1) \times 10^{-4} cm^{-1}$ $E = (102 \pm 2) \times 10^{-4} cm^{-1}$

$a = (6.5 \pm 1) \times 10^{-4} cm^{-1}$ $A = (-89.7 \pm 1) \times 10^{-4} cm^{-1}$,

$B = (-87 \pm 2) \times 10^{-4} cm^{-1}$

An examination of these parameters reveals the presence of very low symmetry (reflected by a large value of 'E') and moderately strong crystal field (as reflected by the large value of 'D') at Mn^{2+} site. This is consistent with the results of crystal structure studies[2] for Mg^{2+} site in HMgN.

The two resultant magnetic axes, K_1 and K_2, can be defined midway between the two Z axes and the two X axes, respectively. EPR spectra of Mn^{2+} for H along the K_1 and the K_2 axes are shown in Figs. VII-4 and 5 respectively. Along these axes the Mn^{2+} spectra due to the two complexes coincide giving only thirty allowed lines alongwith forbidden hyperfine lines. Fig. VII-6 shows the allowed and forbidden hyperfine lines for H along the K_2 axis for the central fine group $+ 1/2 \leftrightarrow - 1/2$. The analysis of these forbidden hyperfine transitions has been carried out using the perturbation expressions of the doublet separations given in Appendix B. From this analysis the following values of quadrupole coupling constants for Mn^{2+} in HMgN have been obtained:

$Q' = -0.16 \times 10^{-4} cm^{-1}$, $Q'' = 1.65 \times 10^{-4} cm^{-1}$.

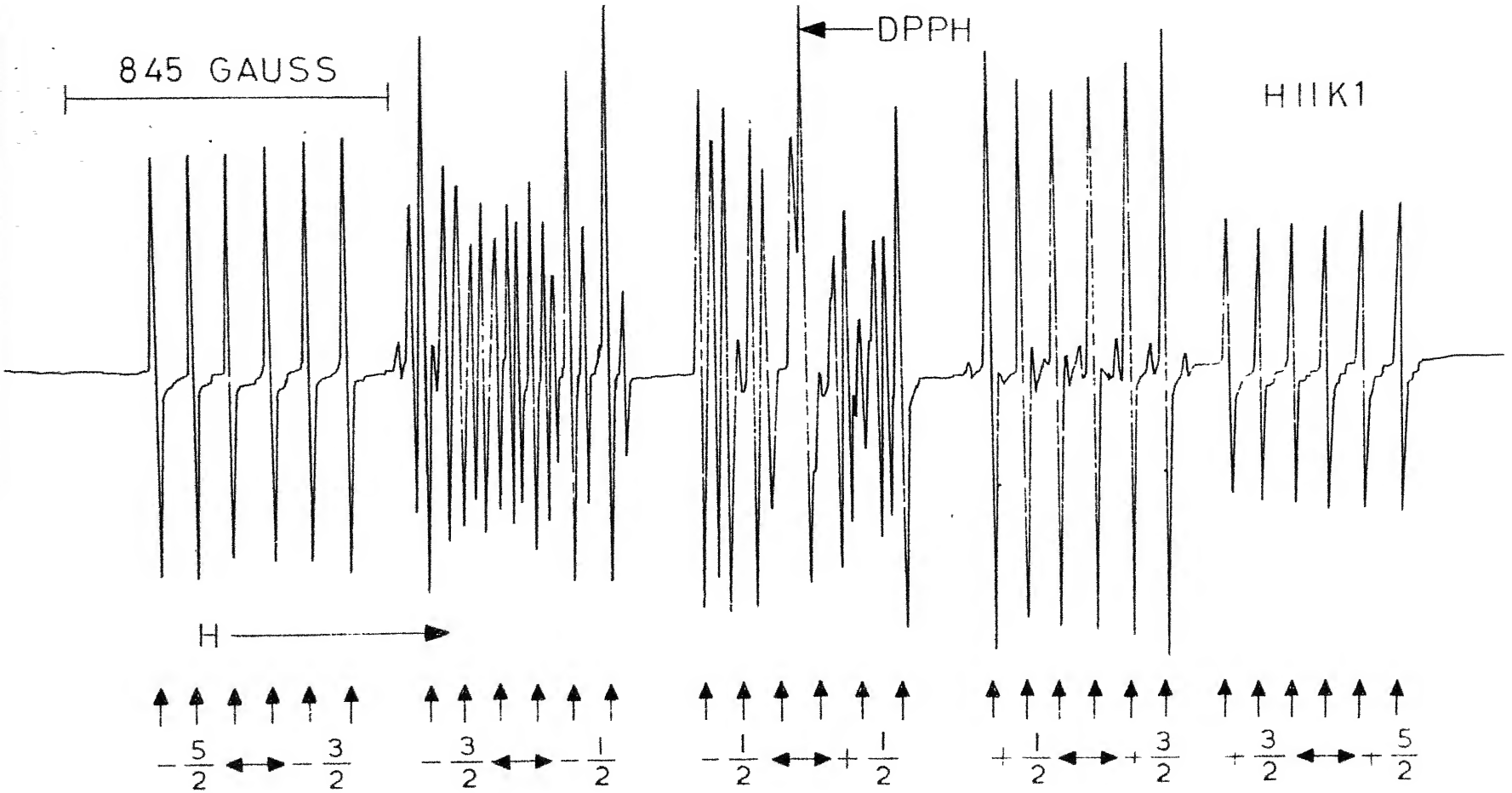

Fig.VII-4: The EPR spectrum of Mn^{2+} in Mg(H_2O)$_6$(ClO$_3$)$_2$ at 300 K for H along the K_1-axis.

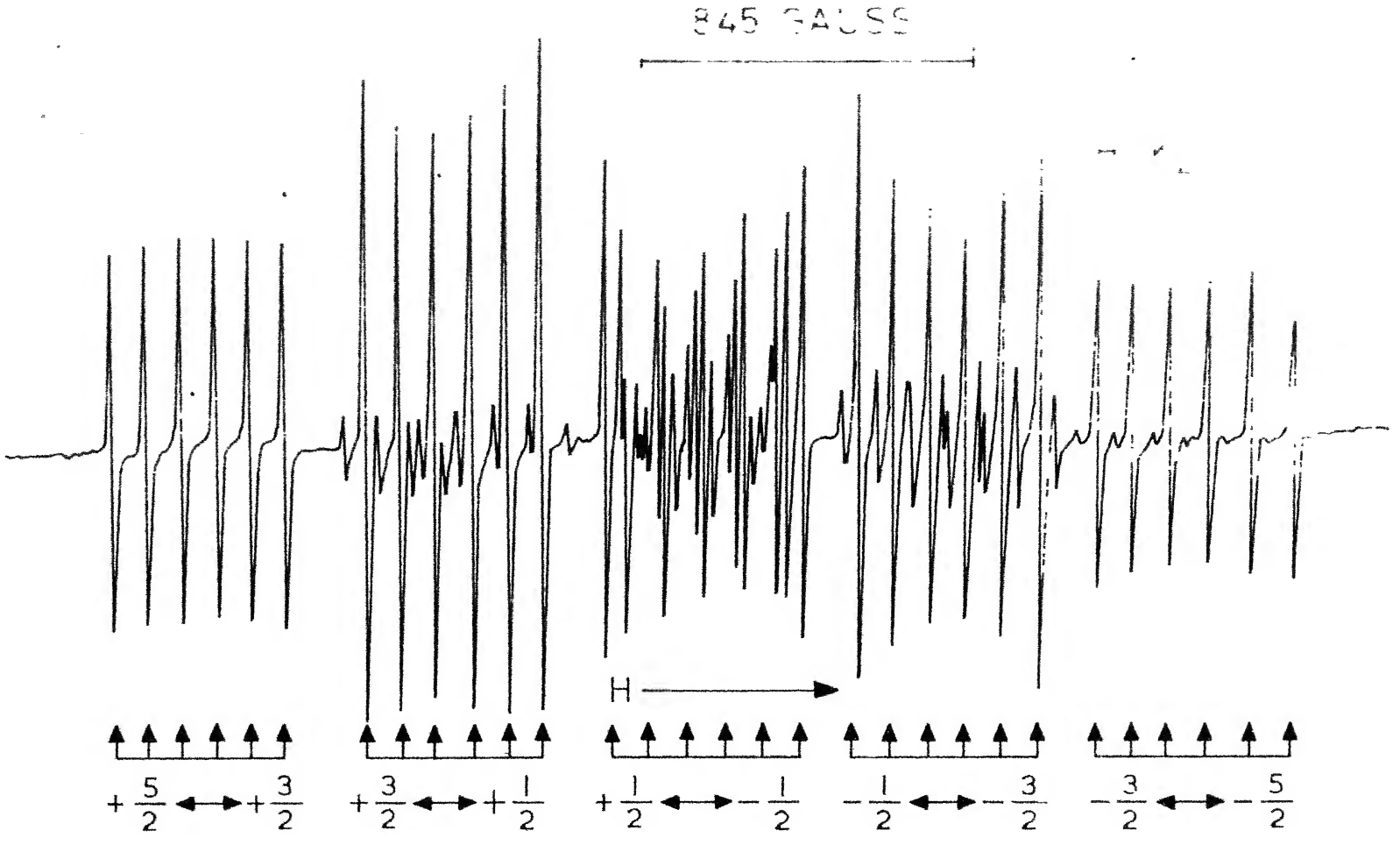

Fig.VII-5: The EPR spectrum of Mn^{2+} in $Mg(OH_2)_6.(NO_3)_2$ at 300 K for H along the K_2-axis.

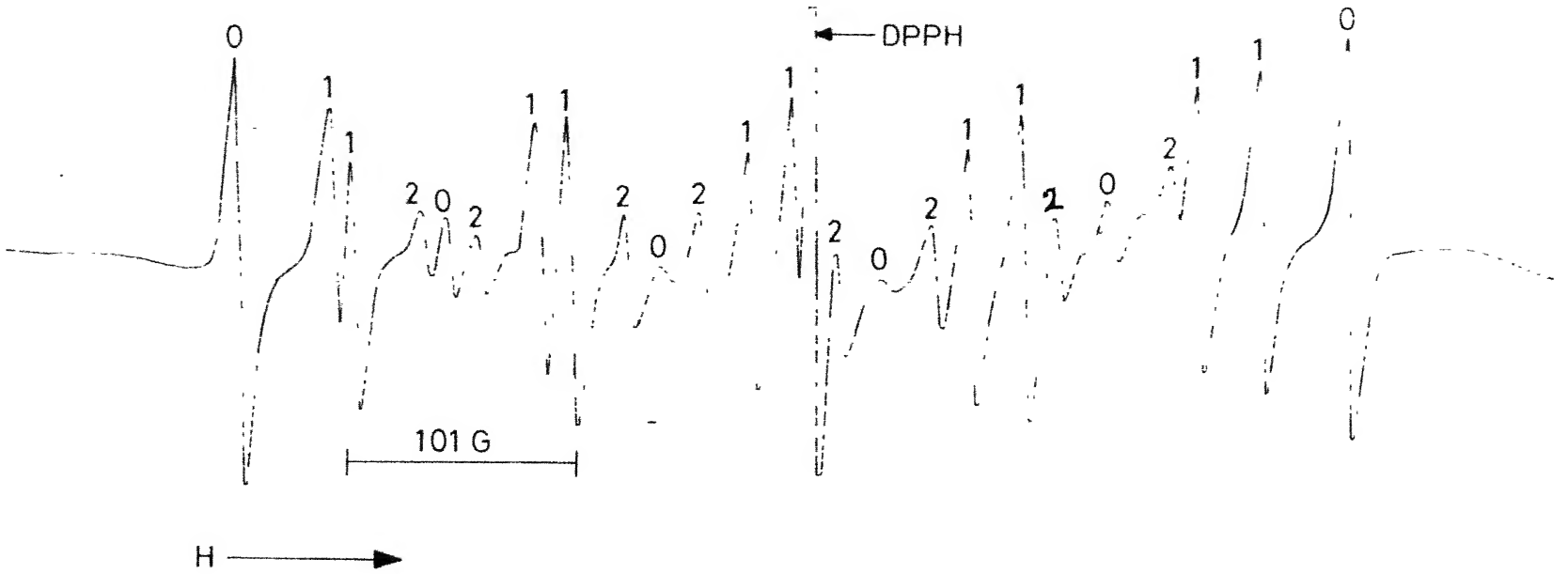

Fig.VII-6: The EPR spectrum of Mn^{2+} in $Mg(OH_2)_6 \cdot (NO_3)_2$ for H along the K_2-axis showing the allowed and forbidden hyperfine transitions in the central group +1/2↔-1/2 at 300 K. The transitions are labeled by a number n so that $\Delta m = \pm n$.

$Ni(OH_2)_6.(NO_3)_2:Mn^{2+}$:

Angular variation studies of Mn^{2+} spectra in HNiN crystals show only one single thirty line spectrum. This indicates the equivalency of the two Mn^{2+} complexes, arising from the substitution of Mn^{2+} for Ni^{2+}, per unit cell. The Mn^{2+} spectrum for H along the Z-axis is shown in Fig. VII-7, and those for H parallel to the X and Y axes are shown in Fig. VII-8. The spectra have been analysed for the spin-Hamiltonian parameters using an orthorhombic spin-Hamiltonian. The best-fit parameters, thus obtained, are as follows:

$g_Z = 1.997 \pm 0.001$ $\quad g_X = 1.998 \pm 0.001$

$D = (-384.2 \pm 1) \times 10^{-4} cm^{-1}$, $\quad E = (109 \pm 2) \times 10^{-4} cm^{-1}$,

$a = (7.5 \pm 1) \times 10^{-4} cm^{-1}$, $\quad A = (-88.6 \pm 2) \times 10^{-4} cm^{-1}$,

$B = (-86.7 \pm 3) \times 10^{-4} cm^{-1}$

Here again the large value of the rhombic component 'E' reveals the presence of very low symmetry at the site of Mn^{2+} substituting for Ni^{2+} in HNiN. In addition, the large value of 'D' reveals the presence of moderately strong crystal field at Mn^{2+} site. This is consistent with the results of crystal structure studies[3] for Ni^{2+} site in HNiN.

Besides the above features of the Mn^{2+} spectra regarding the symmetry and strength of the crystal field, there are additional features in HNiN: Mn^{2+} due to paramagnetic host Ni^{2+} ions. These are as follows:

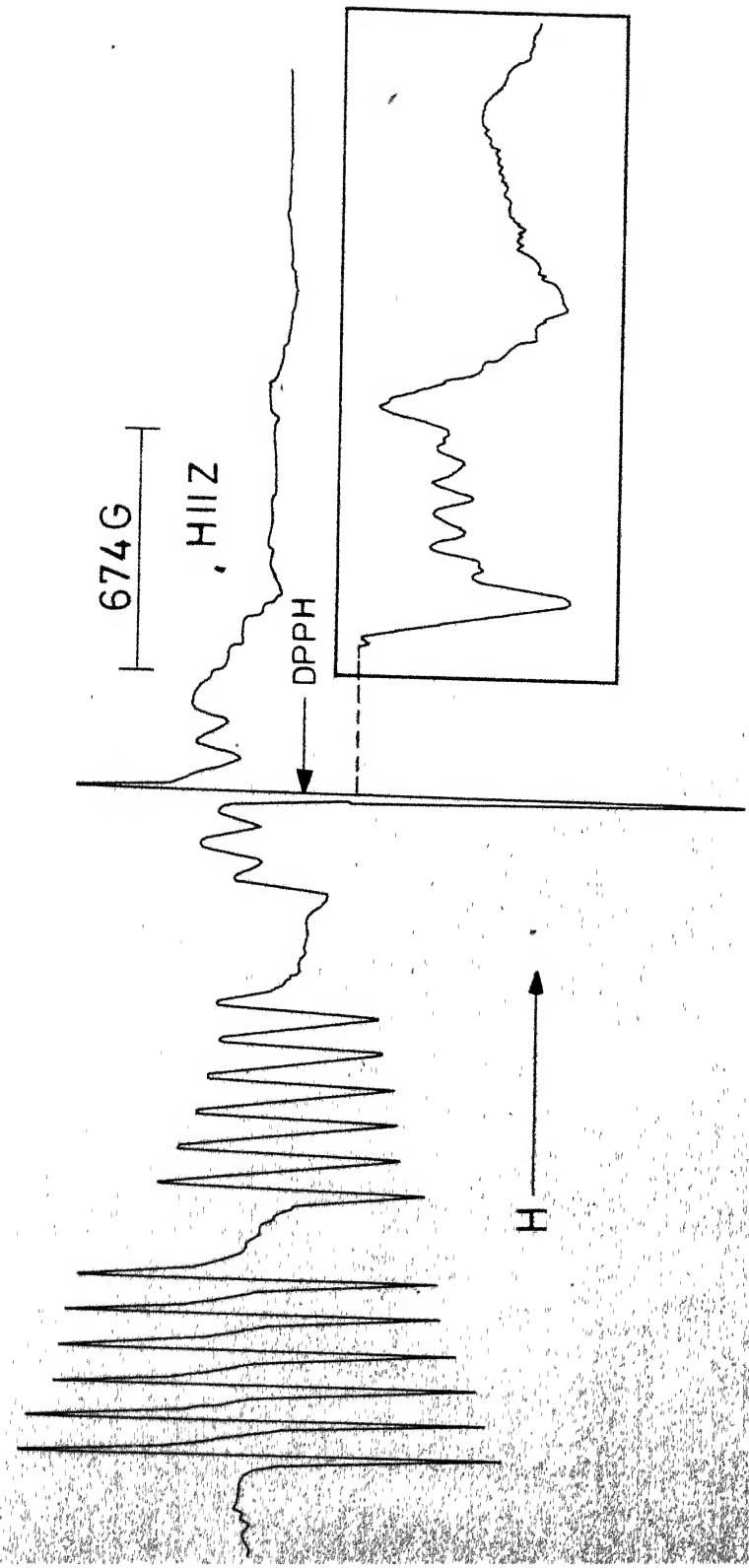

Fig. VII-7: The EPR spectrum of Mn^{2+} in $Ni(OH_2)_6 \cdot (NO_3)_2$ at 300K for H along the Z-axis. The two high field groups recorded with ten times increased gain (x10) are shown in the inset.

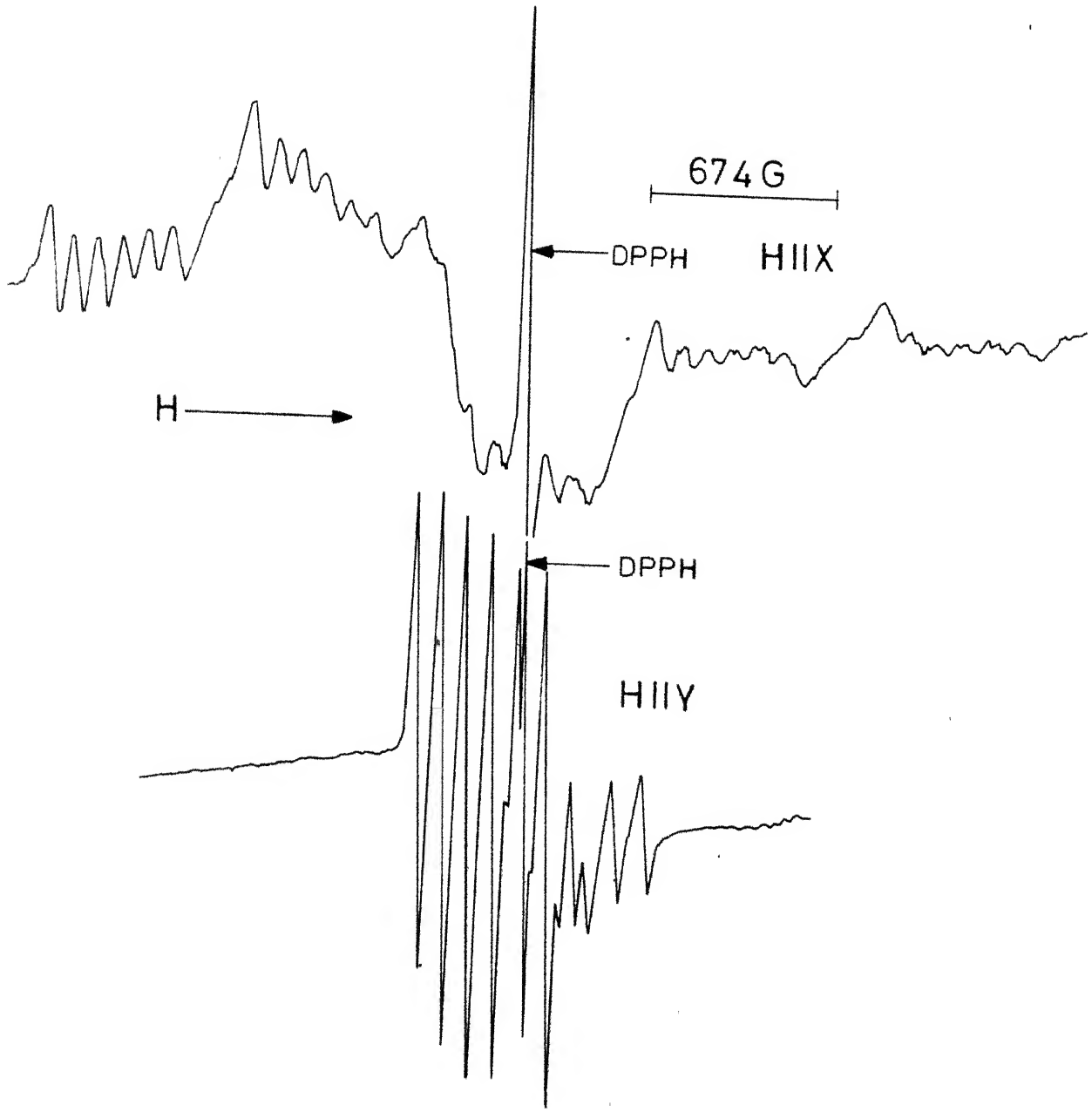

Fig.VII.8: The EPR spectra of Mn^{2+} in $Ni(OH_2)_6 \cdot (NO_3)_2$ at 300K for H along the X and Y axes.

(1) A large anisotropy in the widths of Mn^{2+} resonance lines in HNiN crystals (see Figs. VII-7 and 8).

(2) The widths of Mn^{2+} resonance lines increase with the Zeeman field intensity (see Figs. VII-7 and 8 and Table VII-1). The monotonic increase of Mn^{2+} linewidths for H along the Z-axis is so fast that the two high field fine structure groups are almost completely broadened out and are barely discernible (see Fig. VII-7). For H along the X-axis, the monotonic increase is less faster and all the fine structure groups are visible (see Fig. VII-8).

(3) The g-value of Mn^{2+} in HNiN shows a negative shift from its value generally observed in diamagnetic hosts, e.g. in HMgN: Mn^{2+}.

All the above mentioned observations may be attributed to the magnetic interactions between Mn^{2+} and host Ni^{2+} ions. Observations (1) and (2) can be explained qualitatively in terms of the spin quenching idea, described in Chapter II-C and applied in explaining similar additional features for Mn^{2+} doped $Ni(NH_4)_2(SeO_4)_2 \cdot 6H_2O$ single crystals in Chapter V. Following the earlier discussion, HNiN crystal, with D = -6.07 cm^{-1} and E = -1.86 cm^{-1},[6] is suitable host for the observation of sharp EPR spectrum of Mn^{2+} at 300 K due to spin quenching. Further

Table VII-1

The Zeeman-field intensity (H) and the corresponding linewidth (ΔH) of Mn^{2+} resonance lines for $H \| Z$ in $Ni(OH_2)_6.(NO_3)_2$ single crystals at 300 K.

H (gauss)	ΔH (gauss)
1555	17.7 ± 2
1656	18.5 ± 2
1753	19.4 ± 2
1852	19.4 ± 2
1950	20.2 ± 2
2049	21.1 ± 2
2305	27.0 ± 2
2402	28.6 ± 3
2500	30.3 ± 3
2600	32.0 ± 3
2697	32.0 ± 3
2795	33.7 ± 3
3139	47.0 ± 4
3230	48.8 ± 4
3526	49.0 ± 4
3628	52.2 ± 4
3990	57.0 ± 5
4074	58.5 ± 5

the field dependence of Mn^{2+} linewidths is obvious since the magnetic moment of Ni^{2+}, given by μ_{ins} (Eq.(II.44)) is field dependent. In principle, the field dependence should give information whether or not a narrowing process is operative because the field dependence should be quadratic with narrowing and linear without narrowing. Similar to our earlier observations of Chapters IV and V here also the Mn^{2+} linewidth data could not fit exactly to either of the two forms mentioned above implying the existence of some intermediate case.

The anisotropy of Mn^{2+} linewidth (observation (1)) is a result of the fact that the magnetic moment of Ni^{2+}, μ_{ins} (Eq.(II.44)), is a function of field orientation. This anisotropy has been described in detail in Chapter II-C and for the particular case of Mn^{2+} doped Ni Tutton salts in Chapter V.

Finally, the shift in g-value can be explained to be due to internal magnetic field at the site of Mn^{2+} ions, caused by the moments induced on Ni^{2+} spins due to the polarization effect of the Zeeman field.[9] This causes shift in Mn^{2+} g-value from its value, when diamagnetic divalent cations (e.g. Mg^{2+}) are present in place of Ni^{2+} ions.

REFERENCES

1. A. Ferrari, A. Braibanti, A.M. Manotti Lanfredi and A. Tiripicchio, Acta Crystallogr. 22, 240 (1967).

2. A. Braibanti, A. Tiripicchio, A.M. Manotti Lanfredi and F. Bigoli, Acta Crystallogr. B25, 354 (1969).

3. F. Bigoli, A. Braibanti, A. Tiripicchio and M.Tiripicchio Camellini, Acta Crystallogr. B27, 1427 (1971).

4. B.V. Prelesnik, F.Gabela, B.Ribár and I.Krstanović, Cryst. Struct. Comm. 2, 581 (1973).

5. B. Ribár B. Prelesnik and S. Caric', Z.Krist.137, 318 (1973).

6. L. Berger and S.A. Friedberg, Phys. Rev. 136, A158, (1964).

7. A. Herweijer and S.A. Friedberg, Phys. Rev. B4, 4009 (1971).

8. M.W. Porter and R.C. Spiller, 'The Barker Index of Crystals', Vol. II, W.Heffer and Sons, Cambridge (1956).

9. M.T. Hutchings and W.P. Wolf, Phys. Rev. Letters 11, 187 (1963).

APPENDIX A

LITERATURE SURVEY OF EPR STUDIES OF VARIOUS PARAMAGNETIC IMPURITY IONS IN PARAMAGNETIC HOSTS

Impurity	Host	References
Mn^{2+}	Ni^{2+}, Co^{2+}, Fe^{2+} and Cu^{2+} Tutton salts, $CuSO_4.5H_2O$ and $NiSiF_6.6H_2O$	Ono and Hayashi, J.Phys.Soc. Japan 8, 561 (1953).
Mn^{2+}	$(NH_4)_2Ni_2(SO_4)_3$	Chowdari, J.Phys.Chem.Solids 30, 2747 (1969); Upreti, ibid. 35, 461 (1974).
Mn^{2+}	$Ni(CH_3COO)_2.4H_2O$	Janakiraman and Upreti, J.Chem. Phys. 54, 2336, (1971); Saraswat and Upreti, J.Magn. Resonance 20, 39 (1975).
Mn^{2+}	$NiSO_4.7H_2O$	Janakiraman and Upreti, J.Chem. Phys. 54, 2336 (1971) and Phys. Stat.Sol.(b) 47, 679 (1971).
Mn^{2+}	$(NH_4)_2Ni(SO_4)_2.6H_2O$ and $K_2Ni(SO_4)_2.6H_2O$	Upreti, J. Magn. Res. 14, 274 (1974).
Cu^{2+}, Co^{2+} and Ni^{2+}	$NiSeO_4.6H_2O$	Jindo and Myers, J.Magn.Res. 6, 633 (1972).
Mn^{2+}, V^{2+}, Cu^{2+} and Co^{2+}	α-$NiSO_4.6H_2O$	St. John and Myers, Phys.Rev. B13, 1006 (1976).
Mn^{2+}	$Ni(NH_4)_2(SeO_4)_2.6H_2O$	Present work
Mn^{2+}	$Ni(OH_2)_6.(NO_3)_2$	Present work

Mn^{2+}	$(NH_4)_2Fe(SO_4)_2.6H_2O$	Ohtsuka, Abe and Kanda, Sci. Rep.Res. Inst.Tohuku Univ. 9A, 476 (1957); Janakiraman and Upreti, Chem. Phys. Lett. 4, 550 (1970).
Cu^{2+}	$(NH_4)_2Fe(SO_4)_2.6H_2O$	Gill and Ivey, J.Phys.C7, 1536 (1974) and 8, 4203,(1975).
Ni^{2+}	$FeSiF_6.6H_2O$	Rubins, J.Chem.Phys. 60, 4189 (1974).
Mn^{2+}	$FeK_2(SO_4)_2.6H_2O$	Present work
Mn^{2+}	$CoCl_2.6H_2O$, $CoSO_4.7H_2O$ and Co Tutton salt	Date, J.Phys. Soc. Japan 18, 912 (1963).
Mn^{2+}	$CoCl_2.2H_2O$	Tachiki, J.Phys.Soc.Japan 25, 686 (1968).
Mn^{2+}	$(NH_4)_2Co_2(SO_4)_3$	Chowdari, J.Phys.Chem.Solids 30, 2747 (1969).
Mn^{2+}	$(NH_4)_2Co(SO_4)_2.6H_2O$	Upreti, Chem.Phys.Lett.18, 120 (1973).
Cu^{2+}	$K_2Co(SO_4)_2.6H_2O$	Sastry and Sastry, J.Chem. Phys. 59, 6419 (1973).
Cu^{2+}	$(NH_4)_2Co(SO_4)_2.6H_2O$	Sastry and Sastry, Physica 74, 151 (1974).
Mn^{2+}	$Co(CH_3COO)_2.4H_2O$	Saraswat and Upreti, J.Magn. Res. 20, 39 (1975) and present work.
Mn^{2+}	$CoK_2(SO_4)_2.6H_2O$	Present work
Mn^{2+}	$CoSO_4.7H_2O$	Present work
Cr^{3+}	$K_3Fe(CN)_6$	Mitsuma, J.Phys.Soc.Japan 17, 128 (1962).
Cu^{2+}	$(Cu\text{-}Mn)SO_4.5H_2O$	Branski, Acta Phys.Polonica 34, 301 (1968).

Co^{2+}, Ni^{2+} and Fe^{2+}	$RbMnF_3$	Gulley and Jaccarino, Phys. Rev. B6, 58 (1972).
Cu^{2+}	$Cd(NH_3)_2.Ni(CN)_4 .2C_6H_6$	Nagata, Miyako and Watanabe, J.Phys. Soc. Japan 34, 1158 (1973).
Cu^{2+}	$(CH_3)_4NMnCl_3$	Richards, Phys.Rev. B10, 805 (1974).

LANTHANIDE GROUP HOSTS

Gd^{3+}	$Ln(C_2H_5SO_4)_3.9H_2O$ (Ln=Ce,Nd,Sm)	Bleaney, Elliot and Scovil, Proc. Phys. Soc. A64, 933 (1951).
Gd^{3+}	$Nd(NO_3)_3.6H_2O$	Singh and Venkateswarlu, J.Chem. Phys. 46, 4765 (1967).
Gd^{3+}	$NdCl_3.6H_2O$	Singh, Upreti and Venkateswarlu, J.Chem.Phys. 46, 2885 (1967); Misra and Sharp, ibid. 64, 2168 (1976).
Gd^{3+}	$SmCl_3.6H_2O$	Singh and Venkateswarlu, Proc. Ind. Acad. Sci. A65, 211 (1967); Misra and Sharp, J.Phys.C 9, 401 (1976).
Gd^{3+}	$Sm(NO_3)_3.6H_2O$	Singh and Upreti, Proc. Ind. Acad. Sci. A66, 104 (1967).
Gd^{3+}	$PrCl_3.7H_2O$	Singh, Upreti and Venkateswarlu, J. Chem.Phys. 46, 2885 (1967); Misra and Sharp, Phys. Stat.Sol. (b) 75, 607 (1976).
Gd^{3+}	$Pr(NO_3)_3.6H_2O$	Singh and Venkateswarlu, Proc. Ind. Acad. Sci, A65, 361 (1967).
Gd^{3+}	LnF_3 (Ln=Pr,Ce and Nd)	Sharma, J.Chem.Phys. 54, 496 (1971).

Gd^{3+}	$Ln(C_2H_5SO_4)_3 \cdot 9H_2O$ (Ln = Pr,Nd,Sm,Tb, Dy,Ho,Er,Yb)	Gerkin and Thorsell, J.Chem. Phys. 57, 2665 (1972).
Gd^{3+}	$Ln(C_2H_5SO_4)_3 \cdot 9H_2O$ and $Ln(C_2H_5SO_4)_3 \cdot 9D_2O$ (Ln=Sm,Er)	Bernstein and Dobbs, Phys. Rev. B11, 4623 (1975).
Gd^{3+}	$Ln_2Mg_3(NO_3)_{12} \cdot 24H_2O$ (Ln=Ce,Pr,Nd,Sm,Eu)	Misumi,Isobe and Higa,Nippon Kagaku Kaishi 11, 2039 (1973).
Gd^{3+}	$Ln_2M_3(NO_3)_{12} \cdot 24H_2O$ (Ln=Ce,Pr,Nd,Sm,Eu and M = Co,Zn)	Misumi, Isobe and Higa, ibid. 14, 1829 (1974).
Gd^{3+}	$EuCl_3 \cdot 6H_2O$	Misra and Sharp, Physica 83B, 174 (1976).
Gd^{3+}	$NH_4Nd(SO_4)_2 \cdot 4H_2O$	Malhotra, Bist and Upreti, Chem.Phys.Lett. 28, 390 (1974).
Gd^{3+}	$NH_4Ce(SO_4)_2 \cdot 4H_2O$	Malhotra and Bist, Proc.Nucl. Phys. and Solid St.Phys.Symp. Bombay, 17C, 410 (1974).
Gd^{3+}	$Nd_2(SO_4)_3 \cdot 8H_2O$	Malhotra, Bist and Upreti, J.Magn.Res. 21, 173 (1976).
Gd^{3+}	$Pr_2(SO_4)_3 \cdot 8H_2O$	Malhotra, Solid State Comm. 18, 499 (1976).
Yb^{3+}	TmAl Garnet and TmGa Garnet	Hutchings and Wolf, Phys.Rev. Lett.11, 187 (1963).
Fe^{3+}	TmAl Garnet and TmGa Garnet	Rimai and Bierig, ibid 12, 284 (1964).
Fe^{3+} and Yb^{3+}	TmGa Garnet	Hodges, Solid State Comm. 17 919 (1975).

Gd^{3+} and Fe^{3+}	EuGa Garnet	Hutchings, Windsor and Wolf, Phys.Rev. 148, 444 (1966).
Eu^{2+}	SmS, SmSe and SmTe	Mehran, Stevens, Title and Holtzberg, Phys.Rev.Lett. 27, 1368 (1971).
Mn^{2+}	SmTe	Mehran, Stevens, Title and Holtzberg, Phys.Rev.Lett. 27, 1368 (1971).
Gd^{3+} and Eu^{2+}	SmB_6	Kojima, Kasaya and Koi, J.Phys. Soc.Japan 36, 1206 (1974).
Gd^{3+}	$CsEu(MoO_4)_2$	Otko, Pelikh, Zvyagin, Sov. Phys.-Solid State 14, 2918 (1973).
Gd^{3+}	$Gd_x Eu_{1-x}$ Ultraphosphates	Parrot, Barthou, Canny, Blanfeit and Collin, Phys. Rev. B11, 1001 (1975).

taking the z' - axis along H. Here,

$$S_+ = S_{x'} + iS_{y'}, \quad S_- = S_{x'} - iS_{y'}$$

$$\sigma = \tfrac{1}{2}[D(3\,\mathrm{Cos}^2\,\theta - 1) + 3E\,\mathrm{Sin}^2\,\theta\,\mathrm{Cos}\,2\phi]$$

$$\rho = \tfrac{1}{4}[D\,\mathrm{Sin}^2\,\theta + E(\mathrm{Cos}^2\,\theta\,\mathrm{Cos}\,2\phi - \mathrm{Sin}^2\phi) + 2iE\,\mathrm{Cos}\,\theta\,\mathrm{Sin}\,2\phi]$$

$$\lambda = \mathrm{Sin}\,\theta\,[(D - E\,\mathrm{Cos}\,2\phi)\,\mathrm{Cos}\,\theta + iE\,\mathrm{Sin}\,2\phi]$$

$$P = \tfrac{1}{2}[Q'(3\,\mathrm{Cos}^2\,\theta - 1) + 3Q''\,\mathrm{Sin}^2\,\theta\,\mathrm{Cos}\,2\phi]$$

In the above the hyperfine constant and the g-value are assumed to be isotropic. The assumption is valid for many of the experimentally studied systems.

The eigen values of the above Hamiltonian, with z' as the quantization axis and under the approximation $g\beta H \gg |D|$, $|E|$, $|A|$, to third-order perturbation are given by

$$E_{|M,m\rangle} = g\beta HM + \sigma[M^2 - \tfrac{1}{3}S(S+1)] + AMm + \frac{A^2}{2g\beta H}[m[M^2 - S(S+1)] + M[I(I+1) - m^2]] - \gamma\beta_N Hm + P[m^2 - \tfrac{1}{3}I(I+1)] + \frac{|\lambda|^2}{(2g\beta H)^2}\frac{2Am}{M}[[M^2 - S(S+1)]^2 - M^2]$$

$$+ \frac{|\rho|^2}{(g\beta H)^2} 2AMm\,[2M^2+1-2S(S+1)]$$

$$+ \frac{A^2\sigma}{(2g\beta H)^2} [[S(S+1)-M(M+1)][I(I+1)-m(m-1)](2M+1)$$

$$- [S(S+1)-M(M-1)][I(I+1)-m(m+1)](2M-1)]$$

$$+ \frac{A^3}{(2g\beta H)^2} [[S(S+1)-M(M+1)][I(I+1)-m(m-1)](m-M-1)$$

$$+ [S(S+1)-M(M-1)][I(I+1)-m(m+1)](M-m-1)]$$

Before calculating the doublet separations we give a schematic representation of the allowed and forbidden hyperfine transitions in the electron paramagnetic resonance of Mn^{2+} in an orthorhombic crystalline field. Fig. B-1 at the end shows schematically the allowed and forbidden hf lines in the Mn^{2+} spectrum for positive D and for the external field H at an angle slightly away from the principal Z-axis. The thirty longer vertical lines correspond to the allowed transitions ($\Delta M = \pm 1$, $\Delta m = 0$) and smaller vertical lines numbered from 1 through 50 correspond to the forbidden transitions $\Delta M = \pm 1$, $\Delta m = \pm 1$ for the five groups ($M \leftrightarrow M-1$) while those numbered from 1' through 8' correspond to the forbidden transitions $\Delta M = \pm 1$, $\Delta m = \pm 2$ in the group $M = +\frac{1}{2} \leftrightarrow -\frac{1}{2}$. The relative positions and intensities of the lines in the figure are only qualitative. The identification of the forbidden hf transitions ($|M,m> \rightarrow |M-1, m'>$), for positive D and negative A, is as follows:

1) $|\frac{5}{2}, -\frac{3}{2}> \rightarrow |\frac{3}{2}, -\frac{5}{2}>$ 2) $|\frac{5}{2}, -\frac{1}{2}> \rightarrow |\frac{3}{2}, -\frac{3}{2}>$

3) $|\frac{5}{2}, \frac{1}{2}> \rightarrow |\frac{3}{2}, -\frac{1}{2}>$ 4) $|\frac{5}{2}, \frac{3}{2}> \rightarrow |\frac{3}{2}, \frac{1}{2}>$

5) $|\frac{5}{2}, \frac{5}{2}> \rightarrow |\frac{3}{2}, \frac{3}{2}>$ 6) $|\frac{5}{2}, -\frac{5}{2}> \rightarrow |\frac{3}{2}, -\frac{3}{2}>$

7) $|\frac{5}{2}, -\frac{3}{2}> \rightarrow |\frac{3}{2}, -\frac{1}{2}>$ 8) $|\frac{5}{2}, -\frac{1}{2}> \rightarrow |\frac{3}{2}, \frac{1}{2}>$

9) $|\frac{5}{2}, \frac{1}{2}> \rightarrow |\frac{3}{2}, \frac{3}{2}>$ 10) $|\frac{5}{2}, \frac{3}{2}> \rightarrow |\frac{3}{2}, \frac{5}{2}>$

11) $|\frac{3}{2}, -\frac{5}{2}> \rightarrow |\frac{1}{2}, -\frac{3}{2}>$ 12) $|\frac{3}{2}, -\frac{3}{2}> \rightarrow |\frac{1}{2}, -\frac{1}{2}>$

13) $|\frac{3}{2}, -\frac{1}{2}> \rightarrow |\frac{1}{2}, \frac{1}{2}>$ 14) $|\frac{3}{2}, -\frac{3}{2}> \rightarrow |\frac{1}{2}, -\frac{5}{2}>$

15) $|\frac{3}{2}, \frac{3}{2}> \rightarrow |\frac{1}{2}, \frac{1}{2}>$ 16) $|\frac{3}{2}, -\frac{1}{2}> \rightarrow |\frac{1}{2}, -\frac{3}{2}>$

17) $|\frac{3}{2}, \frac{5}{2}> \rightarrow |\frac{1}{2}, \frac{3}{2}>$ 18) $|\frac{3}{2}, \frac{1}{2}> \rightarrow |\frac{1}{2}, -\frac{1}{2}>$

19) $|\frac{3}{2}, \frac{1}{2}> \rightarrow |\frac{1}{2}, \frac{3}{2}>$ 20) $|\frac{3}{2}, \frac{3}{2}> \rightarrow |\frac{1}{2}, \frac{5}{2}>$

21) $|\frac{1}{2}, -\frac{5}{2}> \rightarrow |-\frac{1}{2}, -\frac{3}{2}>$ 22) $|\frac{1}{2}, -\frac{3}{2}> \rightarrow |-\frac{1}{2}, -\frac{5}{2}>$

23) $|\frac{1}{2}, -\frac{3}{2}> \rightarrow |-\frac{1}{2}, -\frac{1}{2}>$ 24) $|\frac{1}{2}, -\frac{1}{2}> \rightarrow |-\frac{1}{2}, -\frac{3}{2}>$

25) $|\frac{1}{2}, -\frac{1}{2}> \rightarrow |-\frac{1}{2}, \frac{1}{2}>$ 26) $|\frac{1}{2}, \frac{1}{2}> \rightarrow |-\frac{1}{2}, -\frac{1}{2}>$

27) $|\frac{1}{2}, \frac{1}{2}> \rightarrow |-\frac{1}{2}, \frac{3}{2}>$ 28) $|\frac{1}{2}, \frac{3}{2}> \rightarrow |-\frac{1}{2}, \frac{1}{2}>$

29) $|\frac{1}{2}, \frac{3}{2}> \rightarrow |-\frac{1}{2}, \frac{5}{2}>$ 30) $|\frac{1}{2}, \frac{5}{2}> \rightarrow |-\frac{1}{2}, \frac{3}{2}>$

31) $|-\frac{1}{2}, -\frac{3}{2}> \rightarrow |-\frac{3}{2}, -\frac{5}{2}>$ 32) $|-\frac{1}{2}, -\frac{1}{2}> \rightarrow |-\frac{3}{2}, -\frac{3}{2}>$

33) $|-\frac{1}{2}, \frac{1}{2}> \rightarrow |-\frac{3}{2}, -\frac{1}{2}>$ 34) $|-\frac{1}{2}, -\frac{5}{2}> \rightarrow |-\frac{3}{2}, -\frac{3}{2}>$

35) $|-\frac{1}{2}, \frac{1}{2}> \rightarrow |-\frac{3}{2}, \frac{3}{2}>$ 36) $|-\frac{1}{2}, -\frac{3}{2}> \rightarrow |-\frac{3}{2}, -\frac{1}{2}>$

37) $|-\frac{1}{2}, \frac{3}{2}> \rightarrow |-\frac{3}{2}, \frac{5}{2}>$ 38) $|-\frac{1}{2}, -\frac{1}{2}> \rightarrow |-\frac{3}{2}, \frac{1}{2}>$

39) $|-\frac{1}{2}, \frac{3}{2}> \rightarrow |-\frac{3}{2}, \frac{1}{2}>$ 40) $|-\frac{1}{2}, \frac{5}{2}> \rightarrow |-\frac{3}{2}, \frac{3}{2}>$

41) $|-\frac{3}{2}, -\frac{5}{2}> \rightarrow |-\frac{5}{2}, -\frac{3}{2}>$ 42) $|-\frac{3}{2}, -\frac{3}{2}> \rightarrow |-\frac{5}{2}, -\frac{1}{2}>$

43) $|-\frac{3}{2}, -\frac{1}{2}> \rightarrow |-\frac{5}{2}, \frac{1}{2}>$ 44) $|-\frac{3}{2}, \frac{1}{2}> \rightarrow |-\frac{5}{2}, \frac{3}{2}>$

45) $|-\frac{3}{2}, \frac{3}{2}> \rightarrow |-\frac{5}{2}, \frac{5}{2}>$ 46) $|-\frac{3}{2}, -\frac{3}{2}> \rightarrow |-\frac{5}{2}, -\frac{5}{2}>$

47) $|-\frac{3}{2}, -\frac{1}{2}> \rightarrow |-\frac{5}{2}, -\frac{3}{2}>$ 48) $|-\frac{3}{2}, \frac{1}{2}> \rightarrow |-\frac{5}{2}, -\frac{1}{2}>$

49) $|-\frac{3}{2}, \frac{3}{2}> \rightarrow |-\frac{5}{2}, \frac{1}{2}>$ 50) $|-\frac{3}{2}, \frac{5}{2}> \rightarrow |-\frac{5}{2}, \frac{3}{2}>$

1') $|\frac{1}{2}, -\frac{5}{2}> \rightarrow |-\frac{1}{2}, -\frac{1}{2}>$ 2') $|\frac{1}{2}, -\frac{1}{2}> \rightarrow |-\frac{1}{2}, -\frac{5}{2}>$

3') $|\frac{1}{2}, -\frac{3}{2}> \rightarrow |-\frac{1}{2}, \frac{1}{2}>$ 4') $|\frac{1}{2}, \frac{1}{2}> \rightarrow |-\frac{1}{2}, -\frac{3}{2}>$

5') $|\frac{1}{2}, -\frac{1}{2}> \rightarrow |-\frac{1}{2}, \frac{3}{2}>$ 6') $|\frac{1}{2}, \frac{3}{2}> \rightarrow |-\frac{1}{2}, -\frac{1}{2}>$

7') $|\frac{1}{2}, \frac{1}{2}> \rightarrow |-\frac{1}{2}, \frac{5}{2}>$ 8') $|\frac{1}{2}, \frac{5}{2}> \rightarrow |-\frac{1}{2}, \frac{1}{2}>$

Now we calculate the doublet separations for the various fine structure groups. In the following the positive and negative D refer to the relative sign of D with respect to that of A, which is assumed to be negative.

(I) $M = +\frac{1}{2} \leftrightarrow -\frac{1}{2}$:

(i) $\Delta m = \pm 1$ Transitions:

From the eigen value expression given above we obtain,

$$E_{|\frac{1}{2},m+1>} - E_{|-\frac{1}{2},m>} = g\beta H + \frac{A}{2}(2m+1) - \frac{A^2}{2g\beta H}(m^2+m+\frac{1}{4}) - \gamma\beta_N H + P(2m+1) + \frac{|\lambda|^2}{(2g\beta H)^2} \times 288\, A\,(2m+1) - \frac{|\rho|^2}{(g\beta H)^2} 16A\,(2m+1) + \frac{A^3}{(2g\beta H)^2}(2m^3+3m^2+\frac{75}{2}m+\frac{73}{4})$$

For $E_{|\frac{1}{2},m+1>} - E_{|-\frac{1}{2},m>} = h\nu$, the H in the first term on the right hand side gives the field value at which the forbidden transition $|\frac{1}{2}, m+1> \rightarrow |-\frac{1}{2}, m>$ will occur. Denoting this field value by $H_{|\frac{1}{2},m+1> \rightarrow |-\frac{1}{2},m>}$ and putting $\frac{h\nu}{g\beta} = H_o$, we have,

$$H_{|\frac{1}{2},m+1> \rightarrow |-\frac{1}{2},m>} = H_o - \frac{A}{2}(2m+1) + \frac{A^2}{2H}(m^2+m+\frac{1}{4}) + (\frac{\gamma\beta_N}{g\beta})H - P(2m+1) - \frac{|\lambda|^2}{H^2} 72A\,(2m+1) + \frac{|\rho|^2}{H^2} 16A(2m+1) - \frac{A^3}{4H^2} \times (2m^3+3m^2+\frac{75}{2}m+\frac{73}{4})$$

where H in the denominators is also $H_{|\frac{1}{2},m+1> \to |-\frac{1}{2},m>}$ and the parameters A, σ, ρ, λ and P are now in gauss.

Similarly, we get,

$$H_{|\frac{1}{2},m> \to |-\frac{1}{2},m+1>} = H_o - \frac{A}{2}(2m+1) + \frac{A^2}{2H}(m^2+m-\frac{67}{4}) - (\frac{\gamma\beta_N}{g\beta})H + P(2m+1) - \frac{|\lambda|^2}{H^2} 72A(2m+1) + \frac{|\rho|^2}{H^2} 16A(2m+1) - \frac{A^2\sigma}{H^2} 8(2m+1) - \frac{A^3}{4H^2}(2m^3+3m^2-\frac{193}{2}m-\frac{195}{4}).$$

Finally the doublet separation is given by,

$$\Delta H = H_{|\frac{1}{2},m+1> \to |-\frac{1}{2},m>} - H_{|\frac{1}{2},m> \to |-\frac{1}{2},m+1>}$$

$$= \frac{17A^2}{2H} + 2(\frac{\gamma\beta_N}{g\beta})H - 2P(2m+1) + \frac{8A^2\sigma}{H^2}(2m+1) - \frac{67A^3}{4H^2}(2m+1).$$

To the first order approximation we replace H in the above by $H_o - \frac{A}{2}(2m+1)$. Then using the condition that $H_o \gg |A|$ the inverse powers of $H_o - \frac{A}{2}(2m+1)$ can be expanded. The final expression for doublet separations after neglecting small higher order terms is,

$$\Delta H = \frac{17A^2}{2H_o} + 2\left(\frac{\gamma\beta_N}{g\beta}\right) H_o - (2m+1)\left[2P - \frac{8A^2\sigma}{H_o^2} + \frac{25}{2}\frac{A^3}{H_o^2} + \left(\frac{\gamma\beta_N}{g\beta}\right)A\right]$$

(ii) $\Delta m = \pm 2$ transitions:

Proceeding as above, we get for the doublet separation

$$\Delta H = H_{\left|\frac{1}{2},m+1\right> \to \left|-\frac{1}{2},m-1\right>} - H_{\left|\frac{1}{2},m-1\right> \to \left|-\frac{1}{2},m+1\right>}$$

$$= \frac{17A^2}{H} + 4\left(\frac{\gamma\beta_N}{g\beta}\right) H - 8Pm + \frac{32A^2\sigma}{H^2} m - \frac{67A^3}{H^2} m$$

Replacing H by $H_o - Am$ to the first order approximation and neglecting higher order terms, we finally get,

$$\Delta H = \frac{17A^2}{H_o} + 4\left(\frac{\gamma\beta_N}{g\beta}\right) H_o - 2m\left[4P - \frac{16A^2\sigma}{H_o^2} + \frac{25A^3}{H_o^2} + 2\left(\frac{\gamma\beta_N}{g\beta}\right)A\right]$$

(II) $M = +\frac{3}{2} \leftrightarrow +\frac{1}{2}$, $\Delta m = \pm 1$ transitions:

The doublet separations, obtained by using the expression for $E_{|M,m>}$ is,

$$\Delta H = -2A + 2\left(\frac{\gamma\beta_N}{g\beta}\right) H - 2P(2m+1) + \frac{A^2}{H}\left(2m + \frac{17}{2}\right)$$
$$- \frac{|\lambda|^2}{H^2}\left(\frac{256}{3}\right) A + \frac{|\rho|^2}{H^2} 52A - \frac{A^2\sigma}{H^2}(8-10m)$$
$$- \frac{A^3}{H^2}\left(3m^2 + \frac{61}{2} m\right)$$

Again to the first order approximation H in the above is replaced by $H_o - 2\sigma - \frac{A}{2}(2m+3)$ or $H_o + 2\sigma - \frac{A}{2}(2m+3)$ for positive

or negative D respectively. Substituting these expressions for H and recalling the assumption that $H_o >> |D|, |E|, |A|$ we get the following doublet separations after neglecting small higher order terms:

(i) For positive D:

$$\Delta H = -2A + 2\left(\frac{\gamma\beta_N}{g\beta}\right) H_o - 2P(2m+1) - \frac{|\lambda|^2}{H_o^2}\left(\frac{256}{3}\right) A + \frac{|\rho|^2}{H_o^2} 52A$$

$$+ \frac{A^2}{H_o}\left(2m + \frac{17}{2}\right) + \frac{A^2\sigma}{H_o^2}(14m+9) - \frac{A^3}{H_o^2}\left(m^2+19m - \frac{51}{4}\right)$$

(ii) For negative D:

$$\Delta H = -2A + 2\left(\frac{\gamma\beta_N}{g\beta}\right) H_o - 2P(2m+1) - \frac{|\lambda|^2}{H_o^2}\left(\frac{256}{3}\right) A$$

$$+ \frac{|\rho|^2}{H_o^2} 52A + \frac{A^2}{H_o}\left(2m + \frac{17}{2}\right) - \frac{A^2\sigma}{H_o^2}(14m+9)$$

$$- \frac{A^3}{H_o^2}\left(m^2+19m - \frac{51}{4}\right)$$

(III) $M = -\frac{1}{2} \leftrightarrow -\frac{3}{2}$, $\Delta m = \pm 1$ transitions:

Here, we obtain for the doublet separation,

$$\Delta H = -2A - 2\left(\frac{\gamma\beta_N}{g\beta}\right) H + 2P(2m+1) - \frac{|\lambda|^2}{H_o^2}\left(\frac{256}{3}\right) A$$

$$+ \frac{|\rho|^2}{H^2} 52A + \frac{A^2}{H}\left(2m - \frac{13}{2}\right) - \frac{A^2\sigma}{H^2}(10m + 18)$$

$$- \frac{A^3}{H^2}\left(3m^2 - \frac{49}{2} m - \frac{55}{2}\right)$$

To the first order approximation we replace H by $H_o+2\sigma - \frac{A}{2}(2m-1)$ or $H_o-2\sigma - \frac{A}{2}(2m-1)$ for positive or negative D respectively. Substituting these expressions for H and proceeding as above the following expressions are obtained for the doublet separations:

(i) For positive D:

$$\Delta H = -2A - 2\left(\frac{\gamma\beta_N}{g\beta}\right) H_o + 2P(2m+1) - \frac{|\lambda|^2}{H_o^2}\left(\frac{256}{3}\right) A + \frac{|\rho|^2}{H_o^2} 52A + \frac{A^2}{H_o}\left(2m - \frac{13}{2}\right) - \frac{A^2\sigma}{H_o^2}(14m+5) - \frac{A^3}{H_o^2}\left(m^2-17m - \frac{123}{4}\right)$$

(ii) For negative D:

$$\Delta H = -2A - 2\left(\frac{\gamma\beta_N}{g\beta}\right) H_o + 2P(2m+1) - \frac{|\lambda|^2}{H_o^2}\left(\frac{256}{3}\right)A + \frac{|\rho|^2}{H_o^2} 52A + \frac{A^2}{H_o}\left(2m - \frac{13}{2}\right) + \frac{A^2\sigma}{H_o^2}(14m + 5) - \frac{A^3}{H_o^2}\left(m^2-17m- \frac{123}{4}\right).$$

(IV) $M = +\frac{5}{2} \leftrightarrow +\frac{3}{2}$, $\Delta m = \pm 1$ transitions:

In this case, we get,

$$\Delta H = -4A + 2\left(\frac{\gamma\beta_N}{g\beta}\right) H - 2P(2m+1) - \frac{|\lambda|^2}{H^2}\left(\frac{40}{3}\right) A + \frac{|\rho|^2}{H^2} 56A + \frac{A^2}{H}\left(4m + \frac{13}{2}\right) - \frac{A^2\sigma}{H^2}(8m+18) - \frac{A^3}{H^2}\left(6m^2 + \frac{31}{2} m - \frac{67}{4}\right)$$

Replacing H by $H_o - 4\sigma - \frac{A}{2}(2m+5)$ or $H_o + 4\sigma - \frac{A}{2}(2m+5)$ for positive or negative D respectively and proceeding as above we get the following expressions for the doublet separations.

(i) For positive D:

$$\Delta H = -4A + 2\left(\frac{\gamma\beta_N}{g\beta}\right) H_o - 2P(2m+1) - \frac{|\lambda|^2}{H_o^2}\left(\frac{40}{3}\right) A + \frac{|\rho|^2}{H_o^2} 56A + \frac{A^2}{H_o}\left(4m + \frac{13}{2}\right) + \frac{A^2\sigma}{H_o^2}(8m+8) - \frac{A^3}{H_o^2}(2m^2 - m - 33)$$

(ii) For negative D:

$$\Delta H = -4A + 2\left(\frac{\gamma\beta_N}{g\beta}\right) H_o - 2P(2m+1) - \frac{|\lambda|^2}{H_o^2}\left(\frac{40}{3}\right) A + \frac{|\rho|^2}{H_o^2} 56A + \frac{A^2}{H_o}\left(4m + \frac{13}{2}\right) - \frac{A^2\sigma}{H_o^2}(8m+8) - \frac{A^3}{H_o^2}(2m^2 - m - 33)$$

(V) $M = -\frac{3}{2} \leftrightarrow -\frac{5}{2}$, $\Delta m = \pm 1$ transitions:

The doublet separation obtained by using the expression for $E_{|M,m>}$, is

$$\Delta H = -4A - 2\left(\frac{\gamma \beta_N}{g\beta}\right) H + 2P(2m+1) - \frac{|\lambda|^2}{H^2} \left(\frac{40}{3}\right) A$$
$$+ \frac{|\rho|^2}{H^2} 56A + \frac{A^2}{H} \left(4m - \frac{5}{2}\right) - \frac{A^2\sigma}{H^2} (2m+10)$$
$$- \frac{A^3}{H^2} \left(6m^2 - \frac{7}{2}m - \frac{105}{4}\right)$$

Again replacing H by $H_o + 4\sigma - \frac{A}{2}(2m-3)$ or $H_o - 4\sigma - \frac{A}{2}(2m-3)$ for positive or negative D respectively and proceeding as above, we get the following expressions for the doublet separations:

(i) For positive D:

$$\Delta H = -4A - 2\left(\frac{\gamma \beta_N}{g\beta}\right) H_o + 2P(2m+1) - \frac{|\lambda|^2}{H_o^2} \left(\frac{40}{3}\right) A$$
$$+ \frac{|\rho|^2}{H_o^2} 56A + \frac{A^2}{H_o} \left(4m - \frac{5}{2}\right) - \frac{A^2\sigma}{H_o^2} 18m$$
$$- \frac{A^3}{H_o^2} (2m^2 + 5m - 30)$$

(ii) For negative D:

$$\Delta H = -4A - 2\left(\frac{\gamma\beta_N}{g\beta}\right) H_o + 2P(2m+1) - \frac{|\lambda|^2}{H_o^2}\left(\frac{40}{3}\right) A$$
$$+ \frac{|\rho|^2}{H_o^2} 56A + \frac{A^2}{H_o}\left(4m - \frac{5}{2}\right) + \frac{A^2\sigma}{H_o^2} 18m$$
$$- \frac{A^3}{H_o^2}(2m^2 + 5m - 30)$$

The above expressions for the doublet separations have been obtained by using perturbation theory and so will be valid only when $g\beta H \gg |D|$, $|E|$ and $|A|$. Thus the above expressions will be in good quantitative agreement with observations only for systems in which $|D|$, $|E|$ and $|A|$ are small and for situations when the external magnetic field is off only by small angles from the principal axes.

Our expression for $\Delta m = \pm 1$ transitions in the group $M = +\frac{1}{2} \leftrightarrow -\frac{1}{2}$ agrees with the expression for Takeda[+] except for the small term $-\left(\frac{\gamma\beta_N}{g\beta}\right) A(2m+1)$ which we have retained. In the groups $M = \pm\frac{3}{2} \leftrightarrow \pm\frac{1}{2}$ our expressions agree with those of Takeda except for the last terms. To our knowledge no expressions are available for $\Delta m = \pm 1$ transitions in the groups $M = \pm\frac{5}{2} \leftrightarrow \pm\frac{3}{2}$ and for $\Delta m = \pm 2$ transitions in the group $M = +\frac{1}{2} \leftrightarrow -\frac{1}{2}$ for Mn^{2+} in an orthorhombic crystalline field.

[+] T. Takeda, J.Phys. Soc. Japan, 23, 1314 (1967).